An Investigation of the Requirements for Excimer Formation and Charge Stabilization in Model Pi-Stacked Assemblies

Brandon Uhler

Marquette University

AN INVESTIGATION OF THE REQUIRMEMENTS FOR EXCIMER FORMATION
AND CHARGE STABILIZATION IN MODEL PI-STACKED ASSEMBLIES

By

Brandon Uhler, B.S.

A Dissertation submitted to the Faculty of the Graduate School,
Marquette University,
in Partial Fulfillment of the Requirements for
the Degree
of Doctor of Philosophy

Milwaukee, Wisconsin

December 2016

ABSTRACT

AN INVESTIGATION OF THE REQUIRMENTS FOR EXCIMER FORMATION
AND CHARGE STABILIZATION IN MODEL PI-STACKED ASSEMBLIES

Brandon Uhler, B.S.

Marquette University, 2016

Formation of π-stacked excimers plays an important role in many systems, ranging from biological phenomena and polymer formation and function to photovoltaic devices and organic molecular electronics. In these systems, the geometrical reorganization of the ground state upon photoexcitation is still a subject of debate.

In this work, we compare the dynamics of excimer formation and hole (charge) stabilization in fluorene and fluorene-based model systems. We use a variety of gas-phase methods to examine the spectroscopy and dynamics of these systems, including Two-Color Resonant Two-Photon Ionization (2CR2PI), Hole-Burning (HB), Laser Induced Fluorescence (LIF), and Dispersed Fluorescence (DF). In order to quantify the clusters' geometry, minimum, and relative energies, calculations using Density Functional Theory and high level *ab initio* methods are reported. These techniques were applied to better understand the energetic properties and behaviors of these model systems in their ground (S0), excited (S1), and ionized ($M^{+\bullet}$) states to probe the geometrical reorganization resulting in excimer formation and stabilization of charge.

As model systems, we used fluorene based assemblies that are covalently linked by utilizing methylene or cyclohexane bridges, which connect two or more fluorene sub-units together. These are compared with clusters interacting at the van der Waals contact distance (≤ 3.5 Å). It was found that in both covalently linked and vdW bound systems, excimer formation is dominant; however, the excimer state is stabilized by covalent linkage. We also find cases in which the geometric requirements for excimer formation are not met. Almost every system studied displayed the ability to stabilize charge in its ionic state and therefore showed that the requirements necessary to delocalize charge are less stringent than those necessary for excimer formation.

ACKNOWLEDGEMENTS

Brandon Uhler, B.S.

TABLE OF CONTENTS

LIST OF TABLES

LIST OF FIGURES

Chapter 1

Literature Review of Non-Covalent Interactions

1.1   The Formation and Role of Non-Covalent Interactions

A non-covalent interaction is one in which the molecules engaged in the interaction do not share their electrons[1]; this is in direct contrast to a covalent interaction where molecules involved share their electrons and form a strong bond.[2] In comparison with covalent interactions, these are much weaker, and can be more challenging to study, from both the viewpoint of experiment and theory. It is difficult to define non-covalent interactions as *not covalent* due to the fact that there is ambiguity that comes with defining these interactions.[3] Non-covalent interactions usually take advantage of dipole moments and polarizability and therefore are referred to as electromagnetic interactions are grouped into several types,[4] including hydrogen bonding[5-7], van der Waals interactions,[8,9] and pi-stacking.[10,11] Non-covalent interactions are important in a variety of contexts. Although the entirety of this study is focused on gas-phase systems, non-covalent interactions play a significant role in condensed phases. Solvent effects can also be seen as non-covalent. Additionally, non-covalent interactions such as hydrogen bonding have biological significance[13-27] in DNA, RNA, and molecule recognition[28-30]. Concepts relating to structure, stability, and binding sites of certain molecules are commonly found within proteins. The driving force behind the geometry of a large molecule's secondary, tertiary, and quaternary structure, which is crucial to its biological

function,[32] can be attributed, in large part, to non-covalent interaction forces. These

forces can also compete and cooperate with other forces.[31,33,34,154]

Various experimental techniques have been developed to examine non-covalent

interactions. Structural determination, specifically cluster geometry, may be inferred

from microwave spectroscopy.[35-37] Often, the study of molecular clusters requires

techniques capable of discriminating between clusters of different size. For this purpose

a number of mass spectrometric based methodologies, which combine mass spectrometry

with the selectivity inherent to electronic spectroscopy, have been developed. These

include Zero Electron Kinetic Energy (ZEKE),[38,39] Mass Threshold Ionization (MATI),[40]

and Resonant Two-Photon Ionization (R2PI).[41] R2PI techniques will be discussed in

Chapter 2 in detail.

1.2   Impact of π-π Stacking and C-H/π Bonding in Cluster Formation

An important non-covalent interaction that involves the π-electron clouds of two aromatic molecules is referred to as π-π stacking. Here, we observe the non-covalent π-π stacking of two or more substituted benzene rings.[42] Although it is debatable as to which is the more important contributor,[43-45] it is known that both Van der Waals dispersion and electrostatic attraction occur between the aromatic molecules as a result of the presence of multipoles, and more specifically, in the case of benzene, the presence of a quadrupole moment.[10,45] Indeed, the benzene dimer has served as a model system for the study of pi-stacking in the literature, and is a benchmark system for theoretical methods. In the excited state, the pi-stacked system can form an excited dimer, or excimer, which is a topic of focus in this study.[46,47] Although multiple conformers are theoretically possible, to form an excimer, the π-orbitals of the molecular systems must overlap in order to interact with one another most efficiently at a van der Waals distance ≤3.5 Å. This leads to a significant stabilization of the system's excited state.

In the literature, both benzene and toluene[48] have been used as model systems. The two molecules proved to be very beneficial in understanding the non-covalent interactions involved, as well as similar substituted benzenes.[49,50] This has led to experimental and theoretical studies of these interactions and demonstrating the role and importance of both π-π stacking[10] and C-H/π interactions.[51] Benzene demonstrates both of these interactions, with minimum energy geometries corresponding to parallel displaced and t-shaped structure, however, as mentioned before, it has been a great debate in the literature as to which is the global minimum structure.[52,53] Using high level couple

cluster methods, Sherill and co-workers showed that the parallel displaced and t-shaped geometries are separated by an amount as small as 1 kcal/mol.[54]

Bernstein et. al. carried out R2PI studies on the toluene dimers in their excited S_1 state. The spectrum was significantly broadened in respect to the monomer absorption, and hole burning spectroscopy identified two unique features,[55,56] which were assigned to separate conformers. To test this theory, hole-burning was used.[57]

Additional R2PI studies were conducted by Wright et. al. on toluene clusters up to n=8[58], where n is the number of toluene subunits. Spectra of higher order clusters (n > 2) all bore a striking resemblance to the spectrum of the dimer. It was proposed that a "dimer chromophore" exists in every one of these systems which was ultimately responsible for the electronic spectra of higher order clusters. Studies of the ionization potentials of these toluene clusters supplemented these findings.[59] This study revealed a reduction in the ionization potential of the dimer relative to the monomer. This is due to the fact that the cationic charge can be delocalized throughout the π-stacked system of the dimer, which lowers the overall IP. However, there was no significant change in the ionization potential with the comparison of the dimer to larger clusters, which is indicative of a lack of complete π-stacking.
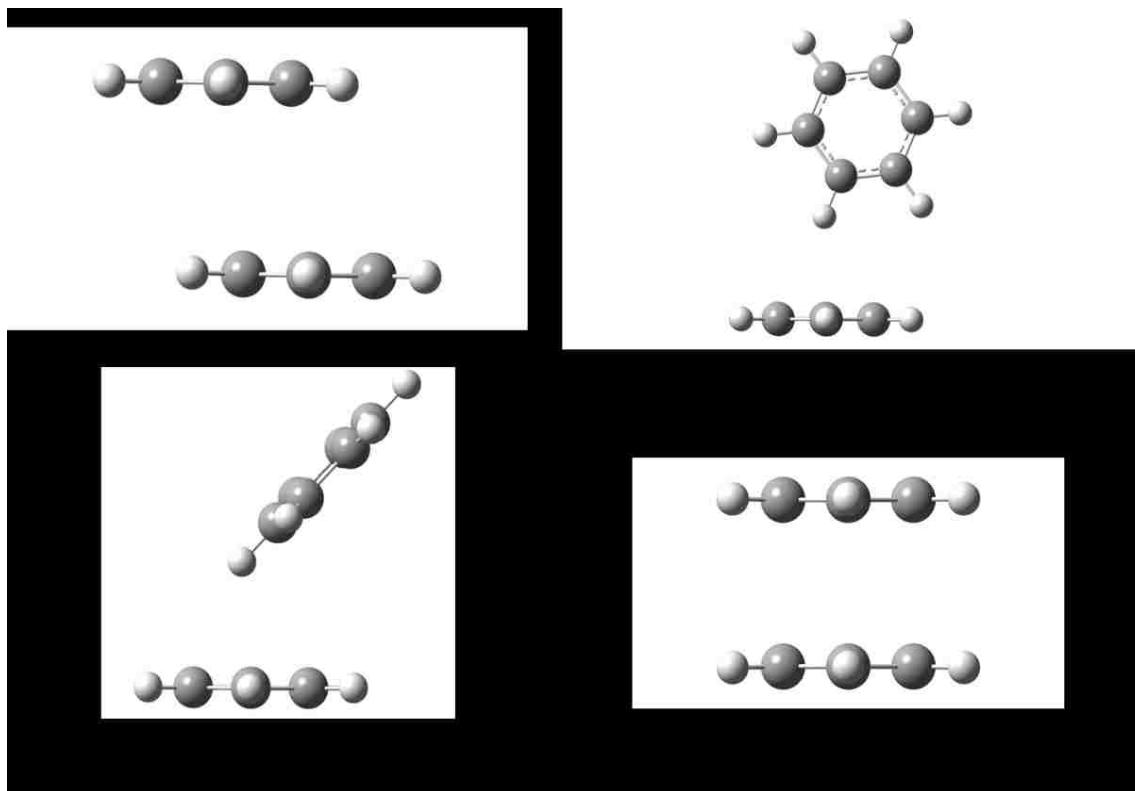
Figure 1.1: Examples of potential benzene dimers. Geometry optimizations were done at the M06-2X/cc-pVDZ level. Calculations show the system's ability to easily adopt either a π-stacked or CH/π bound geometry.

Theoretical[60-62] and experimental[63,64] studies have been done to examine the substituent effects on interactions between aromatic clusters. The aim of these studies was to understand, on a more complete level, non-covalent interactions, and how they function. Halobenzenes proved to be effective prototypical models, where π-π stacking and CH/π bonding compete with other types of non-covalent interactions such as halogen bonding in their clusters. Lu et. al. used a Reflectron Time-of-Flight Mass Spectrometer, to measure the spectra of chlorobenzene and chlorobenzene/benzene aggregates.[65] This study revealed that the S_0-S_1 excitation origin for chlorobenzene dimer contained two distinct features that were shifted relative to the monomer origin. One feature was red-

shifted (i.e., shifted to lower energy) relative to the monomer, while the second was blue-shifted. These two features were attributed to different conformations corresponding to t-shaped and parallel displaced geometries. There was a dependence on the backing pressure with the carrier gas on the relative intensities of the absorptions, which supported the assignments of these features to two different conformations. Other studies of halogen containing benzenes were conducted using one photon R2PI techniques coupled with geometry optimization and TD-DFT calculations.[66-68]

1.3   The Born-Oppenheimer Approximation and Franck-Condon Principle

When considering a description of any molecular system, we start from the Schrödinger Equation, which defines the possible energy states (eigenstates) of the system. The Schrödinger Equation[69] is expressed as follows:

$$\hat{H}\Psi = E\Psi \tag{1.1}$$

where E is the energy of the system, $\hat{H}$ is the Hamiltonian operator, and Ψ represents the system's wavefunction. The Hamiltonian operator describes the system's potential (V) and kinetic (T) energy. Unfortunately, for systems containing for than one electron, there exists no exact solution to the Schrödinger Equation, and therefore approximate methods must be used. In this study, we have used a variety of different computational strategies based upon eq. (1) to examine the electronic and vibrational states, and geometries, of our molecular systems.

One simplifying strategy which helps in solving eq. (1.1) for molecular systems is to consider the relative size of nuclei and electrons. The latter, being much lighter, are necessarily traveling at a much higher speed. Therefore, we can assume that the electrons respond instantaneously (i.e., adiabatically) to any change in the nuclear position. Thus, the nuclear and electronic components of the Schrödinger Equation can approximately be separated. This is called the Born-Oppenheimer approximation.[152] As described by the Born-Oppenheimer Approximation, each electronic state that a molecule is described by its own individual potential energy surface (PES), with unique geometries and vibrational frequencies.

The difference in timescales of nuclear and electronic motion is also crucial in understanding the electronic spectra of molecular systems. One can view the electronic transition as occurring instantaneously on the nuclear timescale, and therefore the most probable electronic transition in the absorption spectrum is a vertical transition which, in turn is described by the Franck-Condon Principle.[70] An electronic transition occurs when an electron moves from one orbital to another and its transition is much faster than any nuclear transition that occurs. Using the Franck-Condon principle, the intensity of the transition can be determined by understanding the system's wavefunctions (their ground state and excited states) and how well they overlap with each other. Therefore, in summary, the overlap of these two states describes the intensity of the excitation of a system, as well as its emission intensity.[70]

1.4   The Exciton Model

An exciton is a delocalized excitation which occurs in systems with multiple

interacting chromophores. The model for exciton coupling has received a majority of its

development through the analysis of crystal structures.[71,72] It can be described as a state

interaction theory. If the electron overlap of intermolecular units is small, the

chromophores of the molecular system can retain their individual traits and remain

separate absorbing chromophores. The physical behaviors of the molecular systems are

not typical, but they can be described using wavefunctions similar to molecular orbital

theory. In order to define the ground state wavefunction of a molecular dimer, the

wavefunctions of both of the absorbing chromophores need to be defined:

$$\Psi_G = \psi_u \psi_v \tag{1.2}$$

Eq. (1.2) represents the ground state wavefunction of the dimer in terms of the

wavefunctions of the two chromophores. The potential between the two molecules can

be described as a Coulombic potential when considering the system's Hamiltonian. In

order to fully apply the exciton model, you must also consider the excited-state of the

chromophores in a similar way to the ground-state consideration. The excited state

wavefunction can be written as:

$$\Psi_E = c_1 \psi_u{}^\dagger \psi_v + c_2 \psi_u \psi_v{}^\dagger \tag{1.3}$$

In eq. (1.3), the dagger labels the particular chromophore wavefunction that is in its

excited state. Using the above equation you can then derive the Schrodinger Equation for

the excited state:

$$H(c_1\psi\dagger_u\psi_v + c_2\psi_u\psi\dagger_v) = E_E(c_1\psi\dagger_u\psi_v + c_2\psi_u\psi\dagger_v)^{73}$$

The evaluation of the consideration of both chromophores reaching their excited state becomes the basis for which the exciton model is formed. Instead of one chromophore absorbing, this is a unique case in which multiple molecules act as effective chromophores that both reach their excited state and whose MO's have an effect on each other.

There are simple cases of exciton splitting that can describe the consequences of light absorbing molecules in systems such as dimers, trimers, and other weakly interacting systems. Often, the formation of an exciton is explained with the framework of a dipole-dipole model, representing the transition dipoles of the monomer electronic states. The orientation of the dipoles determines both the splitting of the excitonic states, and the relative intensities of the two components.[74-76]
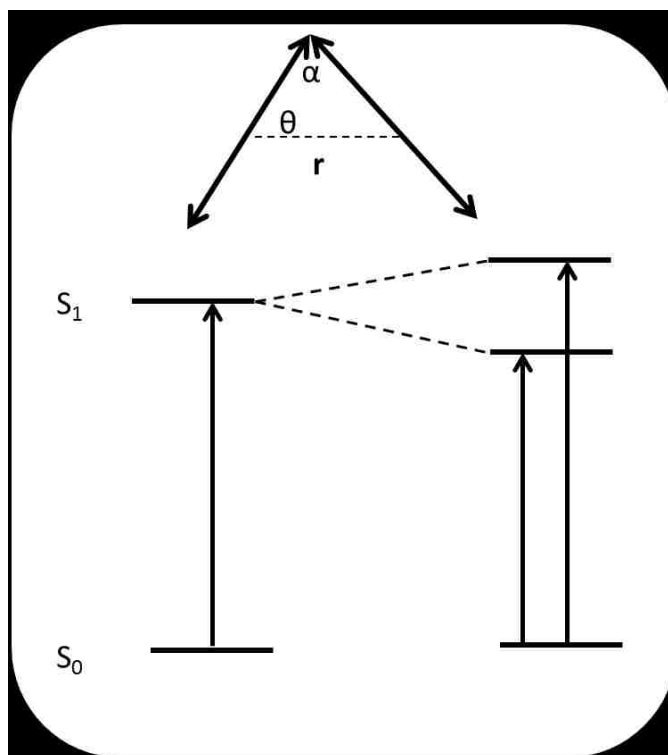
Figure 1.2: A qualitative representation of exciton splitting. A non-zero displacement leads to noticeable level splitting.

Within the dipole-dipole model, important parameters which determine the splitting of the excitonic state include the magnitude of the transition dipole moment, the distance between line of centers of the dipoles, and the relative orientation:[73]

$$\Delta E = \frac{2|\mu|^2}{r^3 ab}(\cos \alpha + 3cos^2\theta) \tag{1.4}$$

The equation shown above describes all models of exciton coupling, but it is best demonstrated by Figure 1.2. It can be seen that there are four different variables that describe the geometry orientation of the molecule and, therefore, the amount of splitting that will be observed experimentally. The first term contains the magnitude of the transition dipole of the monomer in the numerator, and the internuclear distance between

monomer *a* and monomer *b*. The angles in the second term, α and θ, both represents the angles formed by the orientations of the transition dipoles shown in Figure 1.2, where α is the angle between the dipoles, and θ is the angle between the center point of one of one dipole and the direction of the other. No splitting is observed experimentally when the dipoles are either perfectly parallel or in-line with each other as they can either be additive or subtractive, essentially doubling one signal and cancelling the other. The relative intensities of the two excitonic transitions are determined by the relative orientation of the dipoles.

Chapter 2

Experimental Setup and Details

2.1   Overview of Experimental Methodologies

Non-covalent interactions play an important role in a variety of processes, as previously discussed. More specifically, π-interactions have a significant impact on the assembly of polymeric materials used in variety of organic electronic devices.[158] Excimeric interactions, and by association excitonic interactions, are responsible for the efficiency of the formation of these polymeric materials.[159] Even though π-interactions are well known for their ability to stabilize energy and delocalize charge, the geometric requirements and reorganizations involved are not well understood. Therefore, these requirements can be investigated using model systems capable of demonstrating excimer formation and charge delocalization. This chapter is dedicated to describing the experimental and computational methods implemented to better understand these interactions and corresponding geometries therein.

Data acquisition in this study implements two different modes of detection. The first utilizes mass spectrometry.[77] Mass spectrometry is a detection technique that is very sensitive to differences in atomic weight and therefore is a valuable tool in separating and identifying molecules of different masses. A mass spectrometer may be broken down into three components: the ionization source, the mass analyzer, and the ion detector.[78] Molecules can be ionized several different ways for experimental purposes. It is

important to understand the motivation and characteristics so that you may pick an appropriate method. The stability of the molecules, volatility, and its phase or stable state must be considered. Some ionization methods include, but are not limited to, Matrix Assisted Laser Desorption Ionization (MALDI),[79] Electrospray Ionization (ESI),[80] Electron-Impact Ionization (EI)[81], and Photoionization (PI)[82], etc. In this work, we use a linear time-of-flight mass spectrometer (TOF-MS),[83] in which lasers are used to resonantly ionize a molecule (i.e., by excitation through an intermediate electronic state), which imparts selectivity to the mass spectrometry. The ions thus formed are accelerated to ground using a set of grids to which high voltage is applied, and the accelerated ions fly in a field free region (a flight tube of 118 cm) up to a microchannel plate detector, where they are detected.

When this study was initiated, we began by using a 1-Color Resonant 2-Photon Ionization (R2PI) scheme,[41] which is effective when the energy of the intermediate state lies more than halfway to the ionization threshold. In this scheme, illustrated in Figure 2.1, sequential 2-photon excitation leads to ionization. This method suffers from the disadvantage that the beam intensity must be increased to allow two-photon absorption, and the laser is usually tightly focused into the source. When the electronic transition is strong compared with the transition into the ionization continuum, this can easily lead to saturation and broadening of the electronic spectrum.[87]
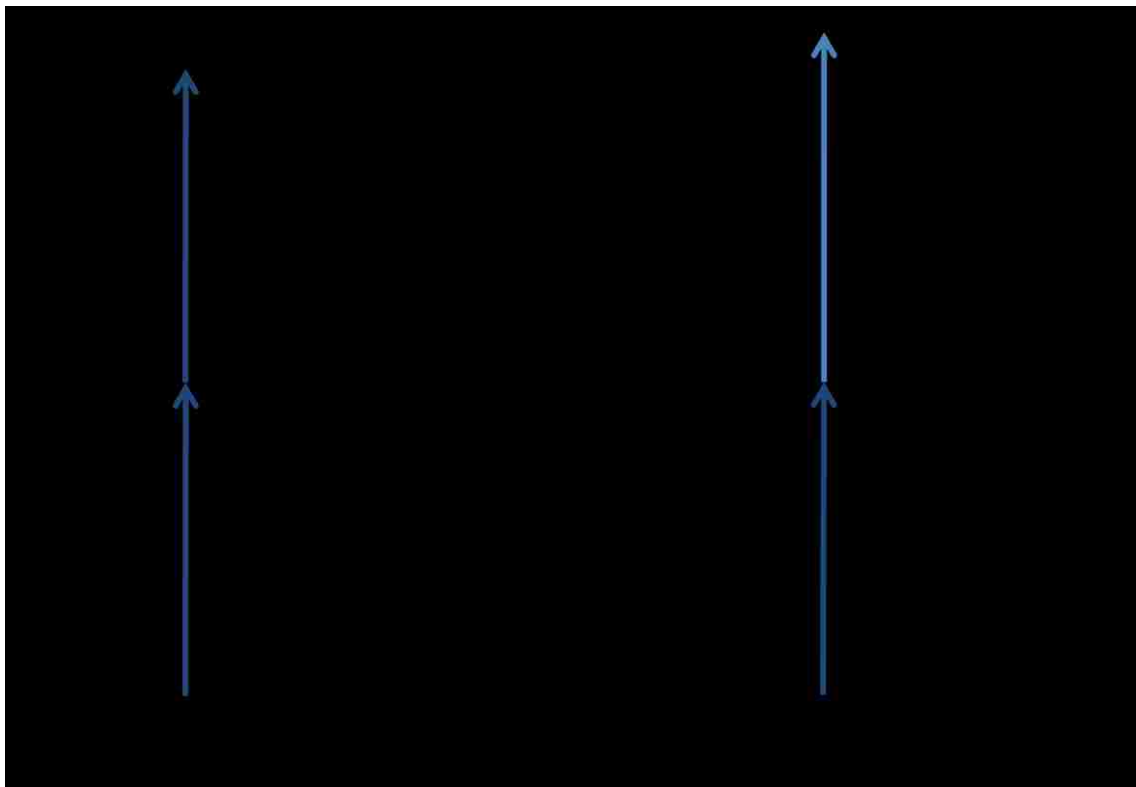
Figure 2.1: A diagram representing the basic concepts and differences between a Resonant 2-Photon Ionization scheme (left) and a 2-Color Resonant 2-Photon Ionization (right). The R2PI scheme on the left provides two photons from the same source, while the 2CR2PI scheme on the right provides two different photons from two different sources.

An alternative approach is the use of 2-Color R2PI (2CR2PI), where a second tunable laser beam, delayed or overlapping the first laser in time, is used to achieve ionization (Figure 2.1). The two laser pulses can be varied in intensity to minimize saturation of the first step while maintaining efficient ionization. In addition, the tenability of the second photon allows the ionization potential to be determined, in experiments where the excitation laser frequency is fixed and the frequency of the ionizing laser scanned. These ion-yield curves show the onset of ionization.

In cases where multiple conformers may be present, the hole-burning method is very useful. Figure 2.2 represents a general timing scheme of this method. In this approach, the 2CR2PI technique is preceded by a 'burn' laser. The burn laser is fixed to a specific wavelength and promotes the associated conformer(s) to the excited state. The 2CR2PI lasers then fire after the burn laser ($\geq$100 ns) and a spectrum is collected. Any features (conformers) associated with the wavelength of the burn laser will be 'burned out' and will not appear in the resulting excitation spectrum, but rather, will appear as a depletion spectrum. This process will be discussed in detail in the next section.
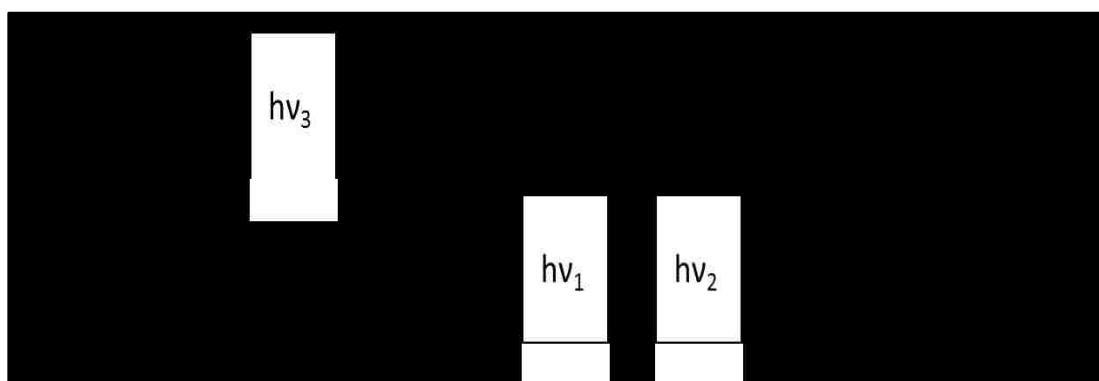
Figure 2.2: A general representation of the timing scheme used to conduct hole-burning experiments for gas-phase experiments.

The mass-based methods are very useful; however, perhaps the most sensitive approach to electronic spectroscopy is through measurement of the fluorescence which occurs following excitation. Fluorene is a molecule that has a fairly long excited state lifetime and therefore can fluoresce very well, which is where it gets its name. Fluorescence techniques were added to provide additional information about the excited and ground states of the systems examined in this work. The specifics of each technique will be discussed in later sections.

2.2   2-Color Resonant 2-Photon Ionization Techniques and Setup

2-Color Resonant 2-Photon Ionization is a useful tool for the analysis of gas phase molecules. Its sensitivity makes it ideal for the detection of such molecules. For this study, a time-of-flight mass analyzer was used and is perfect for particular mass unit weight selection with very high efficiency. With the multi-photon techniques, different combinations of photon application exist. For the sake of this study, we can example two general experimental schemes. Previously mentioned, one setup contains one laser in which you use photons of the same wavelength to first excite the molecule and then reaching the ionization level with a photon of the same wavelength/energy. Since this process is the use of one photon, followed by one more photon of the same wavelength, we can refer to this set up as a resonant two photon ionization (R2PI).[41] Alternatively, you can have two different photon/ionization sources and therefore the photon used to promote the chromophore to its excited state is not the same photon used to ionize it. You can use a photon from one laser to reach the excited state of the molecule, then, you can follow that with a photon of a different wavelength from the other laser that reaches the ionization potential. This setup is often referred to as two-color resonant two-photon ionization (2CR2PI). One could easily imagine more R2PI setups involving more than two photons, as well as more than two photons sources. By using a multi-step ionization process, populating resonant excited states with one photon followed by ionization from another, R2PI and 2CR2PI are used to indirectly monitor the excited state of a molecular system. Thus, an excitation spectrum can be collected. Ionization can occur in different ways through interaction with other molecules, photons, or electrons. A general picture

of what occurs within the scope of this experiment is constant, where the molecule

(labeled M here) ejects one of its electrons to gain a positive, cationic charge:

M + interacting body $\rightarrow M^{+\cdot} + e^-$
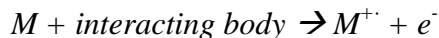
This is how the molecular systems are detected in the 2CR2PI portion of the experiments.

Unlike the Laser-Induced Fluorescence techniques (to be described later), the 2CR2PI

experiment is a time-of-flight technique that cannot detect neutral molecules.

When discussing ionization energy, one can break the discussion down into two

types: vertical and adiabatic ionization.[84] An adiabatic ionization can be described as an

ionization that occurs by the transition from the ground state of the neutral molecule to

the ground state of the ion. Alternatively, a vertical ionization is simply a vertical

transition to the ionic state of the molecule.[84] An adiabatic ionization occurs with the

minimum energy necessary and therefore the adiabatic IP can never be greater than the

vertical IP, only less than or equal to it. A qualitative representation of the energy

necessary to ionize a molecule in both cases is pictured in Figure 2.3. Note that the

vertical and adiabatic ionization energies will be similar if the geometries of the excited

(S_1) and cationic (D_0) states are similar.
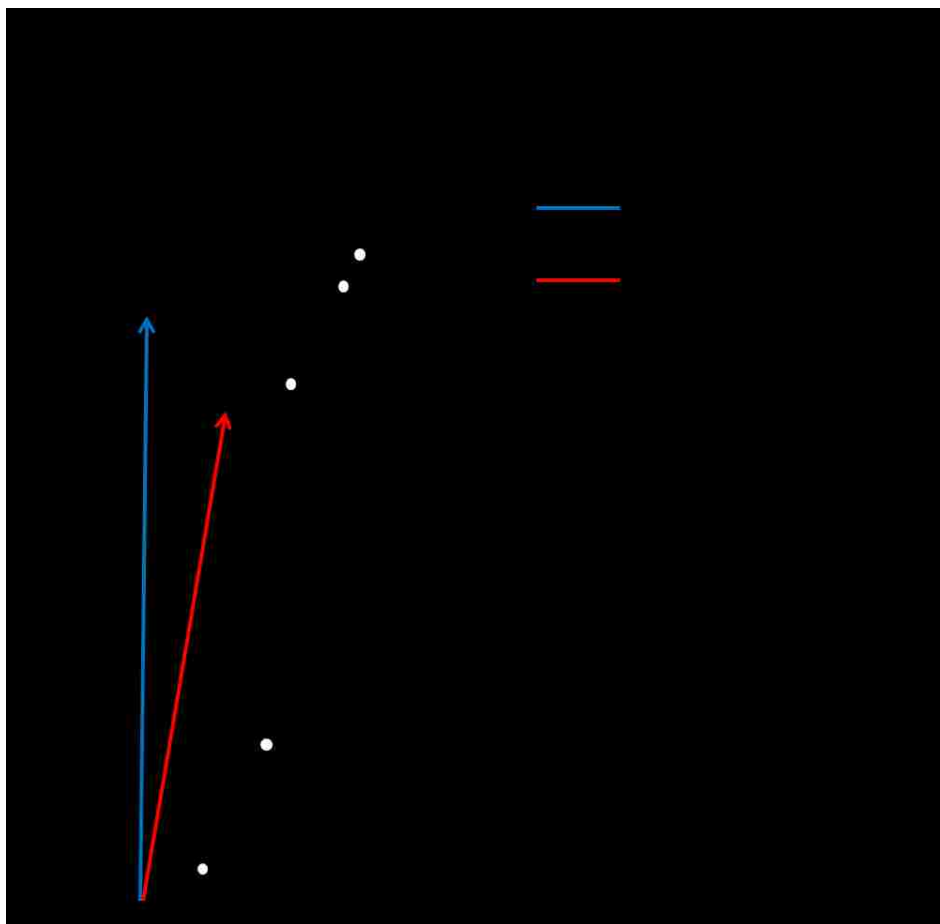
Figure 2.3: The qualitative representation of a molecule transitioning from its neutral state to its ionic state. Pictured in blue is the energy necessary to vertically ionize the molecule while pictured in red is the adiabatic ionization.

In the IP experiments that are conducted in this particular study, a vertical ionization is used to form and collect data towards the resulting cation. The IP experimental technique takes advantage of the same 2-Color technique used for the 2CR2PI experiments. However, here the laser which is scanned is now the ionizing laser. By scanning the ionizing laser we can locate the ionization threshold of the current molecule. The representation of this experimental IP scheme can be found in Figure 2.4.
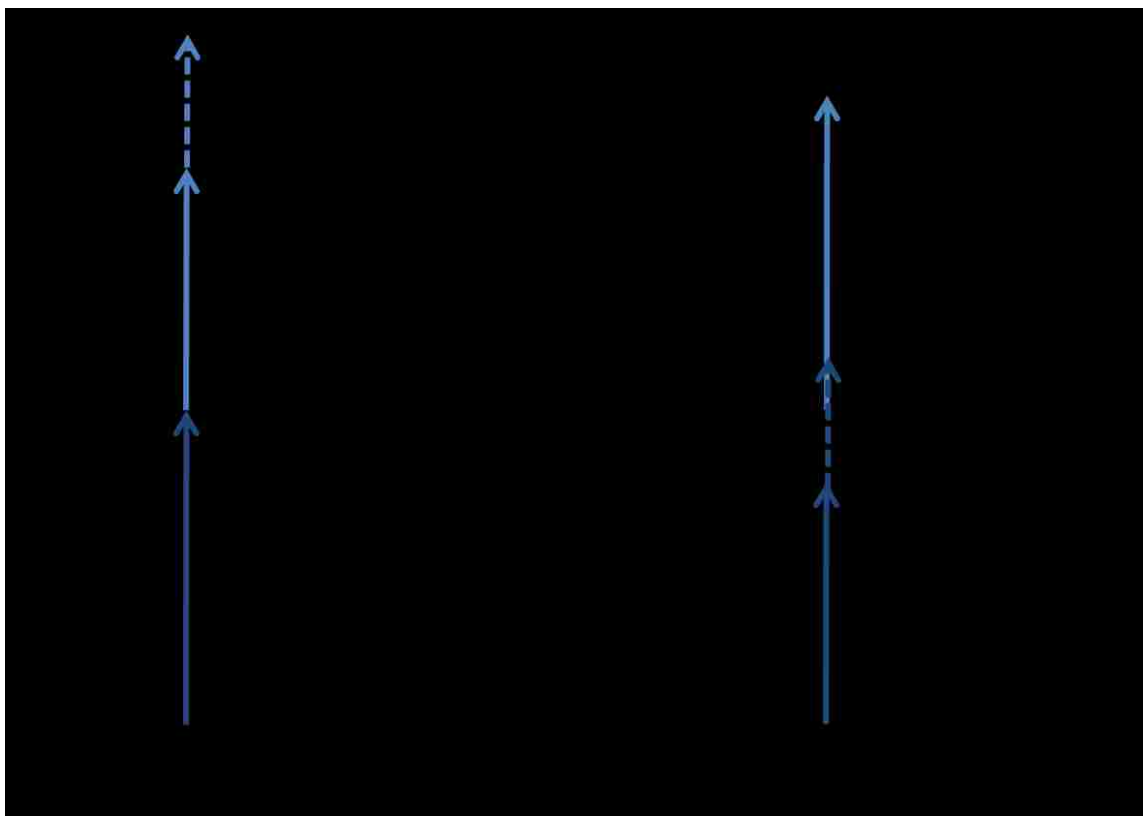
Figure 2.4:   Shown on the left is the experimental scheme utilized when probing the ionization threshold of the sample, thus providing the corresponding IP. Shown on the right for comparison is the 2CR2PI scheme where the excitation laser is being scanned in order to probe the excited state of the sample.

The assumption that the geometry of the resulting ion will be the same or similar to the geometry of neutral molecule from which it was formed is made in this study.[84] This assumption stems from the Franck-Condon Principle in which the overlap of the potential energy surfaces dictate the behavior of the excited and/or ionized sample.[70]

Previously stated, our experiment utilized Time-of-Flight Mass Spectrometer with Multi-Channel Plate detectors (TOF-MS-MCP). This machine utilizes a supersonic

molecular beam[85,86] based upon a General Valve gas nozzle. The pulsed nozzle is capable of cooling the molecules down to <10 K when creating the expansion. This is done to ensure the sample in the experiment is in its lowest energy ground state when entering the experimental chamber. Using He or Ar as a carrier gas, a solid fluorene sample is placed in a sample holder filled with glass wool, and heated to anywhere between 30 and 200 degrees Celsius, about 1-2 bar or 760 torr (~1 atm), ejected from the pulsed nozzle which is about 1.0 mm in diameter. The molecular beam from the nozzle then enters through a 1.0 mm aperture of a skimmer which then allows the narrowed beam to enter the linear flight tube, about 1 meter in length, which is evacuated by various pumps along the apparatus. The specifics of the setup is similar to previous studies.[67,68] The main chamber of the setup is evacuated by a water cooled diffusion pump that allows the area to reach pressures of about 5×10^{-5} mbar in the main chamber and about 1×10^{-6} mbar in the flight tube with the nozzle on. The detector chamber is evacuated by a 250 L/s turbo pump that contains a gate value that can be closed to isolate the detector. Due to the sensitivity of the MCP detectors to moisture, the detector chamber is kept under vacuum at all times. The pressure inside the flight tube could be lowered further by adding liquid nitrogen into a jacket which circumvented the exterior of the flight tube. A schematic representation of the R2PI system that was utilized for this experiment can be found in Figure 2.5.
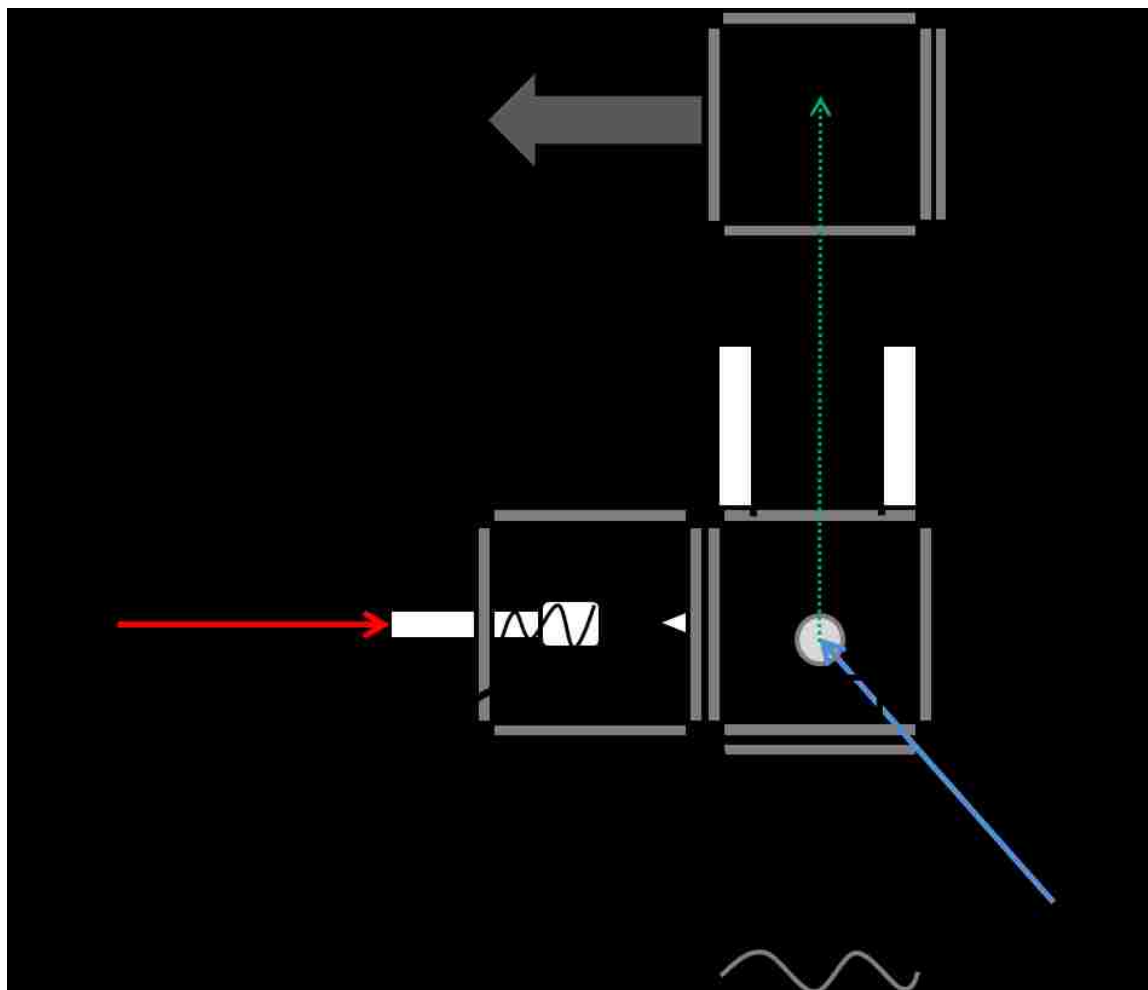
Figure 2.5: A general representation with selected labeled parts of the 2CR2PI instrument used in the studies of the covalent and non-covalent composite fluorene systems.
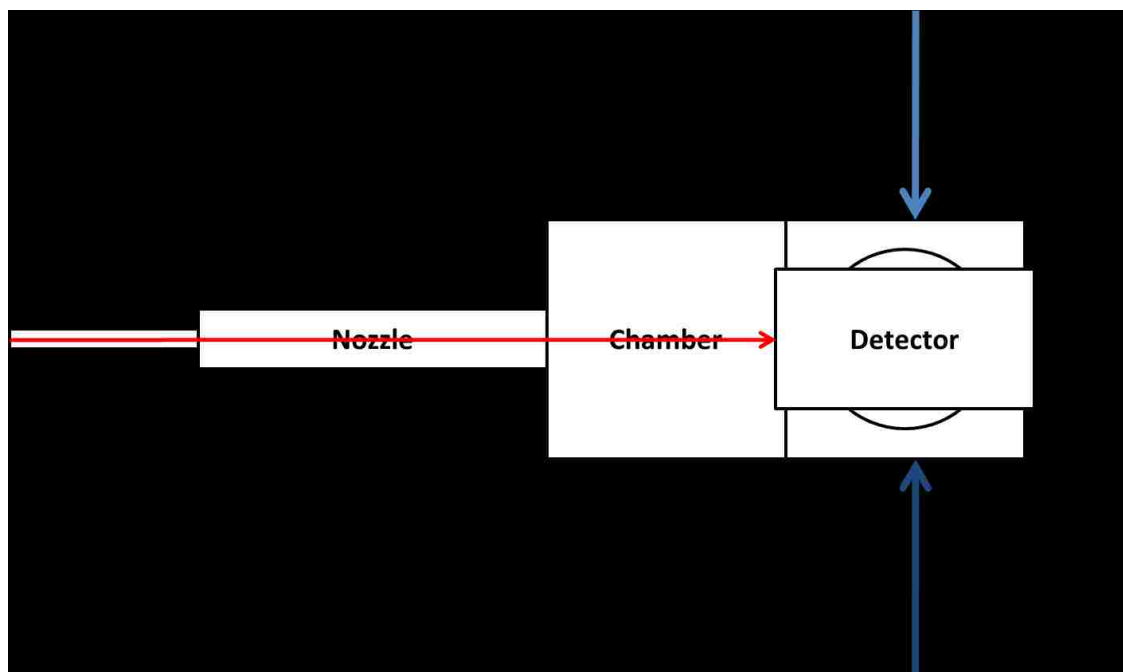
Figure 2.6: A top-down view of the 2CR2PI experimental setup, giving a view of the orientation of the molecular beam and the two independent laser sources entering the ionization chamber.

As discussed above, ionization was achieved with a Resonant Two Photon Ionization scheme. The ionization process was done using frequency doubled laser light, generated from a tunable dye laser pumped by the second-harmonic of an Nd:YAG laser. The doubling process was achieved using a BBO (β-barium borate) crystal, typically yielding pulse energies of about 1.0 to 2.0 mJ. This beam was also focused with a 1.0 m plano-convex lens into the chamber. In 2CR2PI experiments, a second tunable Nd:YAG laser entered the chamber through a window opposite to the excitation laser and acted as the ionization source. In this scenario, the focusing lens of the excitation laser was removed to reduce the possibility of saturation and decrease the one-color R2PI signal contribution, and the ionizing laser was instead focused with a 0.5 m lens. In this setup there needs to be an appropriately timed delay between the two lasers, and that was done by a BNC 565 digital delay generator. As described above, the additional benefits of a two color arrangement are a reduction in power broadening[87], through attenuation of the excitation laser, and the ability to measure ion yield curves and thus the Ionization Potentials. Additionally, by scanning the time delay between the two lasers, an estimate of the lifetime of the excited state can be obtained. In practice, the values thus measured were consistent with those obtained from the more sensitive fluorescence based methods.

Once formed, the ions were accelerated using a conventional three electrode stack. The components of this stack included a repeller plate typically held at a voltage of +2100 V, an extraction plate typically held at +1950 V, and a third plate held constant at ground potential. The accelerated ions then traveled down a 118 cm flight tube, eventually reaching a MCP detector. Since all ions of the same charge acquire the same electrostatic energy, which becomes translational energy in the accelerated ions, ions of

different mass but the same charge will arrive at the detector at different times. This is

the basis of the time-of-flight method. The signal created from the MCP was then

amplified (x25) by a Stanford Research Preamplifier and integrated by a Stanford

Research boxcar system. The data acquisition, as well as the stepping of the laser's

wavelength, was done with a LABVIEW program that typically averaged a ten laser shot

signal in a stepwise fashion.

In the supersonic method described above, weakly bound clusters can easily be

formed as the molecules cool to temperatures < 10 K in the expansion. In such a rapid

cooling, often an equilibrium population of conformers is not achieved, and more than

one conformer may be present.[94] To investigate this consequence an experimental

method known as Hole-Burning (HB) has been developed.[95] The process involves the

same setup as described before with 2CR2PI, with the addition of a third 'burn' laser. It

is necessary for this laser to be aligned perpendicular to or in line with the laser and

molecular beams.

The process works by introducing a photon of a specific wavelength before the

original two-color laser setup fires into the chamber. The two-color scheme is delayed

typically by more than 100 ns and then is fired into the chamber to ionize the sample.

Additionally, active subtraction can be utilized by changing the scanning laser from 10

Hz to 5Hz. This operates on a shot-by-shot basis and subtracts the shot where the

ionizing lasers fire from the shot where all lasers fire. Other than that, the two-color

ionization does not need to be any different. The scheme can be found in Figure 2.2.

The wavelength selected needs to be a specific spectral feature found from a previous

experiment. For this reason, hole-burning is always done as a follow-up to conducting

ionization experiments. If there is reason to believe that multiple conformers exist in the system, usually in systems containing higher order clusters, one can select a feature that is preferably well-resolved to burn out the spectrum. If a spectrum only corresponds to one contributing conformer, then the result of a hole-burning experiment will yield a mirrored spectrum about the y-axis (a repeated spectrum but with all negative values). If a spectrum has multiple contributing conformers, then hole-burning will not deplete the entire spectrum, rather, only the features that correspond to the conformer being burned as a result of the burn laser's wavelength. It should also be noted that hole-burning was not conducted on every sample that was examined. Hole-burning was done on systems in which features in the spectrum were at least moderately resolved. Therefore, it would be clear whether or not particular features belonged to single or multiple conformers.

This is a very helpful supplement to the big picture of the experiment. Knowing whether the spectrum is a result of a single conformer or multiple ones helps in analyzing the data in its entirety.

2.4.1   *Effect of Carrier Gas on Experimental Spectrum*

The experiment makes use of a supersonic expansion, where the molecule of interest is "seeded" in the carrier gas at a low concentration, typically 1% or less. The role of a carrier gas is to aid in the cooling of gas phase sample particles via collisions in the expanding plume.   Temperatures < 10 K are routinely achieved using inert gases as carriers. Typically, argon or helium were used as carrier gases in these experiments. There are pros and cons to using each as carrier gas in supersonic nozzle experiments. Helium suffers from a phenomena often referred to as velocity slipping.[88,89] Due to the difference in mass between helium and the sample, the Helium carrier "slips" past the heavier impurity, leading to a lowering of the collisional cooling, and creating hot bands (Figure 2.7). Hot bands arise from the excitation of molecules lying in thermally excited vibrational states. In contrast, being heaver, Argon does not suffer from velocity slipping. However, being more polarized, Argon has been shown to readily form van der Waals clusters with various aromatic molecules.[90,91]
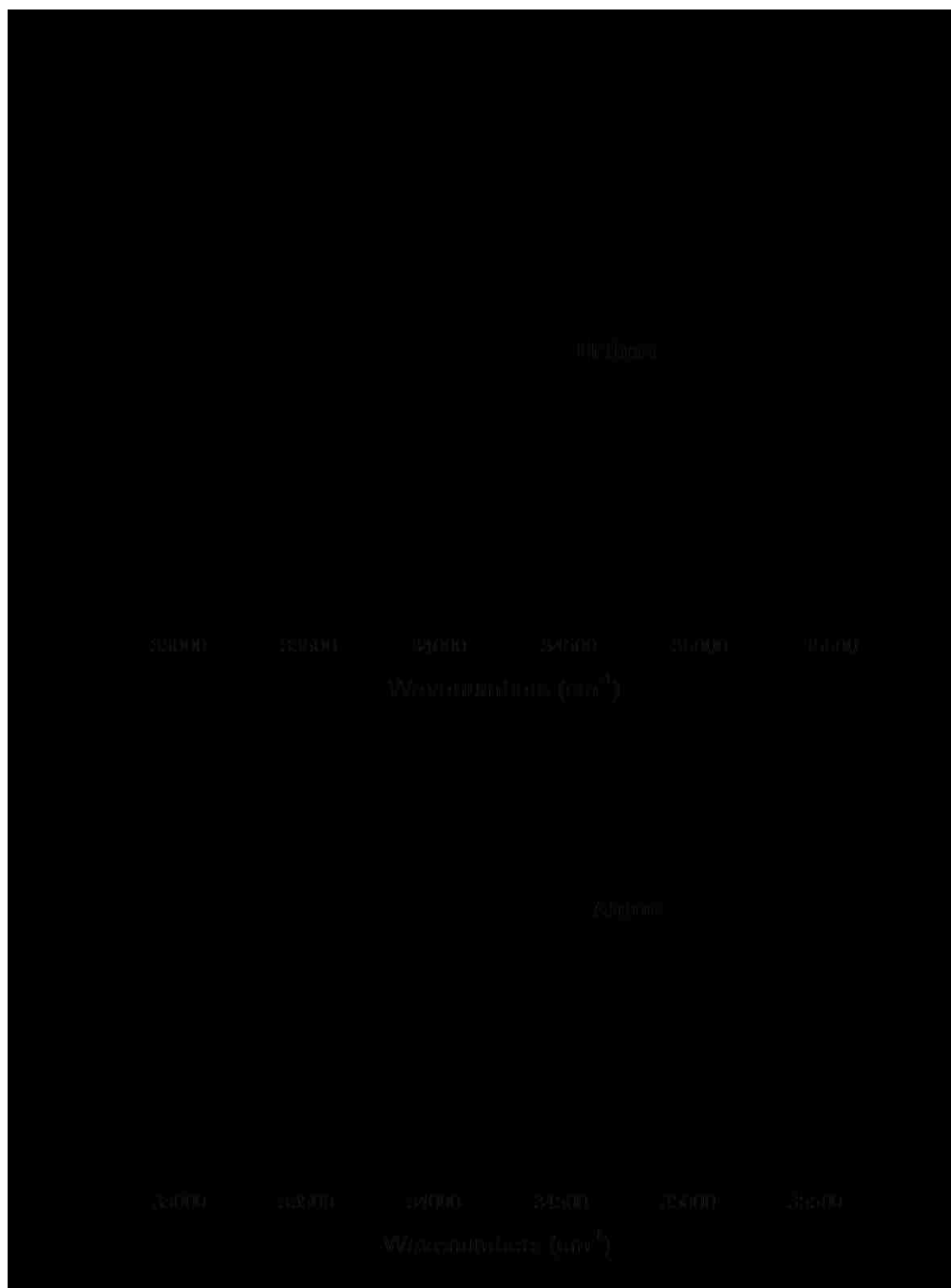
Figure 2.7: A comparison of excitation spectra utilizing different carrier gases. In helium, hot bands can arise as a result of 'velocity slipping.' Hot bands are characteristic of molecules that undergo a transition from an excited vibrational state. This gives rise to the additional low intensity features seen in the Helium spectrum. The hot bands are not observed in the Argon spectrum.

2.3   Laser Induced Fluorescence Techniques and Instrumental Setup

As mentioned previously, one of the defining characteristics of fluorene is its ability to fluoresce due to its relatively long lived excited state. In order to gain additional insight towards the ground and excited states of these fluorene systems, Laser-Induced Fluorescence (LIF) techniques were implemented.[92,93] The biggest downfall of LIF is the inability to mass-select as we are able to do with 2CR2PI. When measuring total fluorescence, anything that can fluoresce will fluoresce and therefore potentially contribute to the spectrum. However, species with very different fluorescence lifetimes can be distinguished by time-gating the detection.   On the plus side, LIF is a very sensitive technique and requires only a single laser, eliminating the need for alignment and timing of multiple lasers. Excitation spectra gathered via LIF, however, can still suffer from similar power broadening[87] effects that arise in the R2PI method as a result of saturating the excited state.

From LIF experiments, one can collect data that, upon analysis, reveals details about the molecule's excited state, ground state, and excited state lifetime. When examining the excited state versus the ground state, a slightly different experimental setup is required. For the excited state, one can scan the laser over a selected range, and by using a mirror, direct the resulting fluorescence towards a Photo-Multiplier Tube (PMT), which serves as the detector. The resulting spectrum is expected to be similar to the excitation spectrum gathered from the 2CR2PI experiments. For probing the ground state, the directing mirror is removed and the resulting fluorescence is sent into a monochromator or spectrograph. This dispersed fluorescence (DF) is measured by

scanning the monochromator with the excitation laser now remaining fixed. The DF

spectrum maps out the energy levels of the ground state as a result. A representation of

the scheme of each process can be found in Figure 2.8.

The laser source used for fluorescence experiments is the same Nd:YAG

INDI/Sirah dye laser as described before with the 2CR2PI experimental setup.

Additionally, the molecular beam source is also the same as used in the ionization

experiments. Thus, discrepancies between the experiments should not arise from a

difference in experimental conditions related to the laser or source. A schematic

representation of the LIF experimental setup can be found in Figures 2.9 and 2.10.
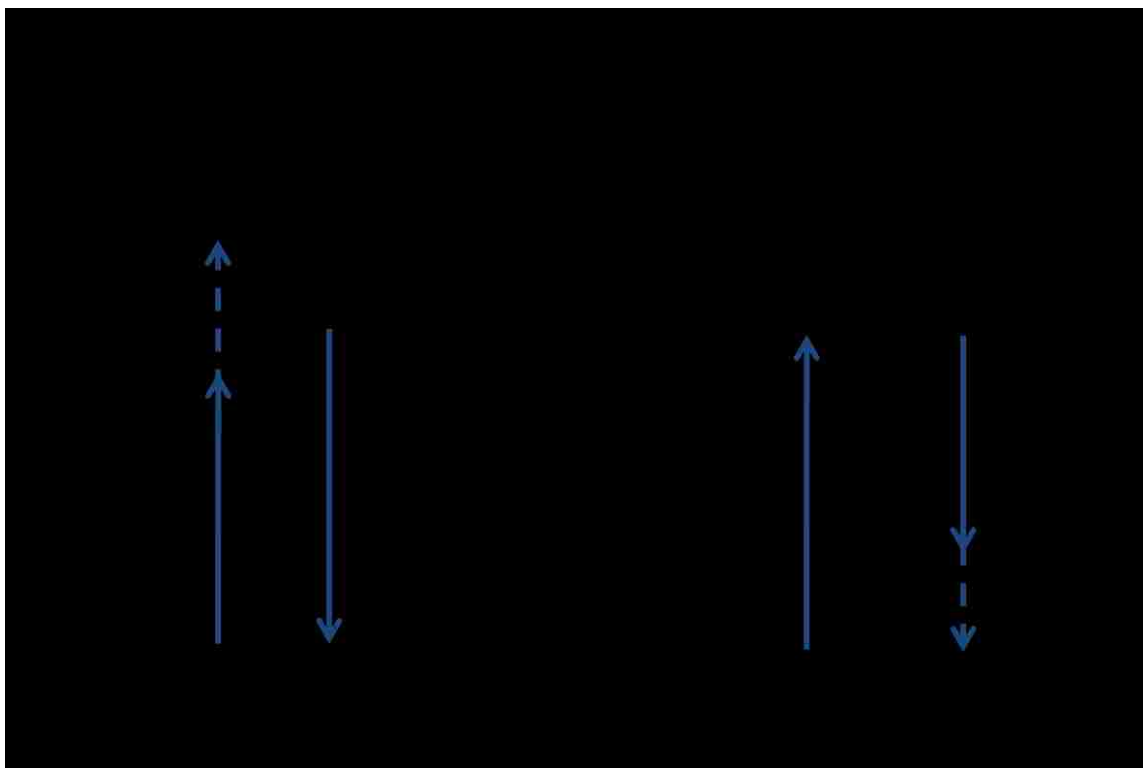
Figure 2.8: A general representation of the difference between total LIF and Dispersed Fluorescence experiments.
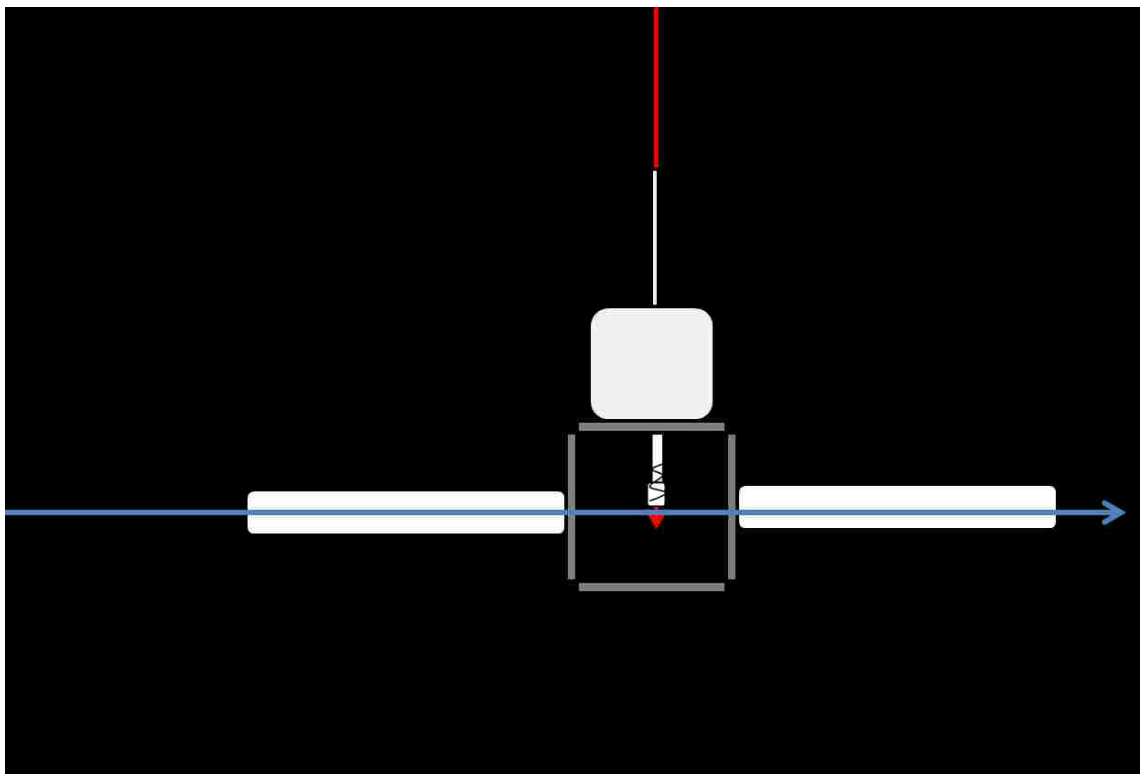
Figure 2.9: A schematic representation of the LIF experimental setup. The molecular beam is introduced vertically into the chamber (kept under vacuum by a diffusion pump) perpendicular to the laser beam.
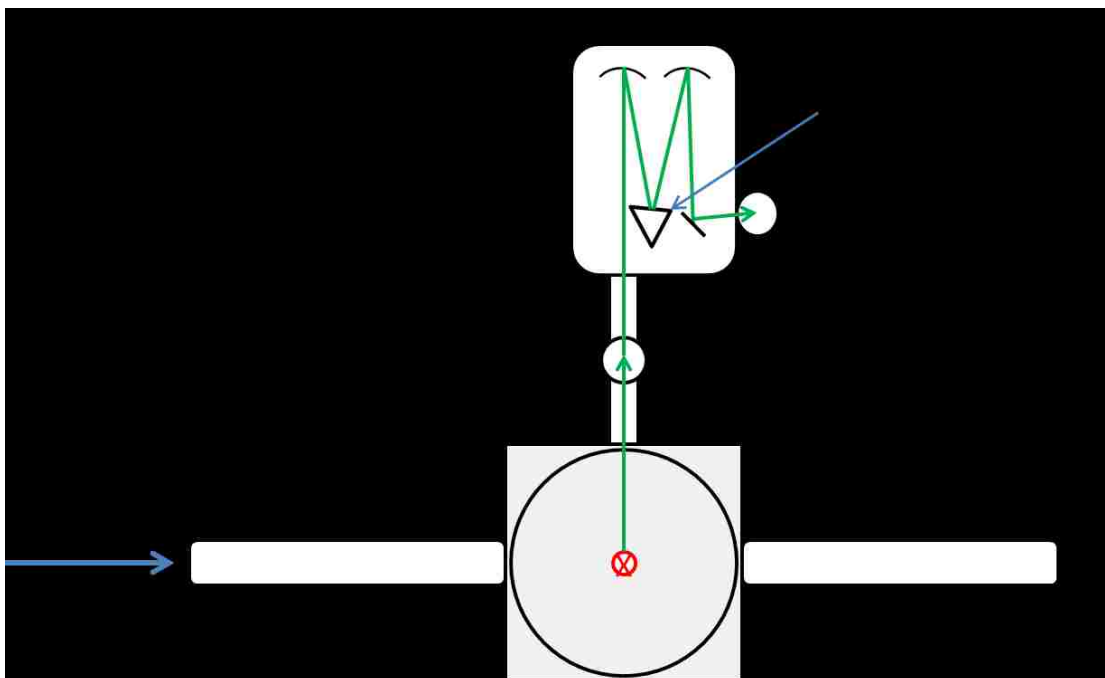
Figure 2.10: A top-down of the LIF experimental setup showing the two different collection methods. For total fluorescence, the fluorescence is directed into the PMT positioned immediately after the chamber. For dispersed fluorescence, the fluorescence is allowed to pass the initial PMT into the monochromator and eventually into the PMT attached to it.

2.4   Computational Methods

Computational chemistry is an invaluable tool which we used to complement our experimental studies. Computational chemistry can easily provide structures of global and local minima on the Potential Energy Surface (PES), provide estimates of energy barriers, the relative stability of different conformers, and predict electronic and vibrational spectra, and ionization potentials. These can be achieved through commercial software packages such as Spartan, or Gaussian. This study makes use of the Gaussian software package.[153] It has become common practice to use computational chemistry to support any findings in research but is capable of supporting discoveries that one would normally not be able to achieve through experiment alone.[96]

While not appropriate for systems such as van der Waals clusters where a quantum mechanical treatment is essential, molecular mechanics was used in this work for covalently linked systems as a way to quickly catalogue the variety of conformers which might be present. Molecular mechanics relies on a classical treatment of the molecules and works by summing the energy from covalent and non-covalent forces. The open-source Avogadro software package[99] was implemented for this treatment which uses force field approximations when performing a conformer search of the system.[100,101] Molecular mechanics were used as a starting point to locate multiple conformers in the ground state, ultimately having those geometries optimized further using more rigorous methods.

Coupled cluster approach is one of several approaches commonly used to treat the problem of electron correlation. It does so by including excitations which correspond to

different arrangements of electrons amongst the molecular orbitals. The CCSD(T) method, which incorporates up to triple excitations, is often referred to as the "gold standard" of calculations.[98] In practice, CC methods utilize an operator that generates all possible excitations through a certain order from the HF wavefunction. To use the model that includes singles and doubles excitation operators (CCSD), the scaling factor with basis set size becomes N^6. If one wants to also include the triples (CCSDT) the scaling factor becomes N^8, making the computational cost expensive for anything but small molecules.[102] Therefore, a different method where the triples are included non-iteratively (CCSD(T)) is more commonly used by researchers. However, this still becomes too computationally expensive for the systems of this study and therefore only CCSD methods were implemented.

The Density Functional Theory (DFT) method is unique due to its evaluation of the system's electron density. DFT methods provide some treatment of electron correlation, but are empirical in the sense that it is impossible to know a priori the correct form of the functional. Thus, while being more accurate than Hartree-Fock methods, DFT methods are less expensive than coupled-cluster and other higher order *ab initio* tratements.[96,98] When deciding which DFT methods to utilize for selected calculations, one will be able to choice between regular, or pure, DFT methods, or hybridized methods. Relevant to this particular study, recent studies have shown that M06 hybrid meta-GGA functionals provide accurate results at low computational cost for non-covalent interactions with no need for counterpoise correction.[103,104]

In investigating many-body molecular systems, one is able to evaluate the dynamics in the presence of time-dependent fields, electric or magnetic alike. The ability

to do this computationally starts with a method referred to as the Time Dependent Density Functional Theory (TD-DFT). In this study, the excitation of molecules is of particular interest and the TD-DFT method is appropriate in predicting the schemes in which these samples undergo excitation transitions. It expands on the ground state energy analysis of DFT methods and extends it to the time-dependent excited states. Normally, one can consider the original time-dependent quantum theories described by the wavefunction and the time-dependent Schrödinger equation (viewed as multi-body systems), but with the TD-DFT method, the system can be treated as a one body system quantified as the electron density.[97] Using TD-DFT methods, one can analyze the impact that time-dependent electric and/or magnetic fields have on dynamical characteristics that include photon-absorption, particular excitation energies, and frequency dependent aspects of the molecular system.

In computational chemistry, the mathematical representations of orbitals are achieved by using basis functions centered on the atomic positions.[97] There exist many different types of basis sets used to solve the Schrödinger Equation to uncover a system's total energy. The least amount of basis functions that can be applied to a given system (i.e., where the number of molecular orbitals generated is just sufficient for the number of electrons) is referred to as the minimal basis set.[97] For example, we have the elements contained within the 1s orbital row, hydrogen and helium; only one basis set for the s-type orbital is required to account for all the electrons in the system.

Perhaps the most well-known and maybe most commonly used basis sets are the Pople and Dunning basis sets. The Pople basis sets include 3-21G, 6-31G, etc., and can be referred to as split valence basis sets. However, more recently, Dunning et. al.[105]

developed basis set that are commonly referred to as 'correlation consistent, polarization valence split' basis sets.[98] Abbreviated, the basis set is often written as cc-pVnZ, with n being an integer representing the zeta level chosen for the calculation (can be double, triple, or quadruple, labeled D, T, and Q respectively).

Chapter 3

**Geometrical Requirements for Excimer Formation and Hole Stabilization:
Covalently and Non-Covalently Linked Fluorene Dimers ((F)$_2$ vs. F2)**

3.1   Introduction to Excitonic Coupling in the Fluorene Dimer

The study of molecular dimers and excimer formation is a rich and complex area of molecular spectroscopy. Excimers exhibit a unique spectral behavior due to an interaction of weakly coupled chromophores. Excimeric behavior was originally discovered back in 1954.[106] Studies originally were aimed at various covalently linked biphenyls. Over time, experimental techniques and technology has significantly improved and has made it possible to look at much more complex systems[107,108] like carbazole,[109] and diphenylmethane.[110] The addition of new experimental and theoretical techniques has resulted in the realization that the electronic communication between multi-chromophoric systems is complicated, and a simple dipole-dipole treatment may not be sufficient in many cases.[111] The treatment of the interaction between molecules in crystals with dipole models did not provide satisfactory explanations. Vibrational motions of the molecules play a large part in the communication between the molecules and therefore require a vibronic treatment of the data.

A drawback to gas phase beam experiments, as implemented here, is that there is often uncertainty regarding the structure of the probed systems, particularly in weakly bound van der Waals where many conformers may be nearly isoenergetic, and the non-

equilibrium distribution often produced in jet-cooled samples makes it difficult to determine a priori the conformational distribution. Conformations corresponding to the global energy minimum may not be preferentially formed. Moreover, molecules in the gas phase are not limited by crystal packing or solvent effects like molecules in the solid or liquid phase, respectively.

Supersonic molecular beam technology, the method used in this study, has provided better insight into excitonic interactions and systems with very weak excitonic coupling have been studied. Naphthalene[112-117] dimer and trimer have been extensively studied and has provided a good starting point for the possibility of π-stacked excimer formation. For example, Wessel and Syage reported a broad red-shifted $S_1 \leftarrow S_0$ spectrum for the dimer which demonstrates facile excimer formation upon excitation.[118] Significant previous work on excimers and their formation in aromatic systems predates this study[119], covering the excited state and ground state through the measurement of DF spectra[120-122].

Fluorene has been well studied previously using similar experimental techniques.[123-126] Fluorene has also been shown to efficiently transport energy and undergo electron transfer in light harvesting assemblies.[127] However, much still remains unknown about the details of the molecule's behavior as a result of clustering. Fluorene is known for its ability to fluoresce, but in addition to that, it is known for its ability to form an excimer as a result of dimer formation.[128-132] However, the details of the ground state structure of the fluorene dimer and the geometrical reorganization which accompanies excimer formation remain unclear, motivating the present study reported in this chapter, which compares the processes of excimer formation and hole stabilization in

the van der Waals dimer of fluorene compared with a novel covalently linked

bichromophore, where the fluorene moieties are linked at the 9 position through a

methylene spacer.
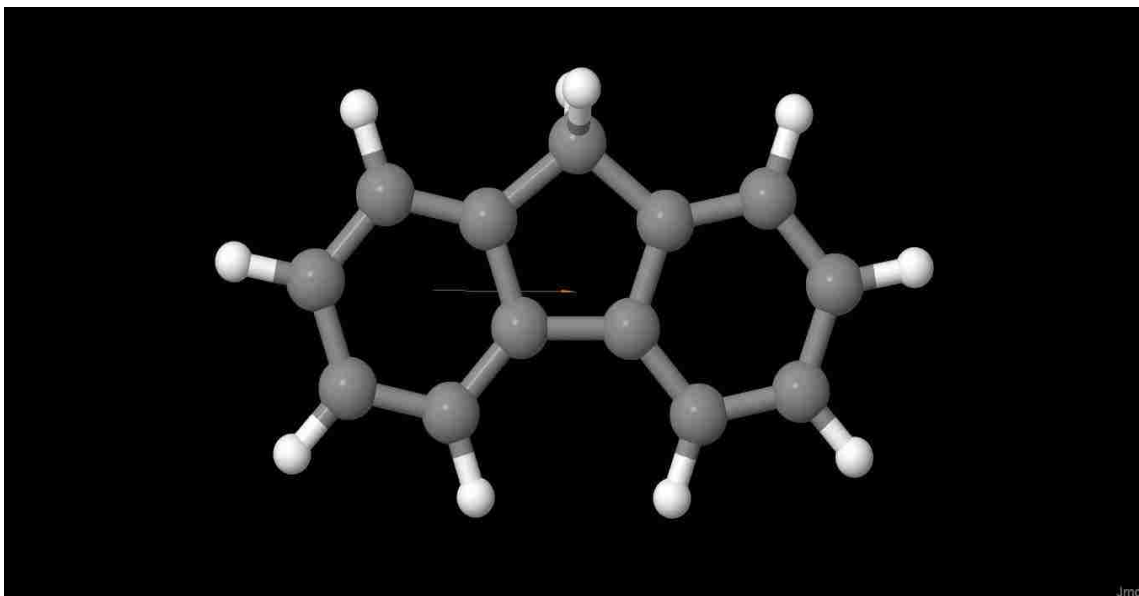
Figure 3.1: The calculated transition dipole[133] upon excitation for the fluorene molecule. As it can be seen, the transition dipole is in the plane of fluorene.

The covalently linked fluorene chromophores were synthesized and characterized

by the Rathore group.[134] These systems, referred to as Fn, where n is the number of

fluorene molecules contained in the chain, are shown in Figure 3.2. If the terminal

fluorenes of the chain contains hydrogen instead of methyl groups at the C9 position,

then they are labeled as FnH2. The van der Waals clusters are referred to as (F)n. For

this portion of the study, the dimer is the focus and therefore all values of n can simply be

replaced with 2, i.e., (F)$_2$ and F2. The representations shown in Figure 3.2 are qualitative

pictures and do not depict the actual experimental geometries of these molecules.
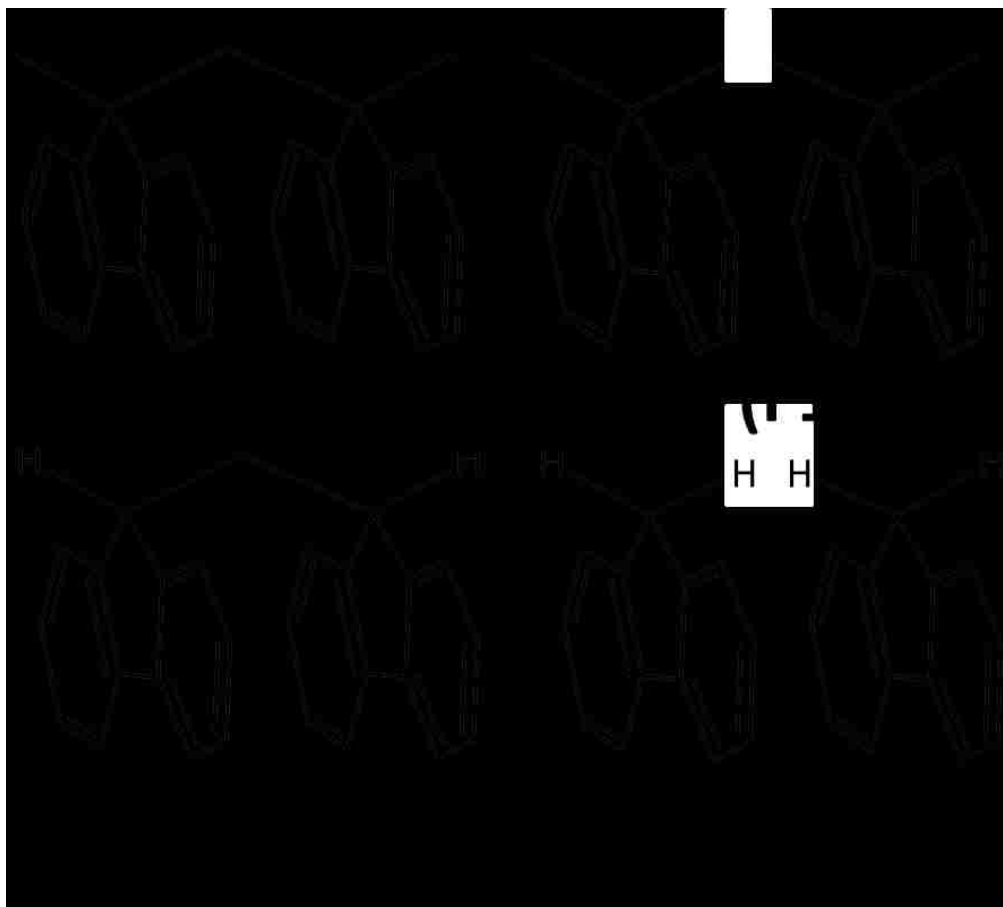
Figure 3.2: Molecular representations of the terminology used when referencing these fluorene composite systems. The structural differences range from being covalently linked with a methylene bridge at the C9 position, to having terminal methyl or hydrogen groups at the C9 position.

In Figure 3.3 the R2PI spectra of the relevant monomers, i.e., fluorene and F1 are shown. The results show the dramatic spectral simplification achieved with a jet-cooled molecular beam, where the rotational contours are collapsed due to the low rotational temperature (< 20 K) in the expansion. Each spectrum displays a clear origin transition, with the position of the origin for fluorene found at 33788 cm^{-1}, while that for F1 found at

33695 cm^{-1}. Interestingly, the addition of the methyl groups does not significantly change the spectrum, indicating that the methyl torsional modes are not Franck-Condon active in the electronic spectrum.
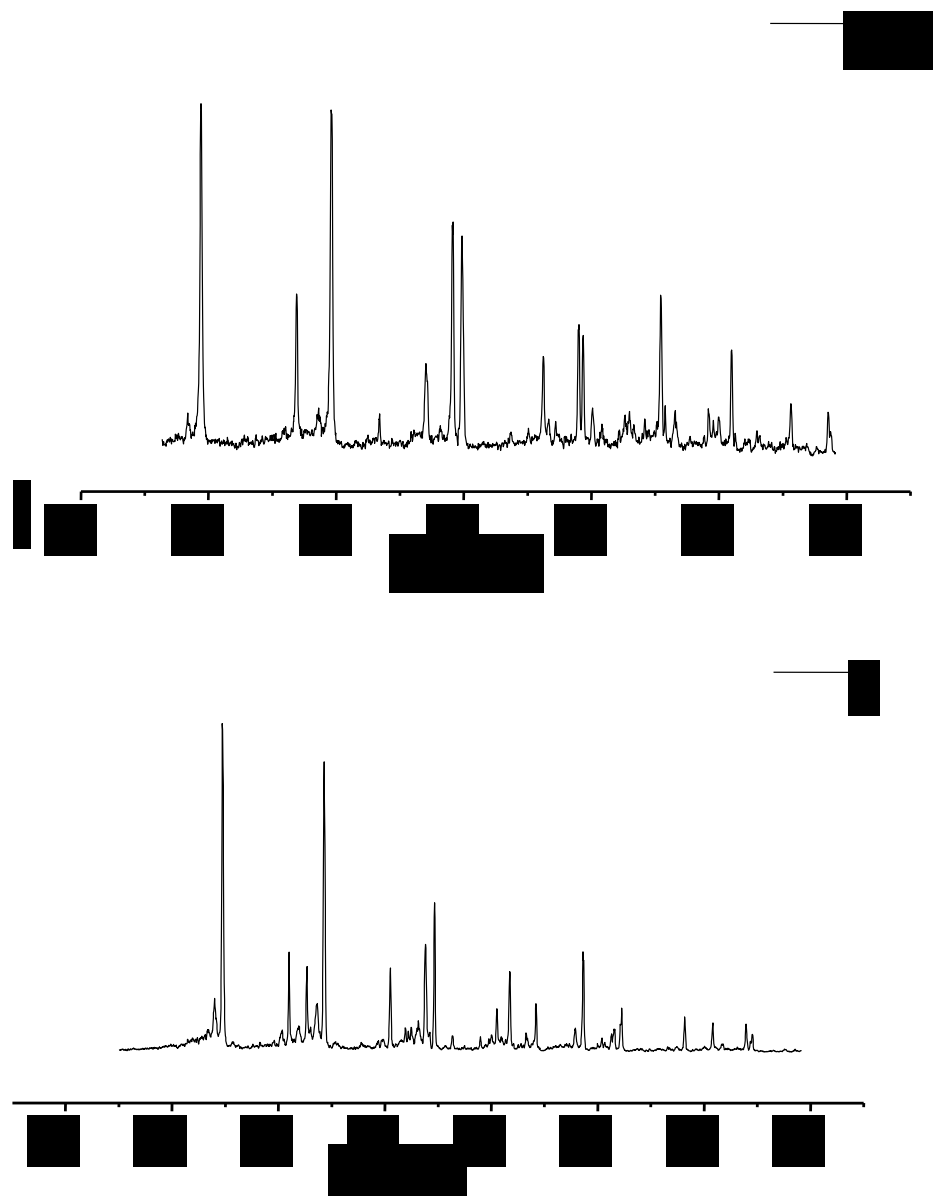
Figure 3.3: (Top) The R2PI spectra for the fluorene monomer. (Bottom) The R2PI spectra for the F1 monomer.

The goal of this work, as previously mentioned, was to compare excimer and hole stabilization in the covalently linked[155] fluorene bichromophore (F2) with the van der Waals (vdW) dimer. There had been a number of earlier studies of the vdW fluorene dimer. For example, fluorescence experiments had been conducted by Beck and Wessel[135] and Saigusa and Itoh,[136] both revealing similar results towards the formation of the dimer. The spectrum of the dimer displayed a red-shift relative to the monomer, and a splitting of the origin transition in the spectrum with complicated structure that was assigned to excitation of torsional vibrations. We carried out a range of studies of both dimers using both ionization and fluorescence techniques.

3.2   R2PI and LIF studies of the fluorene vDW dimer

First, we used the 2CR2PI technique to examine the electronic spectroscopy of the dimer. Using our pulsed general valve molecular beam source and ionization methods, the spectrum of the vdW dimer was successfully captured and can be seen in Figure 3.4.   The lowest energy feature is found at 33788 cm^{-1}, significantly red-shifted (i.e., shifted to lower energy) by some 200 cm^{-1} with respect to the monomer transition. The moderate red-shift can be attributed to the additional stabilization of dimer in the excited state. Under the assumption from previous studies that fluorene dimer forms an excimer, a red-shift of the spectrum is expected, as illustrated in Figure 3.5.
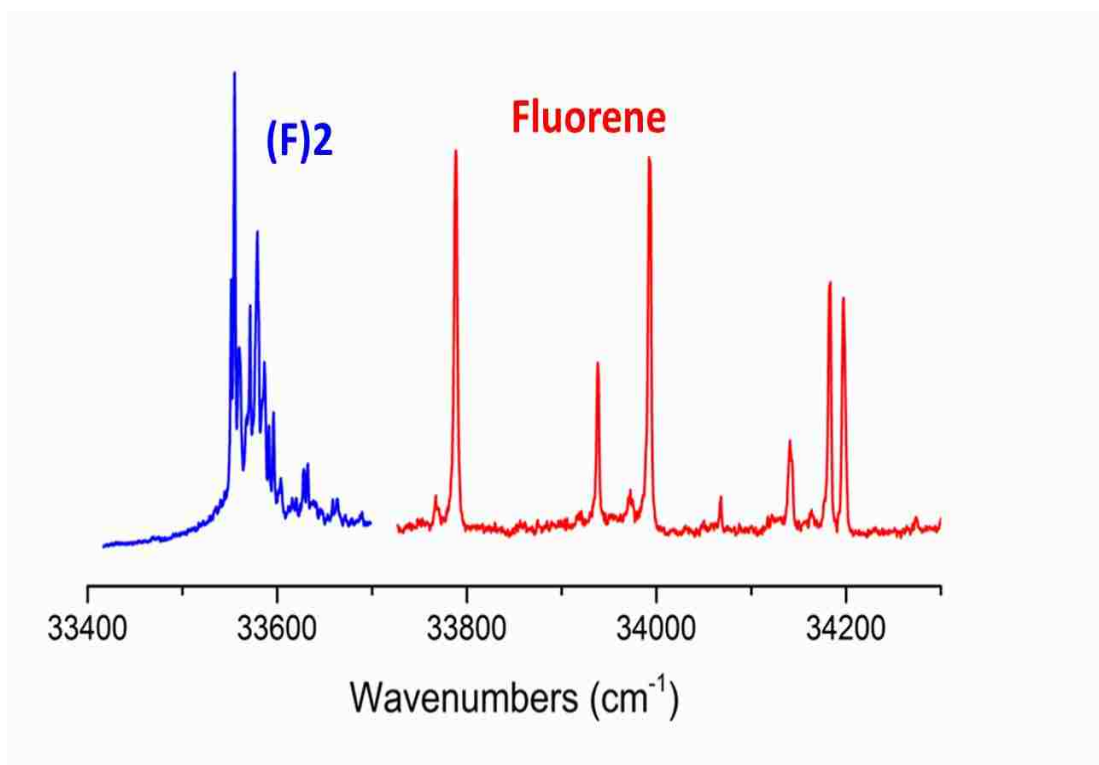
Figure 3.4:   The selected 2-Color Resonant 2-Photon Ionization Spectra of Fluorene monomer (pictured in red trace) and the red-shifted Fluorene dimer (pictured in blue trace).
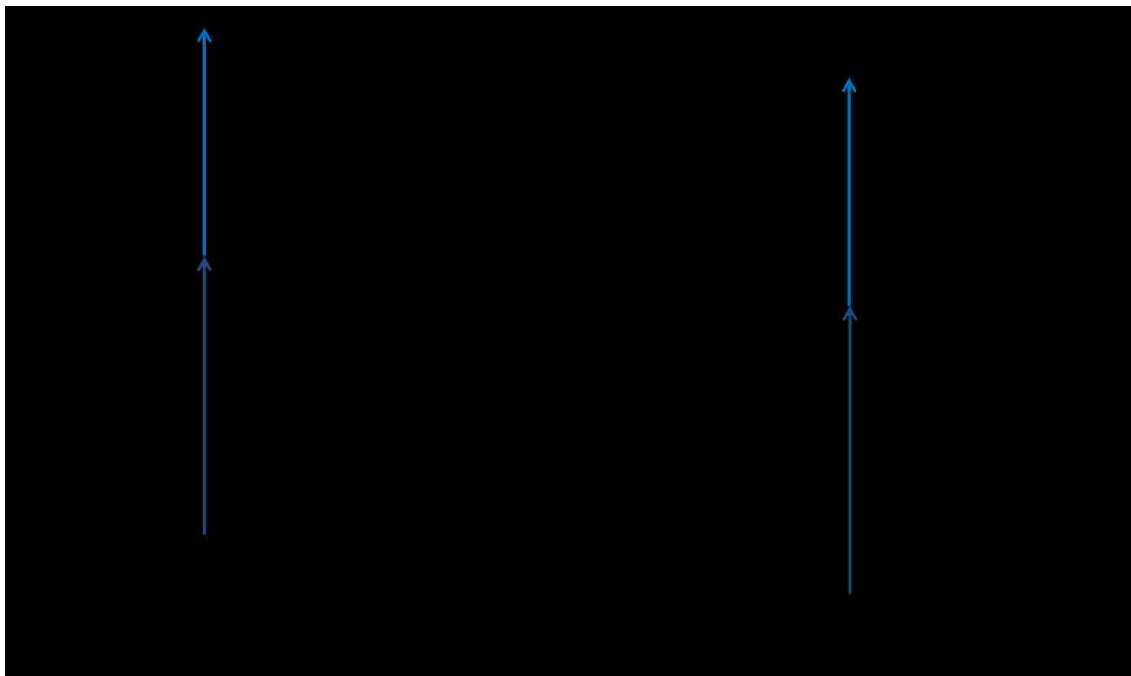
Figure 3.5: Representation of when a red-shift is observed from experimental data. This scheme demonstrates when there is a lowering in the binding energy as a result of stabilization upon excitation of the system. A blue-shift, on the other hand, would result in higher energies.

An expanded view of the origin region of the van der Waals dimer is shown in Figure 3.6. The spectrum displays two split excitonic components, with a splitting of roughly 20 cm^{-1}, and each contains clear torsional structure. This is informative in several respects. First, the similar intensity of the two components suggests that the orientation of the two dipoles is far from parallel. Recalling the excitonic model, the resulting splitting of the spectrum will be a consequence of the orientation of the transition dipoles relative to each other. Second, the torsional structure apparent in the spectrum shows that a geometrical reorganization between the ground and excited state must take place.

In order to rule out the possibility of multiple conformers contributing to the spectrum of the van der Waals dimer, we carried out hole-burning experiments. Figure 3.6 shows the resulting hole-burning spectrum (negative going features as hole-burning results in depletion of intensity) recorded when the burn laser was tuned to the lowest energy feature in the dimer spectrum. The HB spectrum appears to be nearly identical to the two-color spectrum. This is a result characteristic of only one contributing conformer. If there had been more than one conformer, then complete depletion would not have been the result. Instead, only the features associated with that particular frequency would have been burned out. It is now clear that upon excitation, while several conformers may be able to form, only one conformer is contributing to the collected spectrum. At this stage, the identity of that conformer has not been made.
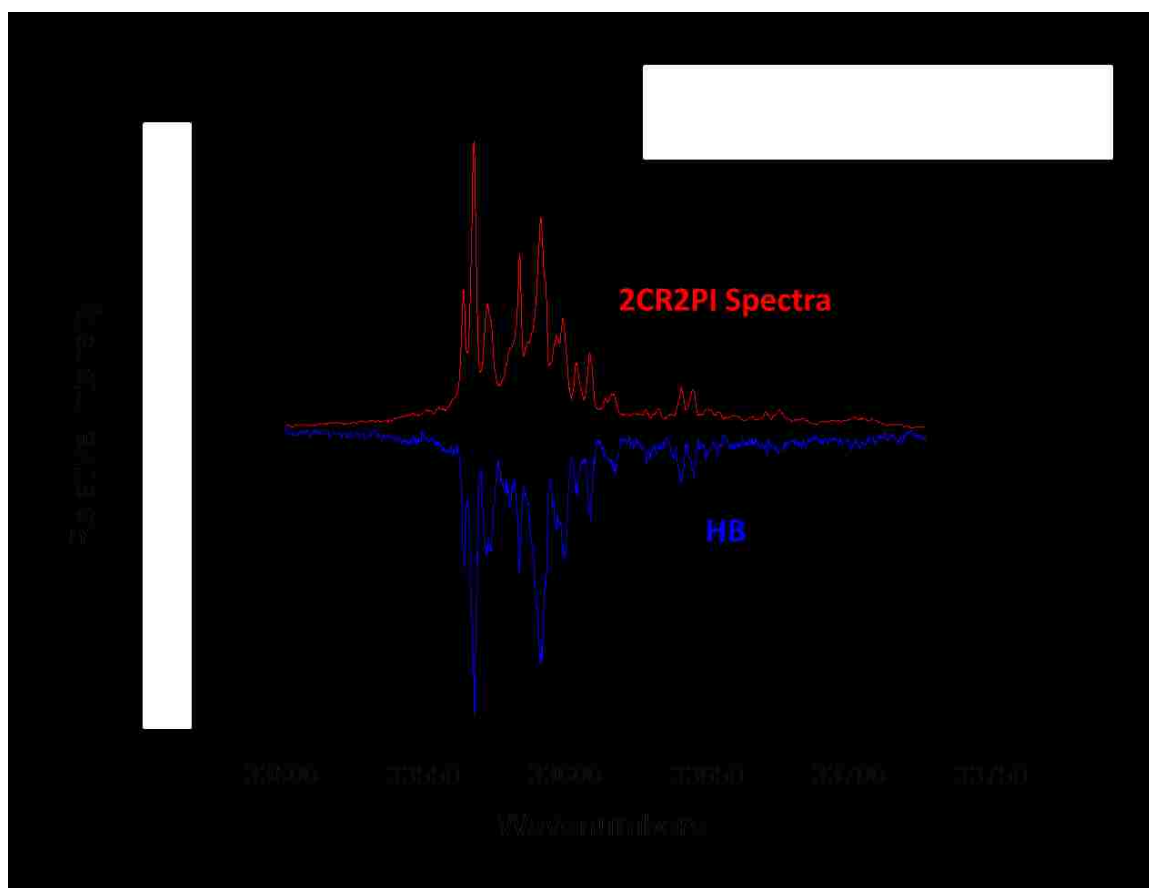
Figure 3.6: Hole-burning spectrum of the vdW fluorene dimer. A burn of the low frequency mode of the spectrum reveals a complete depletion of the spectrum (blue trace).

To obtain ion yield curves, we used 2CR2PI experiments where the excitation laser was fixed on a given transition in the electronic spectrum and the ionizing laser scanned to find the ionization threshold. Ion yield curves for the fluorene monomer and dimer can be seen in Figure 3.7. When plotting the IP curves, it is important to keep in mind that the energy value that is used to describe the ionization threshold is the total energy given to the system (the energy of both lasers). The energy of the excitation photon is added to the energy of the ionization photon in order to get the vertical IP of the molecular system. Taking this into account, looking at the results of the fluorene monomer reveals an IE of 7.885 ± 0.005 eV. This is in good agreement, but better determined, than previous ionization potential measurements that have been reported for fluorene.[137]
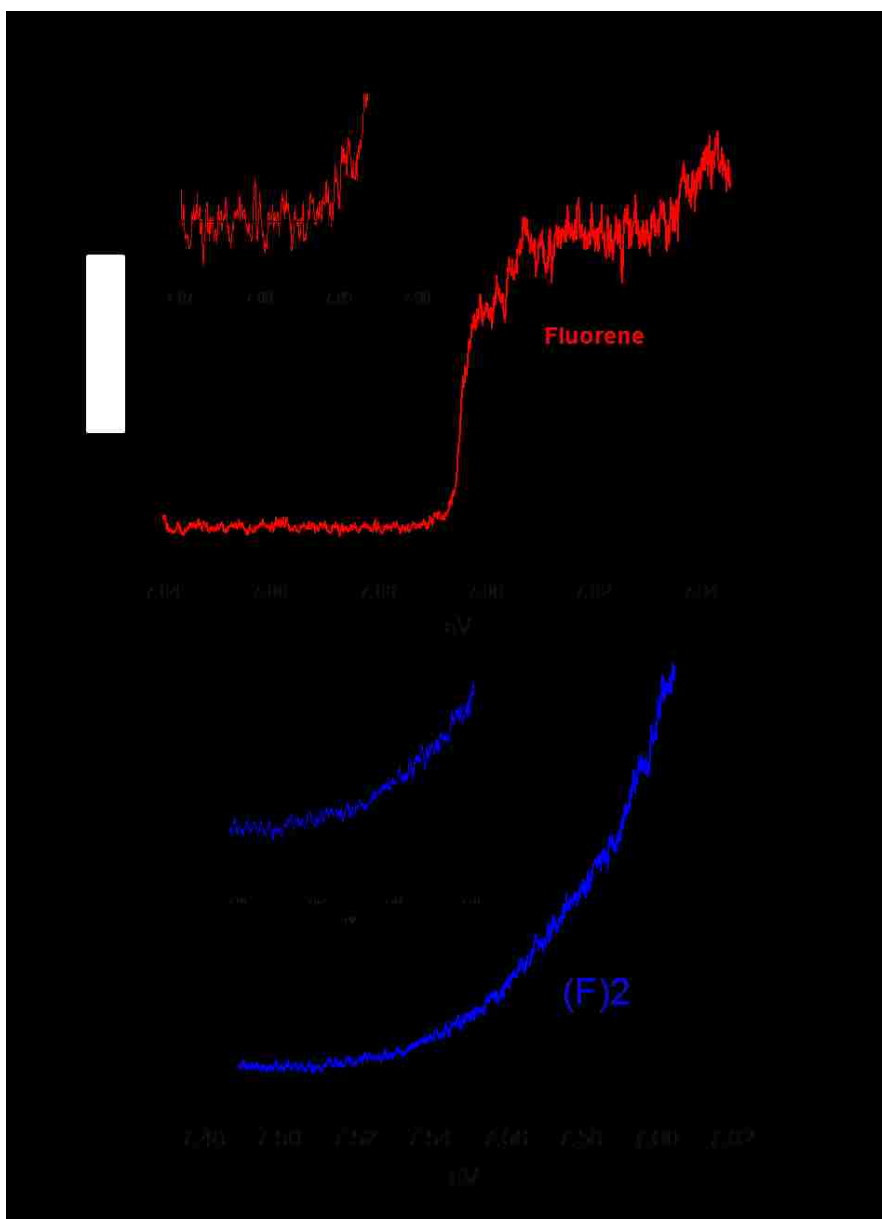
Figure 3.7: Ionization Potential curves of the fluorene monomer (left) and dimer (dimer). In the promotion to the dimer state, we see from the curves pictured a lowering of ionization energy by more than 0.3 eV.

The results shown in Figure 3.7 indicate that the IP of the dimer is much lower than that of the monomer; the IP is decreased from 7.885 to 7.52 ($\pm$ 0.01) eV, a difference of about 0.35 eV. Therefore, from the experiment, the energy required to remove an electron from the dimer is less than that of the monomer, which reflects the stabilization of the resulting hole by delocalization over both chromophores in the bichromophoric assembly.

The total LIF portion of the experiment was conducted in order to investigate any possible discrepancies in the excited state spectrum. The results of the LIF experiment can be seen in Figure 3.8. Observing the spectrum, one may notice that both the dimer and monomer signals are featured in the same spectrum. LIF lacks the mass-selection that the 2CR2PI experimental technique has, and therefore molecules of specific sizes cannot be filtered out. This leaves the experiment vulnerable to any impurities that have the potential to fluoresce. However, the purity of the samples is often checked via NMR before testing and then checked again using the mass-spectrometer in the 2CR2PI experimental setup. The reproduction of both the monomer and dimer was considered successful, both origin bands appearing at the same location as seen in previous experiments. A direct comparison of the 2CR2PI and LIF dimer spectra can be seen in Figure 3.9. Although the detection method for R2PI and LIF is different, we observe the same non-resonant behavior of the dimer in both cases, yielding the same complex splitting patterns in both spectra.
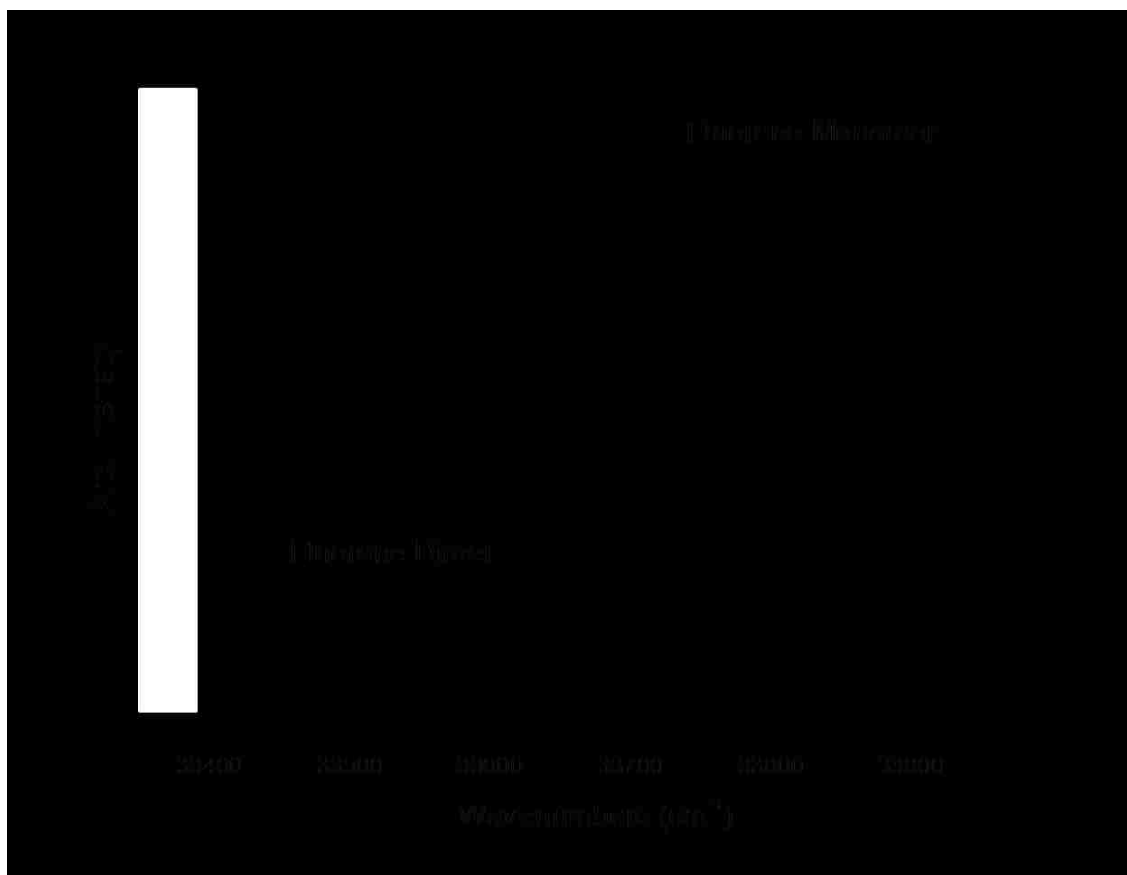
Figure 3.8: The total Laser-Induced Fluorescence Spectrum of Fluorene. As LIF lacks the mass selection that the 2CR2PI technique has, spectra of both monomer and dimer appear in the same trace.
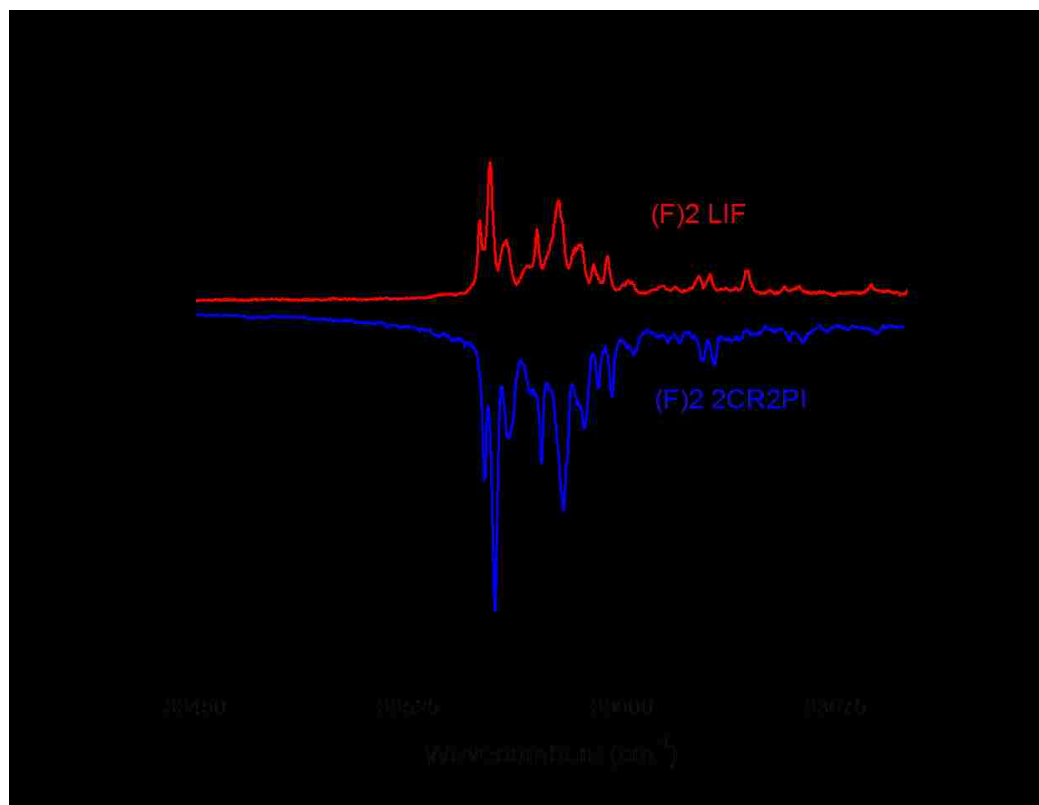
Figure 3.9: A comparison of the (F)$_2$ 2CR2PI (blue trace) and total LIF (red trace) spectra. In both cases the dimer exhibits the same complex splitting pattern of the red-shifted origin transition.

The vdW fluorene dimer was then examined using the Dispersed Fluorescence (DF) techniques. Using an excitation wavelength of about 596 nm, a DF spectrum was successfully obtained. The results can be found in Figure 3.10. The resulting spectrum shows broad, excimer-like activity. The peak of the feature appears at about 360 nm. This value is well shifted to the red of the laser (laser spike appears at the far left of the spectrum). Not much can be gathered from the DF spectrum of (F)$_2$, due to its overall lack of resolution, but it provides useful supplemental data to the big picture of these systems.
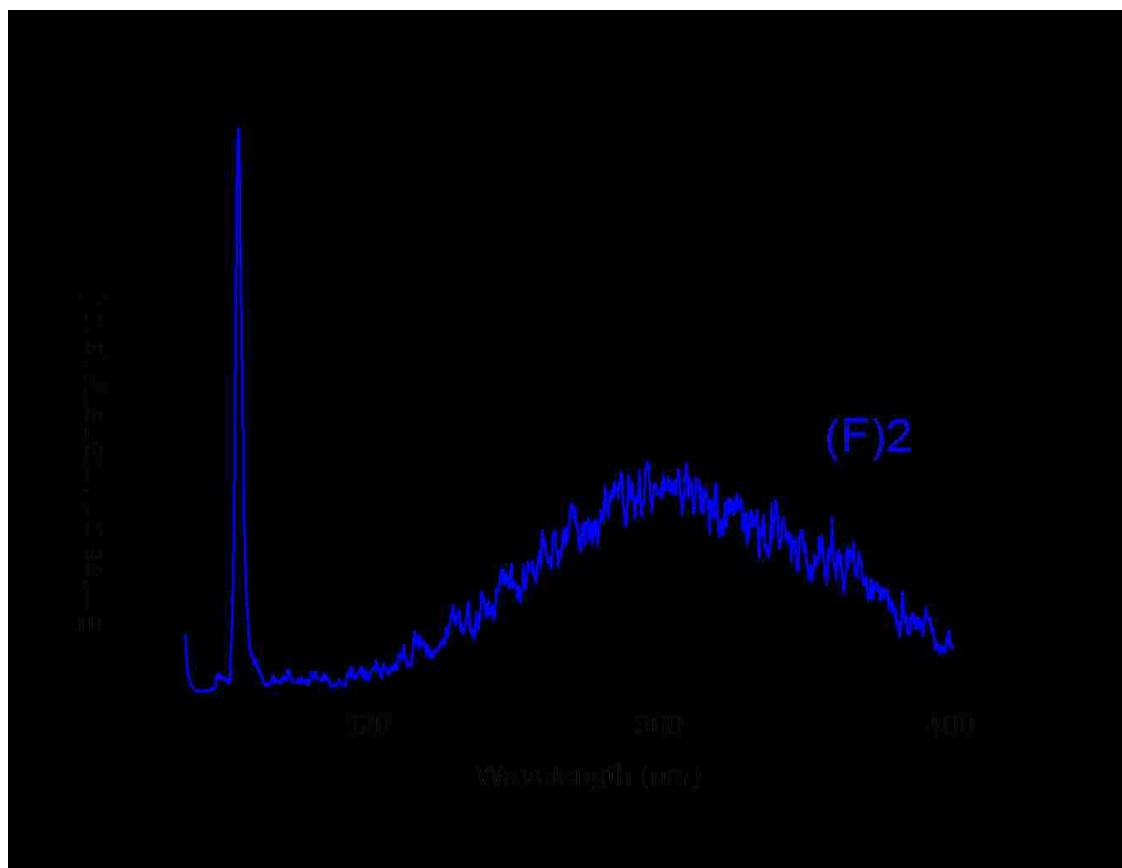
Figure 3.10: The Dispersed Fluorescence spectrum of the vdW fluorene dimer. It exhibits broad, excimer-like emission with the peak of the trace occurring at about 360 nm.

3.3   R2PI and LIF studies of the covalently linked dimer, F2

Under the assumption that the fluorene dimer can form an excimer, the question now becomes, if two fluorene molecules are covalently linked together, what impact will it have on its ability to form an excimer and stabilization of the hole in the ionic state?

The spectrum for F1 has been already collected and was briefly discussed in an earlier section. The covalently linked dimer, F2, is compared against the spectrum of F1 as F1 will be considered the "monomer" of the F2 composite molecule. Using the same experimental setup and beam source for F2, a 2CR2PI spectrum was collected. The results can be seen in Figure 3.11. Similar to the vdW dimer, the origin transition of F2 is red-shifted relative to the origin of the monomer. However, that is where the similarities end. The amount that the spectrum is red-shifted, as well as the spectrum itself, is different from results from the vdW experiment.
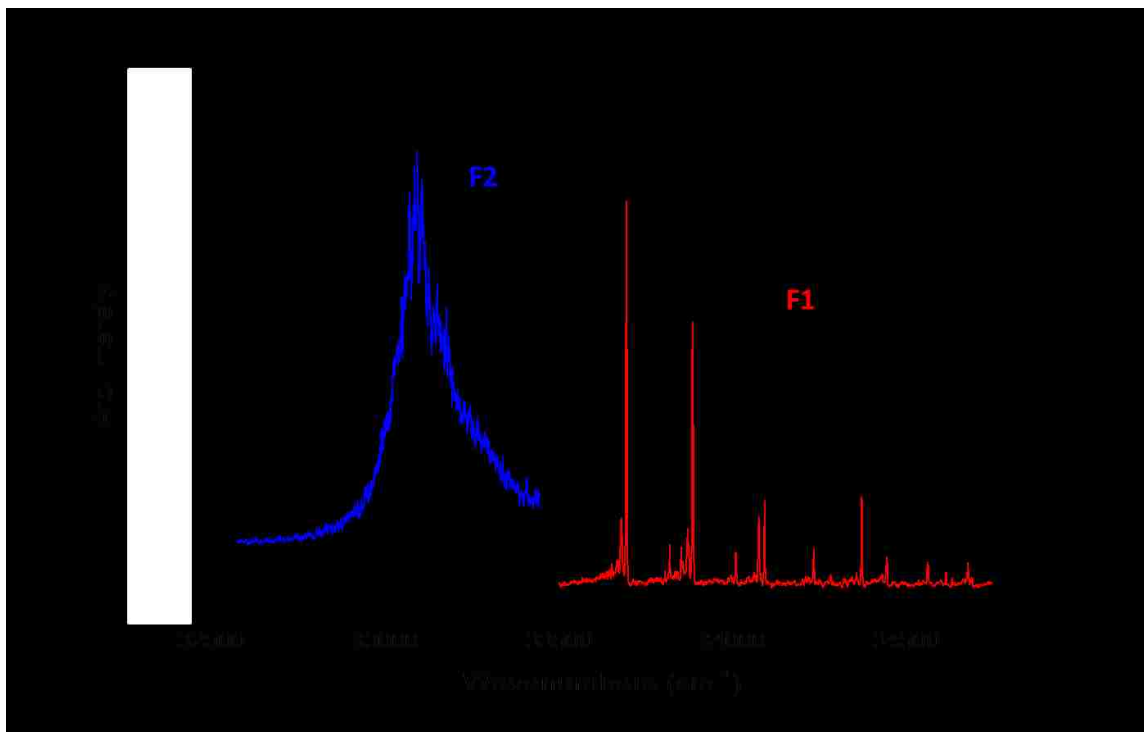
Figure 3.11: 2CR2PI spectra of the composite F1 (red) and F2 (blue) molecule. The transition from F1 to F2 results in a broad, unresolved spectrum that is red-shifted by about 600 cm^{-1}.

Observing the spectra of F1 and F2 we can point out differences that we saw before in the vdW case. The shape of the origin transition has changed and it has been red-shifted relative to the monomer. However, in the covalently linked case, a red-shift of about 600 cm^{-1} is observed. This is a significant red-shift and one that is far more indicative of stabilization as a result of a promotion to the systems excited state. In addition to the red-shift, the spectral shape is incredibly broad and bears no resemblance to the original monomer spectrum, in that no individual resolvable features seem to appear.

Next, with the large red-shift from F1 to F2 in mind, the IP curves of both of these samples were taken. The results can be found in Figure 3.12. Taking into account the

results of the vdW dimer having an IP lowering of more than 0.3 eV, one can expect the

lowering of the IP from F1 to F2 to be even lower than that because of its red-shift, which

was three times as large as the fluorene dimer. However, the results are not what were

expected. At the same time though, they are not in disagreement with the prediction. For

the IP of F1, the curve yielded a value of about 7.815 eV. This value is slightly lower

than the fluorene monomer but that was expected as we saw a small discrepancy in the

location of the origin transitions of the fluorene monomer and F1. When we move on to

the dimer, the IP curve shows a lowering of energy, to about 7.53 eV. The overall drop

in energy is slightly less than 0.3 eV. This concludes the ionization portion of the

experiment and now the focus is shifted to fluorescent techniques.
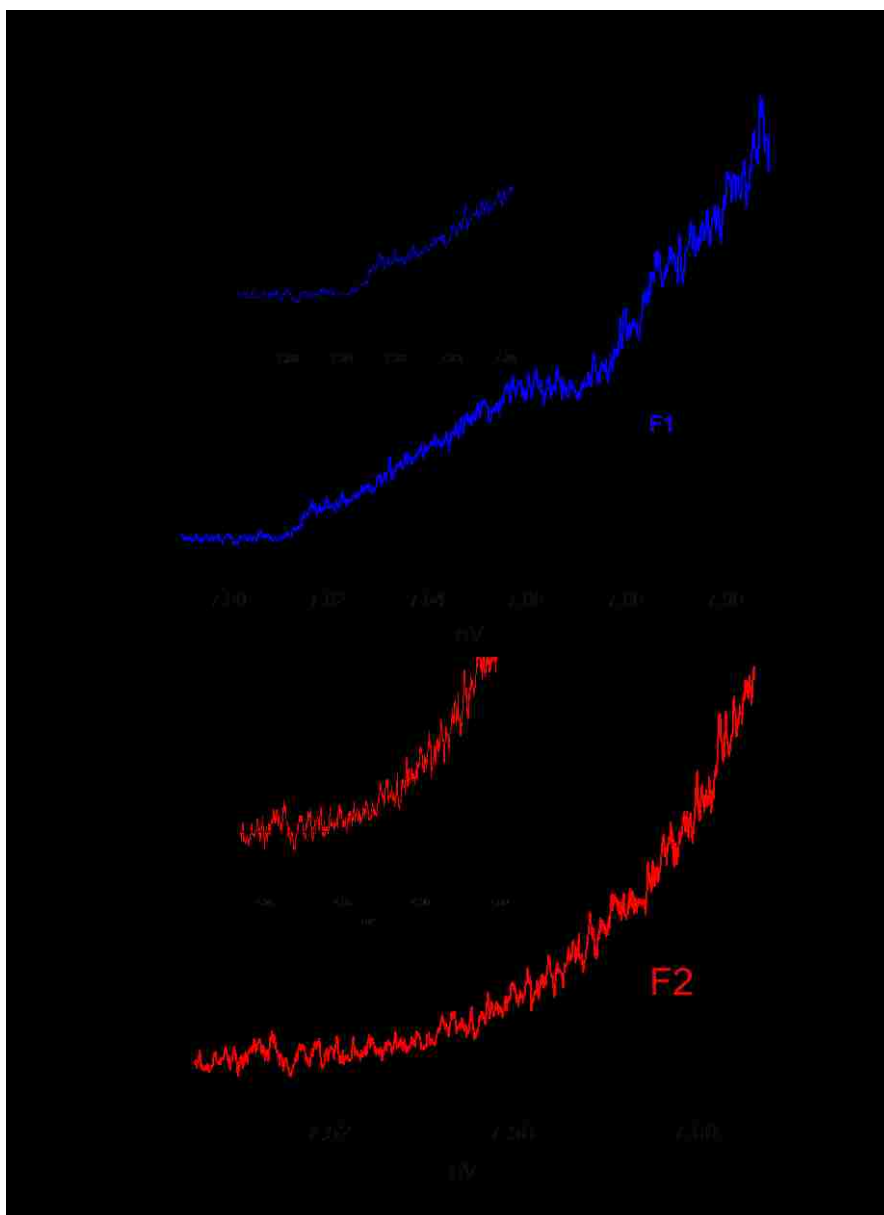
Figure 3.12: Ionization Energy curves of the F1 (blue) and F2 (red) composite fluorene molecules. The ionization of F2 is revealed to be slightly less than 0.3 eV lower than that of the F1 molecule.

Ionization experiments on F2 and the vdW fluorene dimer have revealed that there is an enhanced ability to delocalize charge as a result of their dimer geometries. This is behavior that is expected upon the formation of an excimer. To supplement the previous findings, fluorescence can now be used to verify findings towards the excited state, and add information about each sample's ground state with Dispersed Fluorescence.

After seeing that the vdW dimer exhibits the same excited state behavior in both the 2CR2PI and total LIF experimental procedures, as was expected, the focus was then turned to the F2 composite molecule. The evolution of the origin band of F2 from F1 is of a bit more interest because of its large red-shift and its broad, unresolved characteristic. The LIF experiment was done on F2 to see what results fluorescence detection techniques would yield. As it turns out, as seen in Figure 3.13, the total LIF spectrum is identical to the spectrum collected from the earlier 2CR2PI experiments. We observe the same unresolved, broadened origin transition. Therefore, for both F2 and $(F)_2$, the results of the total LIF verified the spectra of their excited state.
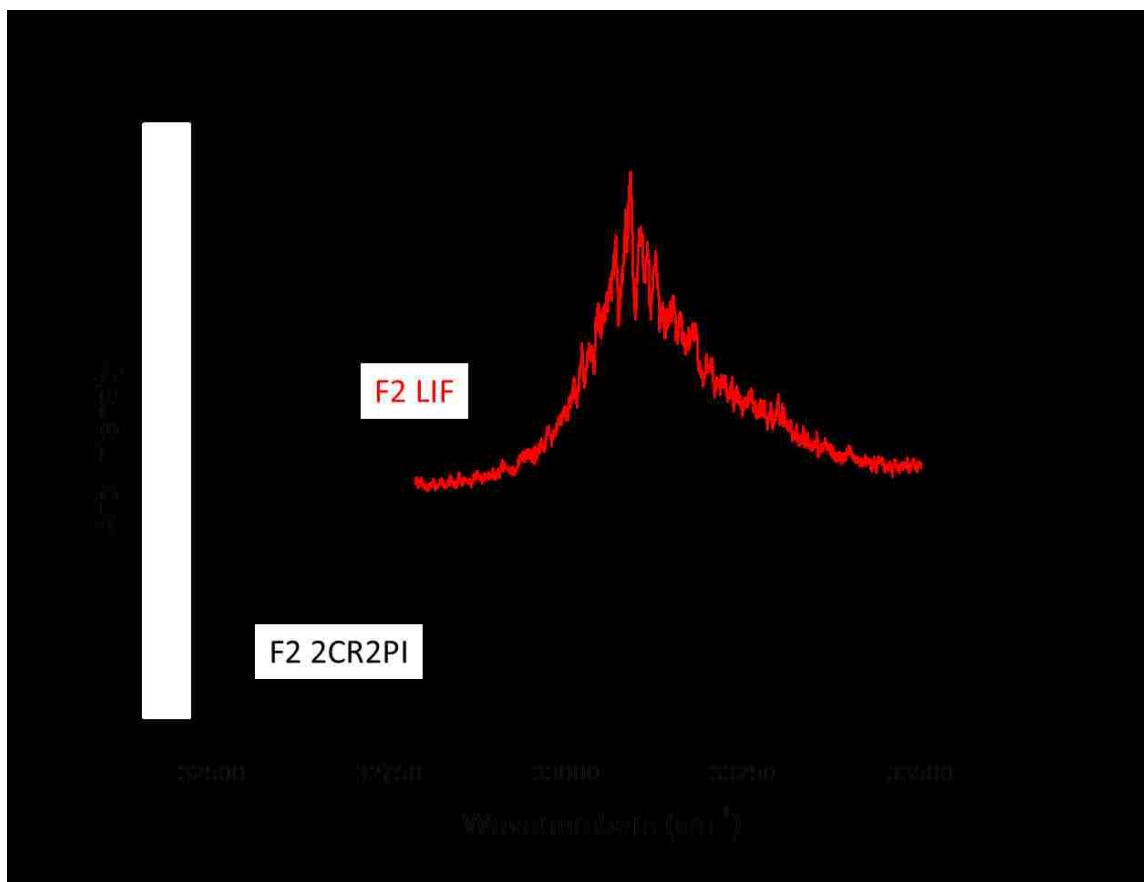
Figure 3.13: The comparison of the F2 2CR2PI (black trace) and total LIF (red trace) spectra. The molecule exhibits the same broad excited state spectral shape in both cases.

The excited state for F2 has been verified by 2CR2PI and total LIF techniques. With this, the focus of the experiment was shifted towards the ground state behavior of the covalently linked dimer. The ground state can be studied with the same Dispersed Fluorescence techniques as $(F)_2$. For the DF experiments, the wavelength used to excite the molecule was the origin transition, or in F2's case, the most intense features of the origin transition since there was no distinguishable, well-resolved origin features.

The excitation wavelength used for this experiment was 604 nm. The results of this experiment can be found in Figure 3.14. Similar to the results that were found in

previous experiments done on (F)$_2$, the DF spectrum exhibits a broad, unresolved shape

that is shifted far to the red of the laser peak. The peak of this broad feature in F2's DF

spectrum appears at about 400 nm, 40 nm to the red of the most intense part of (F)$_2$'s

feature.
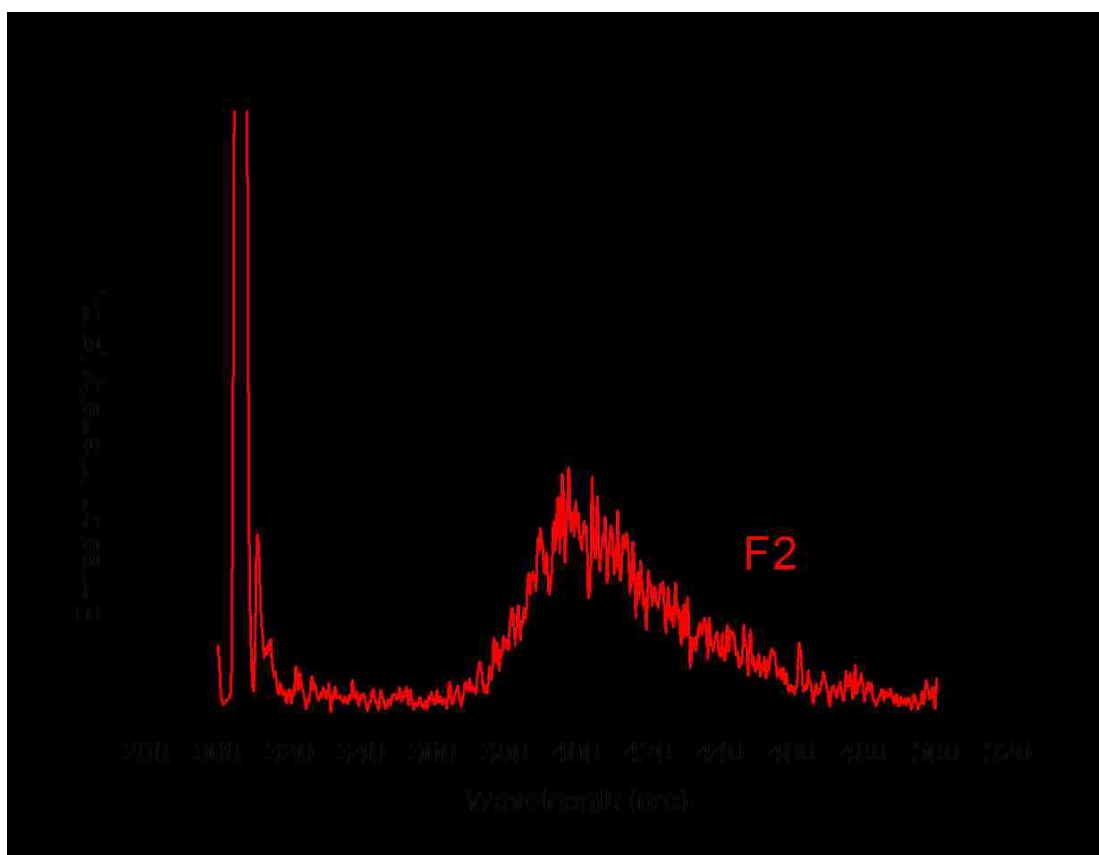
Figure 3.14:   The Dispersed Fluorescence spectrum of the F2 composite molecule. It exhibits broad, excimer-like emission with the peak of the trace occurring at about 400 nm.

The DF of F2 and (F)$_2$ have been superimposed in Figure 3.15 in order to better

analyze the two. From the comparison, it can be seen that the composite F2 molecule is

roughly 40 nm to the red of the DF of (F)$_2$. In order to verify the accuracy of these

findings, a solution phase fluorescence spectrum is included in the DF comparison in

Figure 3.15. The solution phase and gas phase spectrum of F2 seem to match fairly well verifying that what is seen in the gas-phase spectrum is real.

This concludes the experimental portion of the F2 and (F)$_2$ investigation. The data has revealed a lot about the molecules at first glance, but upon further analysis and supplemental computational studies, even more can be uncovered about the molecular systems. Knowing the geometry of the molecules in these gas-phase techniques is difficult and will always have an element of uncertainty. However, combining this data and comparing it against each other will give insight into the geometry-sensitive details about these systems' (potential) excimer formation.
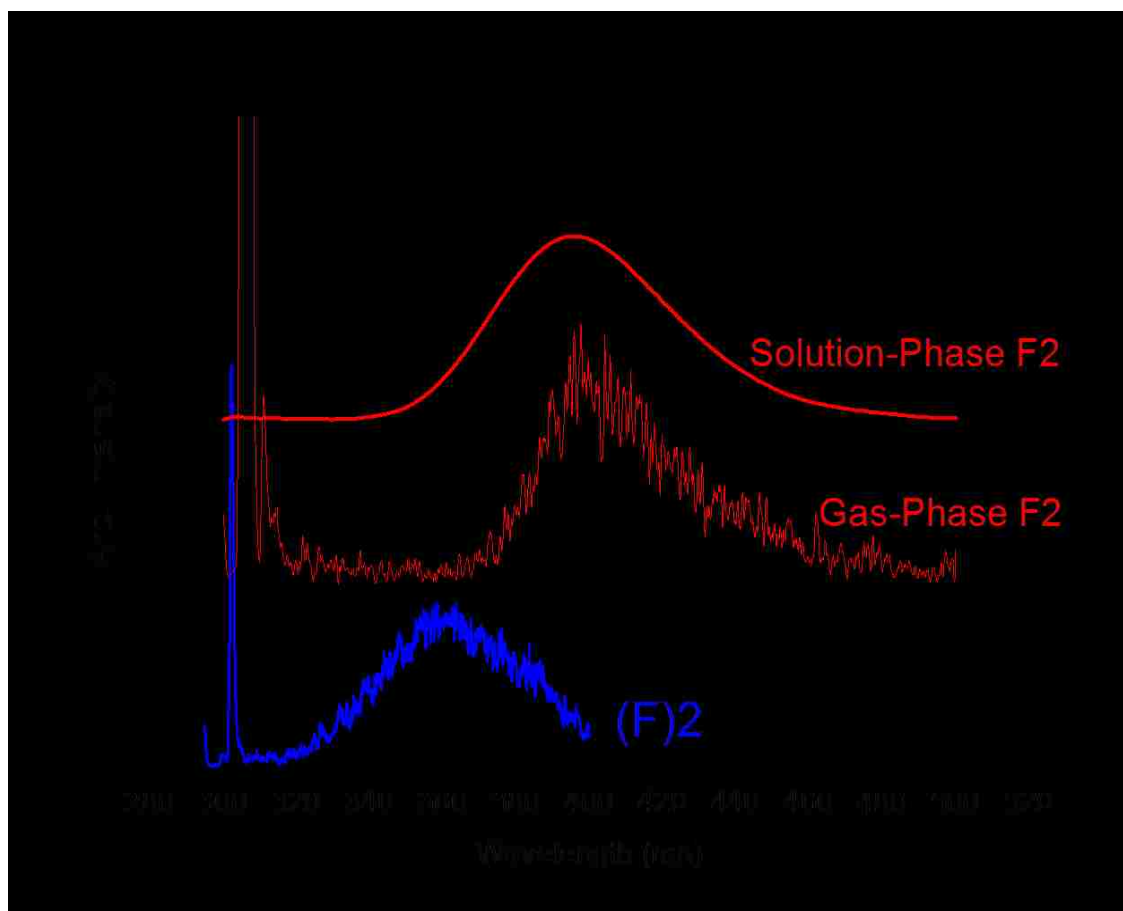
Figure 3.15: A comparison of the DF spectra of (F)₂ and F2. F2 has been previously studied with solution-phase fluorescence techniques and has been plotted against the gas-phase spectrum as reference.

3.4   Computational Studies of (F)$_2$ and F2

Experimental data has been gathered for the vdW fluorene dimer and the covalently linked F2 composite molecule. Overall, each molecule shared similarities and differences and these comparisons give valuable insights about how these dimers are behaving as a result of excitation. It is known from the exciton model that the formation is very sensitive to the geometry of the system[111]. In the analysis of the data of these two systems, we continue to operate under the assumption that the fluorene dimer forms an excimer based on previous studies. With this assumption, we must ask, what geometry is responsible for this excimer and how does the excited state geometry of F2 compare?

Computational methods have proven to be an effective way to identify local and global minimum energy structures in a system.[138,139] A number of different conformers could be present here. Even if the lowest energy conformer can be identified, it is most likely not the only conformer present, and there is no guarantee that it will even be present at all. After conducting the hole-burning experiments, it is known that one conformer is contributing to the spectrum. Therefore, in optimizing potential minimum energy structures, the computational results can then be matched against the experimental results to provide better analysis. In Figure 3.16, some selected ground state geometries have been optimized at the M06-2X/cc-pVDZ level of theory. It can be seen from the structures that the geometry seems to favor varying types of π-stacking, with the transition dipoles potentially being near perpendicular, or parallel to one another.
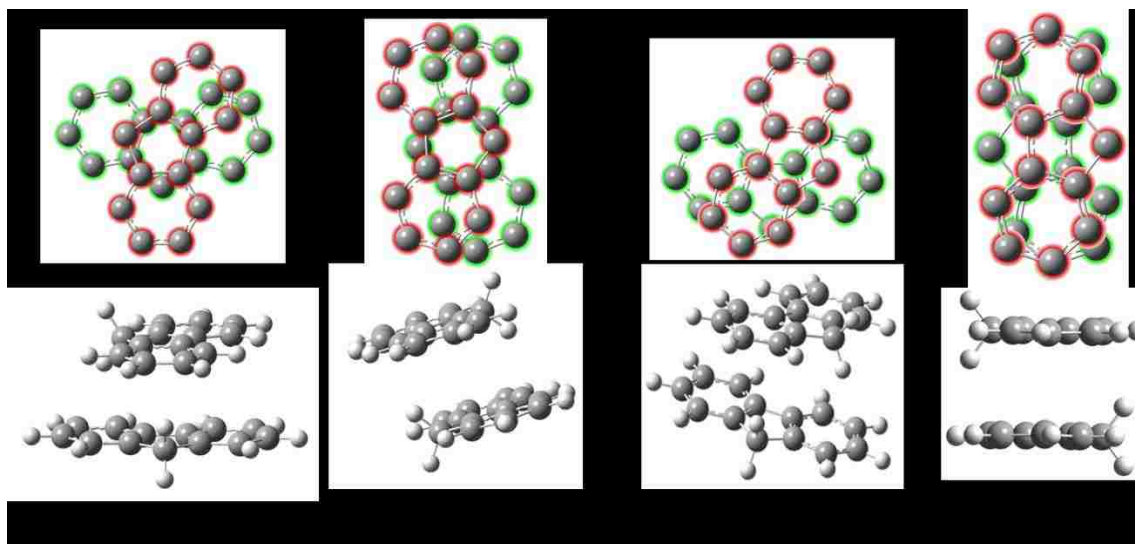
Figure 3.16: A selection of geometry optimized ground state structures for the vdW fluorene dimer with corresponding relative energies. The potential geometries pictured include orthogonal arranged structures as well as a parallel displaced arrangement.

The results of these calculations show that the binding energies of the conformers are nearly isoenergetic, and therefore it is possible for all these conformers to form in the gas-phase. However, if we remember from the exciton model, if the system were to adopt a parallel geometry, then a splitting pattern with one very intense feature and one very weak feature would be observed. This is not the intensity ratio that is observed. Therefore, the minimum energy geometry cannot be assumed to be the only conformer contributing. At the same time, however, the data collected strongly favors that of some sort of excimer formation for the vdW dimer, with the most probable geometry being completely π-π stacked in the excited state. The excited state splitting and intensity ratios are difficult to match with experiment using TD-DFT methods. Calculations

overestimate the splitting by 10-40 times.[140,141] Therefore, a different theoretical

treatment is required.

Revisiting the excited state 2CR2PI spectrum of $(F)_2$ might reveal the answer to

the discrepancy in potential geometries. The spectrum has a complex splitting pattern that

one would expect to be a 'perpendicular' stacked geometry, but with fluorescence data

favoring excimer formation, one would expect the dimer to be completely π-stacked for

maximum energy and charge stabilization. In an attempt to understand what might be

happening, the line shapes of the dimer spectrum were analyzed. Using the Origin

software package, a number of different peaks were tested to see if there were any

potential fits. After a few attempts, Lorentzian peaks were fitted to the spectrum. The

result can be seen in Figure 3.17. Using a portion of the spectrum, for Lorentzian peaks

were fitted to the spectrum, with a cumulative peak fit to the spectrum to show how well

the individual peaks fit overall. In all, four peaks were fit to the selected portion of the

spectrum with the cumulative peak resembling the overall spectrum shape fairly well.

Ultimately, this is a fairly arbitrary fit due to the fact that this spectrum could be made up

of any number of peaks, but, this fit seems to work well with four Lorentzian peaks. It is

important to note that Lorentzian peaks seem to provide the best fit. Line shapes in

spectra can be described as homogenous or inhomogeneously broadened, or Lorentzian

and Gaussian line shapes, respectively. Each type of broadening has specific causes

associated with it that give rise to that line shape in the experiment. In this case, the fit

points to homogeneous broadening in the spectrum. Under the description of

homogeneous broadening there is lifetime broadening, with the line width having a direct

relationship with the lifetime of the system (in this case, the lifetime of the dimer). The

line width of the fitted Lorentzian peak corresponds to a lifetime on the order of several picoseconds.[142] In previous lifetime measurements, it was estimated that the excited state lifetime for the fluorene monomer was on the order of about 15 ns. When the $(F)_2$ vdW dimer is formed, the excited state lifetime is extended to about 54 ns.[128] This lifetime extension is indicative of an increased stabilization in the excited state of the dimer, which is in good agreement with data showing a red-shift of the dimer spectrum and the large lowering of the IP.

Relative energies were then calculated using the minimum energy structures of the $(F)_2$ dimer at the M06-2X level of theory. Figure 3.18 shows that in the ground state, an orthogonal conformer is nearly iso-energetic with the parallel displaced conformer. A π-stacked geometry in the ground state is a maximum. Coupled Cluster (CCSD) calculations were done as a follow-up and show the same trend. When promoted to the excited state, the π-stacked conformer becomes the minimum, while the orthogonal conformer is now the highest in energy. Due to the splitting and intensity ratios found in the 2CR2PI and LIF spectrum of $(F)_2$, the orthogonal conformer is more likely to be found than the parallel displaced, as the parallel geometry would led to intensity ratios that would make the origin appear as one peak (one very large feature and one very small feature).
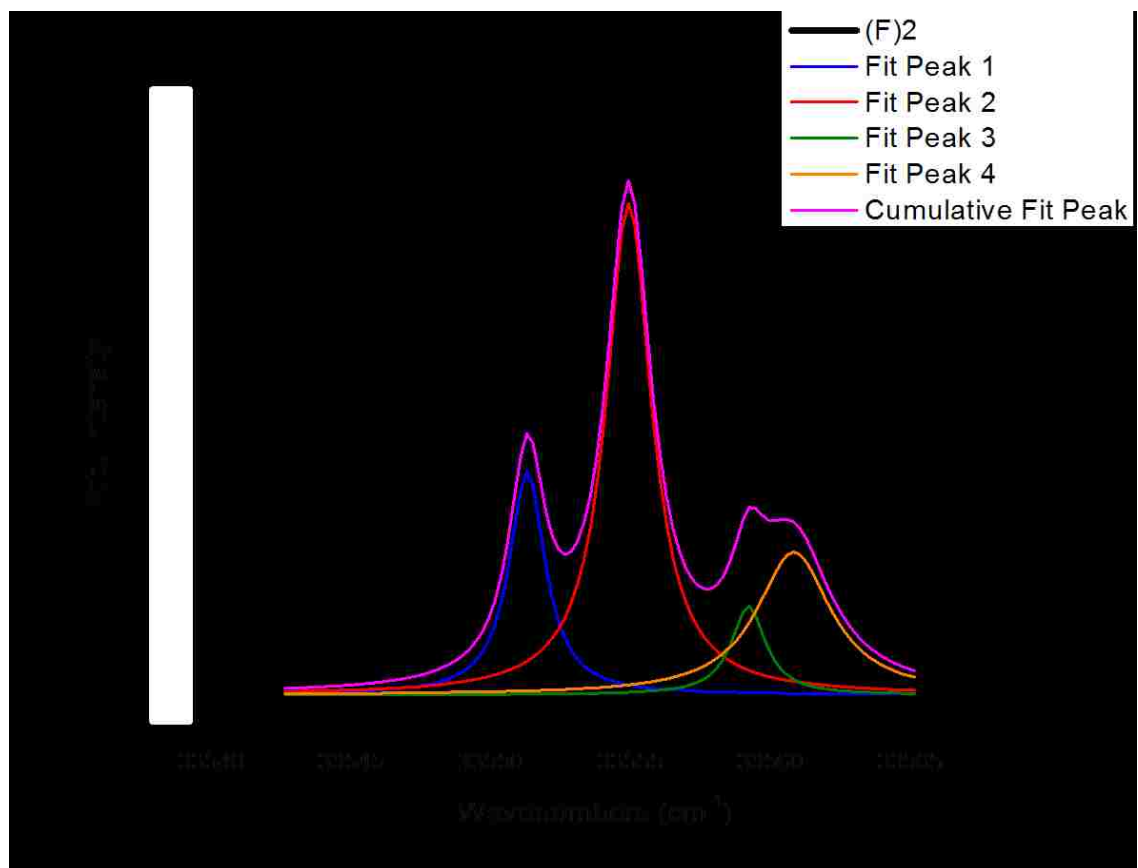
Figure 3.17: A selected portion of the Fluorene dimer with fitted Lorentzian curves. Four curves were fitted to the spectrum with a cumulative curve (plotted in magenta trace) included to show the overall shape compared to experimental results (plotted in black trace).
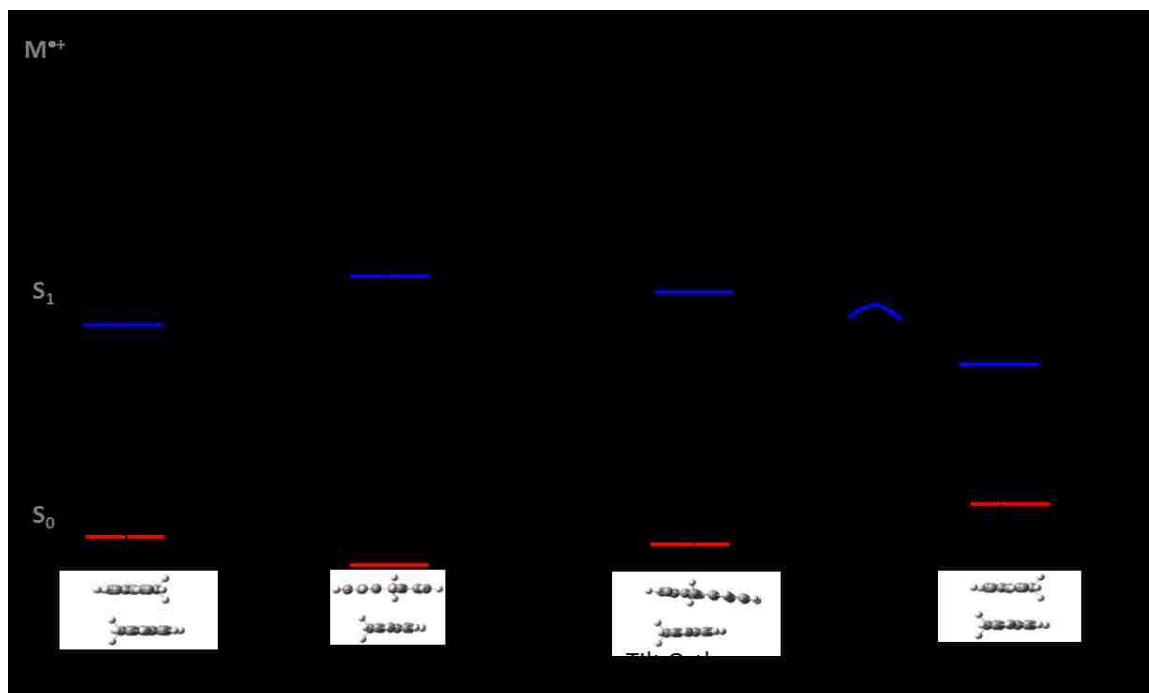
Figure 3.18: Calculated energies of the orthogonal, tilt orthogonal, parallel displaced, and π-stacked geometries of the vdW fluorene dimer. The calculations reveal the ideal conformation for both the ground-state and excited-state of the system. Asterisks indicate optimized structures.

Details of the excited state of each potential $(F)_2$ geometry were also investigated using TD-DFT computational techniques. In Tables 3.1, 3.2, 3.3, and 3.4, the S_1, S_2 and electronic coupling constants, V_{ab} are shown. The coupling values for each geometry are going to be large overestimations, as mentioned before, due to these calculations being purely electronic. Additionally, excited state calculations have yielded predicted oscillator strengths of the S_1 and S_2 transition, as well as the potential molecular orbitals involved. The oscillator strengths, f, for the orthogonal geometry of $(F)_2$ show a similar intensity ratio, while the tilted orthogonal geometry is roughly 2:1. Additionally, relative to all other geometries, the orthogonal $(F)_2$ possesses the smallest electronic coupling constant. The ratios are in good agreement with what is observed experimentally, where

the excitonically split origin features posses similar intensities, and therefore, support the idea that the starting geometry for $(F)_2$ is an orthogonal-type geometry.

Table 3.1: S_1, S_2, and V_{ab} Coupling Values for $(F)_2$ Orthogonal Geometry

	E, eV	E, kJ/mol	E, cm^{-1}	transition	coefficient	f
S_1	4.83	466.39	38987.87	83 -> 90	0.12464	0.1348
				85 -> 89	0.13728	
				85 -> 91	0.10319	
				87 -> 90	0.23264	
				87 -> 92	-0.20939	
				88 -> 89	0.55961	
				88 -> 91	-0.13261	
S_2	4.87	469.92	39281.93	83 -> 89	0.11126	0.1853
				85 -> 90	0.16742	
				86 -> 90	0.10991	
				87 -> 89	0.52578	
				87 -> 91	-0.17662	
				88 -> 90	0.22612	
				88 -> 92	-0.21918	
V_{ab}	0.02	1.76	147.03			

Table 3.2: S_1, S_2, and V_{ab} Coupling Values for $(F)_2$ Tilted Orthogonal Geometry

	E, eV	E, kJ/mol	E, cm^{-1}	transition	coefficient	f
S_1	4.78	460.89	38526.74	87 ->90	0.1327	0.1242
				87 ->91	-0.11967	
				88 ->89	0.60918	
				88 ->90	0.12913	
S_2	4.9	472.78	39521.01	85 ->89	0.17303	0.214
				87 ->89	0.45291	
				87 ->90	-0.30267	
				87 ->91	-0.13826	
				88 ->89	-0.13826	
				88 ->90	0.22814	
				88 ->92	0.1623	
V_{ab}	0.06	5.94	497.13			

Table 3.3: S_1, S_2, and V_{ab} Coupling Values for (F)$_2$ Parallel Displaced Geometry

	E, eV	E, kJ/mol	E, cm^{-1}	transition	coefficient	f
S_1	4.52	436.39	36479.04	87 -> 90	-0.16192	0.000
				88 -> 89	0.66978	
S_2	4.85	468.34	39151.2	83 -> 89	0.15267	0.000
				84 -> 90	-0.1489	
				87 -> 92	0.20225	
				88 -> 89	0.10082	
				88 -> 91	0.61882	
V_{ab}	0.17	15.97	1336.1			

Table 3.4: S_1, S_2, and V_{ab} Coupling Values for (F)$_2$ Stacked Geometry

	E, eV	E, kJ/mol	E, cm^{-1}	transition	coefficient	f
S_1	3.47	335.18	28018.27	88 -> 89	0.70061	0.000
S_2	4.28	413.10	34532.77	85 -> 89	0.18967	0.0526
				88 -> 90	0.55951	
				88 -> 91	0.35101	
V_{ab}	0.4	38.96	3257.25			

Recently, Leutwyler et. al.[143] published work showing how benzene dimer underwent geometry rearrangement as a result of being promoted to its excited state. In the study, they outline how the minimum energy geometry is t-shaped in the ground state and rapidly rearranges to the π-stacked excimer upon excitation. If this same scheme is applied to the (F)$_2$ system, we see that the data supports a geometrical rearrangement.
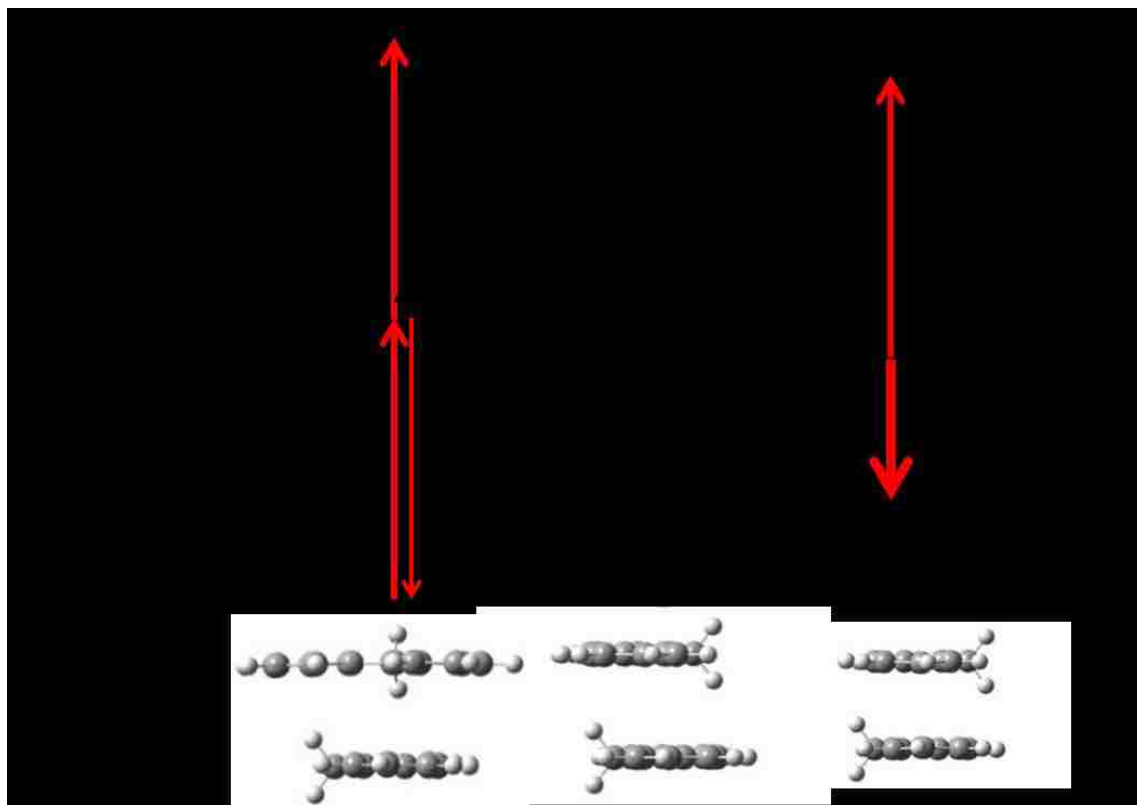
Figure 3.19: A scheme for the formation of an excimer and cation with non-covalent fluorene dimer.

Figure 3.19 serves as a general representation of the geometrical rearrangement that (F)$_2$ must undergo in order to form an excimer. The 2CR2PI and LIF spectra showed resolved splitting and a 200 cm^{-1} red-shift, and with the TD-DFT results, agree with the orthogonal geometry discussed before. However, the Dispersed Fluorescence shows a broad excimer like emission. Therefore, upon excitation, the orthogonal conformation rapidly rearranges to the π-stacked conformation. Once this has occurred, it can be ionized or it can emit from the excimer well. We assume there is a high density of states in the excimer well, and therefore once it has been populated, it will not reverse back to the orthogonal conformation. This rearrangement is evident in the excitation spectra

having Lorentzian line shapes indicative of lifetime broadening. This accounts for the

rapid rearrangement of $(F)_2$ that takes place over several picoseconds. This also accounts

for the excimer-like emission that is evident in the Dispersed Fluorescence spectrum.

The same theoretical treatment was given to the F2 composite system. Multiple

ground state structures were found for the covalently linked system. In Figure 3.20 the

conformers can be generalized as either 'open' or 'closed.' The closed conformer is the

lowest in energy and not nearly iso-energetic with any of the other conformers. This is

expected as the only way for the rings to interact with one another is through a closed,

parallel arrangement, while all open conformers have CH/π bonding as their main

interactions.
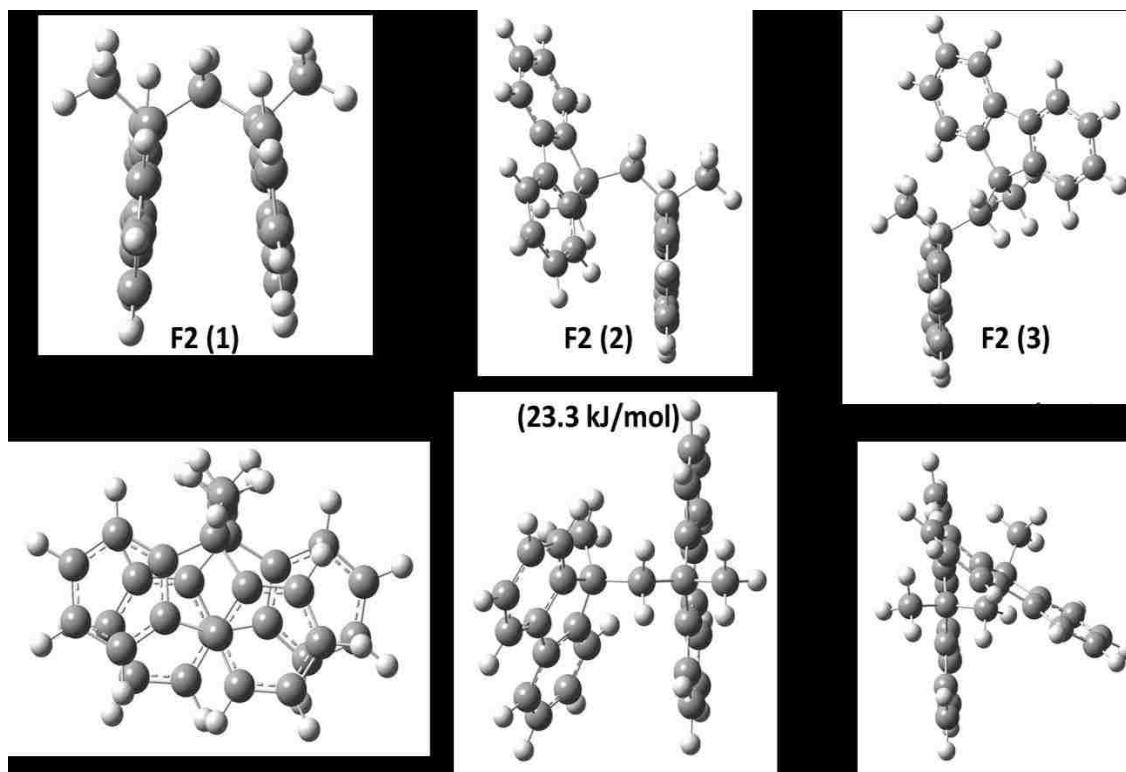
Figure 3.20: Selected geometry optimized ground-state structures of the F2 composite molecule. Potential geometry arrangements, pictured above, include either the 'closed' or 'open' conformation, with the closed option being lowest in energy.

Following the ground state optimizations, the relative energies of structures in their ground and excited states were collected. In Figure 3.21, the structures considered here are the lowest energy open conformation, the closed/staggered, and closed π-stacked conformers. Similar to the $(F)_2$ dimer, the π-stacked geometry is a maximum in the ground state due to the proximity of orbitals that are the same phase. Also similar to $(F)_2$, the π-stacked geometry is a minimum when promoted to the excited state.
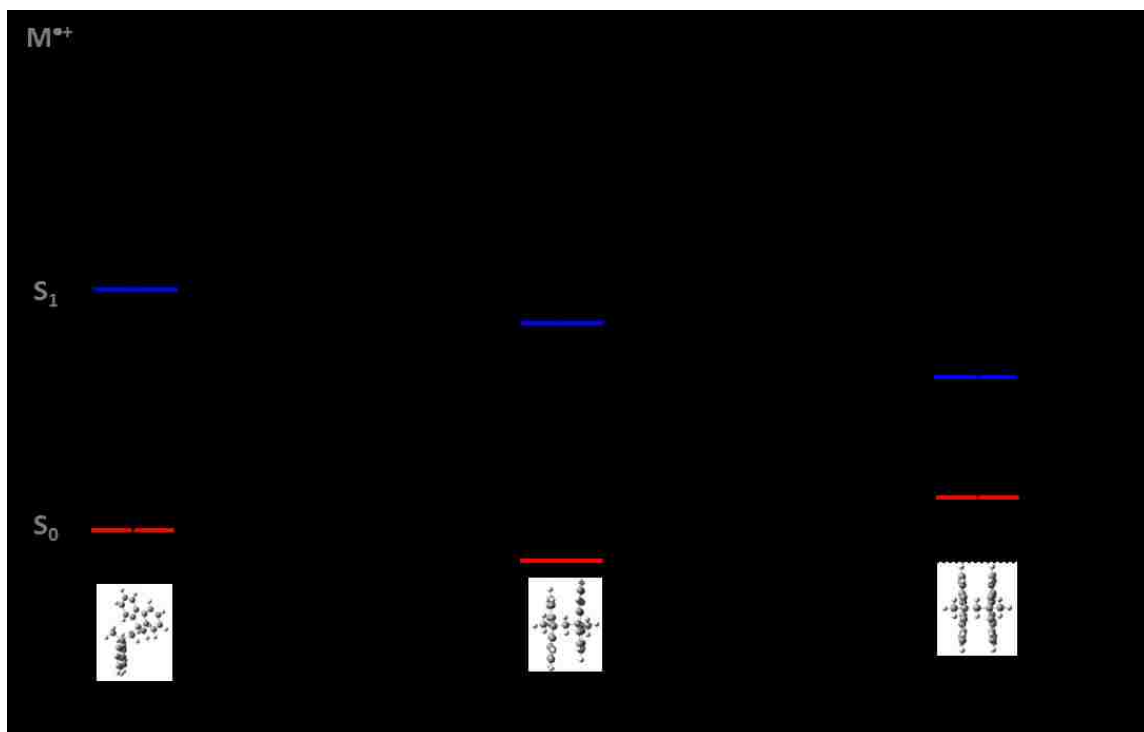
Figure 3.21: Calculated relative energies of selected conformers of the F2 composite molecule. Calculations reveal that with the methylene linker the stacked conformer is the ideal geometry in both the ground and excited states.

In the case of $(F)_2$, a rapid rearrangement of the ground state geometry to the π-stacked geometry occurred in order to form an excimer. However, F2's minimum energy in the ground state is the closed/staggered conformer. Using the same scheme as $(F)_2$, Figure 3.22 offers the mechanism for which F2 forms an excimer. The closed/staggered geometry resembles the π-stacked geometry and therefore would not require a significant rearrangement in order to form the excimer. This provides more direct access to the excimer well.

A follow-up treatment of TD-DFT calculations were completed on F2, similar to $(F)_2$. The S_1, S_2, and V_{ab} coupling constant values are shown in Tables 3.5, 3.6, and 3.7.

However, unlike $(F)_2$, we assume F2's starting geometry is the closed conformer, and therefore forms a 'pre-excimer' that has more direct access to the excimer well. Experimentally, a broad, unresolved origin feature was observed for F2. This is in good agreement with the TD-DFT results, specifically the oscillator strengths, f. In the closed conformation, the transition dipoles are in line with one another, being either additive or subtractive. This orientation would lead to excitonic intensity splitting ratios of one strong feature and one weak feature.

Table 3.5: S_1, S_2, and V_{ab} Coupling Values for F2 Open Geometry

	E, eV	E, kJ/mol	E, cm^{-1}	transition	coefficient	f
S_1	4.79	461.93	38614.51	96 ->100	-0.10971	0.1486
				98 ->100	0.39265	
				98 ->101	0.24987	
				99 ->100	-0.37141	
				99 ->101	0.23636	
S_2	4.89	471.76	39436.84	94 ->100	0.14123	0.339
				96 ->101	0.14445	
				98 ->100	-0.34571	
				98 ->102	-0.18839	
				99 ->100	-0.17804	
				99 ->101	0.42290	
				99 ->103	0.17488	
V_{ab}	0.05	4.92	411.17			

Table 3.6: S_1, S_2, and V_{ab} Coupling Values for F2 Closed Geometry

	E, eV	E, kJ/mol	E, cm^{-1}	transition	coefficient	f
S_1	4.69	452.96	37864.45	96 ->100	0.11756	0.0137
				98 ->101	0.28137	
				98 ->103	0.10025	
				99 ->100	0.59797	
S_2	4.85	467.98	39120.57	94 ->100	-0.17021	0.2343
				96 ->101	0.18380	
				98 ->100	0.28963	
				98 ->102	0.34941	
				99 ->101	0.38781	
				99 ->103	0.18008	
V_{ab}	0.08	7.51	628.06			

Table 3.7: S_1, S_2, and V_{ab} Coupling Values for F2 Stacked Geometry

	E, eV	E, kJ/mol	E, cm^{-1}	transition	coefficient	f
S_1	3.22	311.14	26009.83	99 ->100	0.70109	0.000
S_2	3.88	373.91	31257.81	96 ->100	0.20845	0.000
				99 ->101	0.65578	
V_{ab}	0.33	31.39	2623.99			
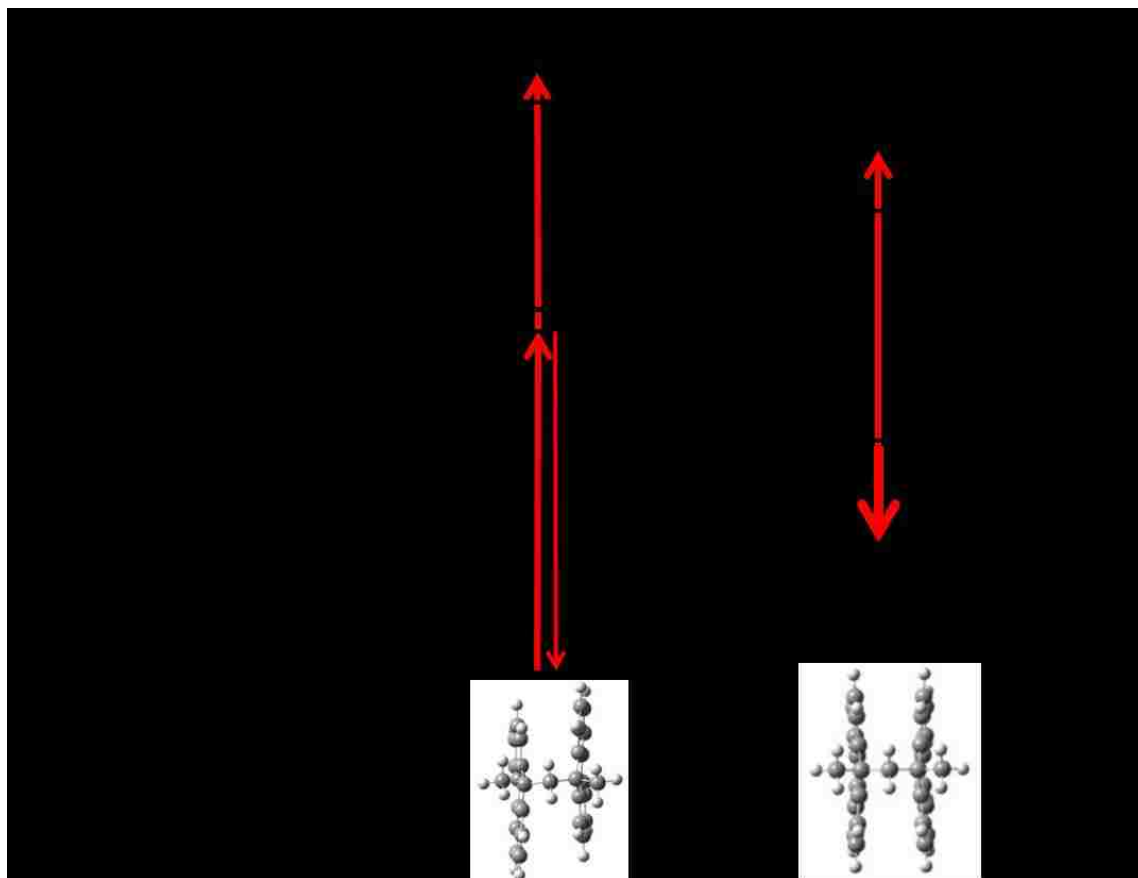
Figure 3.22: A scheme for the formation of an excimer and cation in the covalently linked F2 composite system.

The lack of a barrier to complete rearrangement to the π-stacked geometry accounts for the extended red-shifts in both the excitation and Dispersed Fluorescence spectra relative to what was found in the case of $(F)_2$. It is also assumed here that once F2 has populated the excimer well, it will not be able to return to its original geometry.

3.5   Summary

In this chapter data has been presented for detection methods by ionization and fluorescence of the $(F)_2$ vdW dimer and the F2 composite molecule.   Experiments that have been conducted on the vdW dimer of fluorene are in good agreement with results found in previous studies and publications. It was found that the spectrum of the fluorene dimer red-shifts about 200 cm^{-1} relative to the origin transition of the fluorene monomer spectrum. Using the same techniques to investigate the properties of the F2 composite molecule, F2 red-shifts about 600 cm^{-1} relative to the origin transition of the F1 monomer. The vdW fluorene dimer is already assumed to form an excimer and details about F2 indicate that it most likely forms one as well. To supplement these findings, ionization energies were also investigated for both $(F)_2$ and F2. There was a slight discrepancy in the overall lowering of the IP of these two systems; however, this was only due to the starting IP of each respective monomer. In both cases, the IP was lowered to about 7.52 eV. This is a significant lowering of the IP in both cases and shows that both of these systems can delocalize (cationic) charge efficiently. Additionally, hole-burning studies were conducted on $(F)_2$, but not F2. The HB experiments found that there was only one contributing conformer responsible for the spectral behavior associated with $(F)_2$. Due to the low resolution and overall broadness of the F2 spectra, most likely due to high vibronic activity as a result of poor Franck-Condon overlap between the ground state and excited state, HB experiments were not attempted.

Since both $(F)_2$ and F2 are assumed to form excimers, questions arose as a result of their disagreement in red-shift quantities. The difference in red-shifts between them is more than 400 cm^{-1}. Therefore, if they both presumably form excimers, and they both lower the IP to the same level, why are their excited state stabilizations significantly different? This uncertainty was able to be addressed via fluorescence experiments. Dispersed Fluorescence spectra were collected for $(F)_2$ and F2. The results agreed with previous findings showing additional stabilization in the excited state of the F2 composite molecule. The DF of $(F)_2$ and F2 showed broad, unresolved activity throughout that was located well to the red of the laser origin. These broad, red-shifted features reinforced the idea that excimers are forming in both cases. The two spectra resembled each other very well with the difference being the location of the most intense portion (peak) of the broad features. The peak of the F2 feature is located at about 400 nm, about 40 nm to the red of the peak of $(F)_2$. With that, it is clear that covalently linking the two F1 units together increased the stability of the excimer formed following electronic excitation.

The geometrical details by which F2 forms a more efficient excimer than $(F)_2$ came into question. Follow up computational studies were done to answer this question. Preliminary geometry optimization calculations were done using the M06-2X level of theory to find potential conformers for $(F)_2$ and F2. Additionally, relative energy levels for the ground and the excited states of selected geometries were calculated followed by TD-DFT calculations. Lorentzian line shapes were also fitted to portions of the $(F)_2$ spectrum, indicative of lifetime broadening. With this supplemental material, it was concluded that $(F)_2$ engages in a geometry reorganization shortly after reaching its excited state. Upon excitation, $(F)_2$ adopts a perpendicular stacked geometry, giving rise

to the complex splitting that is seen in the excitation spectrum. On the order of a picosecond timescale, the geometry is rearranged to a completely π-stacked geometry, the geometry responsible for excimer formation. Once the excimer has been formed, the dimer is then rapidly ionized from that excimer-well. F2, being covalently linked, starts in a "pre-excimer" geometry that allows for efficient access to the excimer well once it has been excited. This leads to a larger red-shift in the 2CR2PI spectrum, and an excimer profile further to the red than $(F)_2$ in the DF spectra. Wavefunction stability tests were done as a follow up to verify the stability of the minimum energy structures. Additionally, for ionic calculations, the spin operator $\langle S^2 \rangle$, expected to be 0.75 for doublets, was never different by more than 5% after spin annihilation and therefore spin contamination was not considered an issue.[98]

Our findings have been confirmed by more extensive theoretical studies carried out in the Rathore group, by Maxim Ivanov and Marat Talipov, using a benchmarked DFT method that was found to provide excellent results for the benzene dimer.[157] These theoretical studies support the conclusion that the excimeric state is stabilized in the covalently linked dimer, due to its ability to form a perfect sandwich type structure. Additionally, these studies revealed an energy barrier of about 30 kJ/mol between the tilted orthogonal and π-stacked geometries. In contrast to excimer formation, the geometrical reorganization required for hole stabilization is apparently less restrictive.

Chapter 4

The Non-Covalent F1 Dimer: Why Does Excimer Formation Not Occur?

4.1   F1 Significance and its Relevance to F2 and (F)$_2$ Excimer Formation

In the last chapter we discussed the excimer formation and hole-stabilization

properties of the vdW fluorene dimer and the F2 composite fluorene molecule. In both

cases excimer formation was observed, however, the condition by which that formation

was met varied with F2 being the optimal system for excimer formation. For each

system, the fundamental monomer used to make these bichromophoric samples is

geometrically different. The F1 molecule is a 9,9' dimethylfluorene. In previous

experiments it was shown that the addition of the two methyls, being orthogonal to the

transition dipole at the C9 position, would not dramatically alter the behavior of the

molecule and was confirmed through the similarity of the electronic spectra of fluorene

and F1 (Figure 3.3 in Chapter 3).[144] Building off of this evidence, it is interesting to

compare the results presented above with the corresponding van der Waals dimer of the

F1 molecule. Linking two F1 molecules together with a methylene bridge has proven to

be very beneficial to the formation of an excimer, but removing that geometrical

restriction and allow the F1 molecule to cluster with non-covalent interactions, would the

same (or at least similar) excimer results be observed experimentally?

4.2   R2PI spectra of the F1 dimer

The same set of experimental methods described above was used to investigate the F1 vdW dimer. In contrast to the fluorene vdW system, prior to this study nothing was known about the electronic spectroscopy of F1 and its clusters. The data collected for the dimer will be used to compare to the observations presented above for fluorene dimer and F2. Because the experimental spectrum of the dimer was unknown, we first used the mass resolving capability of 2CR2PI experimental technique to do so. Figure 4.1 displays 2CR2PI spectra of the F1 vdW dimer and monomer.

In comparison with the fluorene dimer, the spectra of the F1 vdW dimer have striking differences. First, the dimer spectrum displays a small number of very narrow features, which show no obvious evidence of lifetime broadening. These features might reflect the vibronic features of a single electronic system, the features of two split excitonic systems, or electronic band systems from different conformers. Second, in comparison with the fluorene vdW dimer, the red-shift of the F1 dimer from the monomer origin is much smaller, around 50 cm^{-1}. This means that there is not as large of stabilization in the excited (S_1) state.
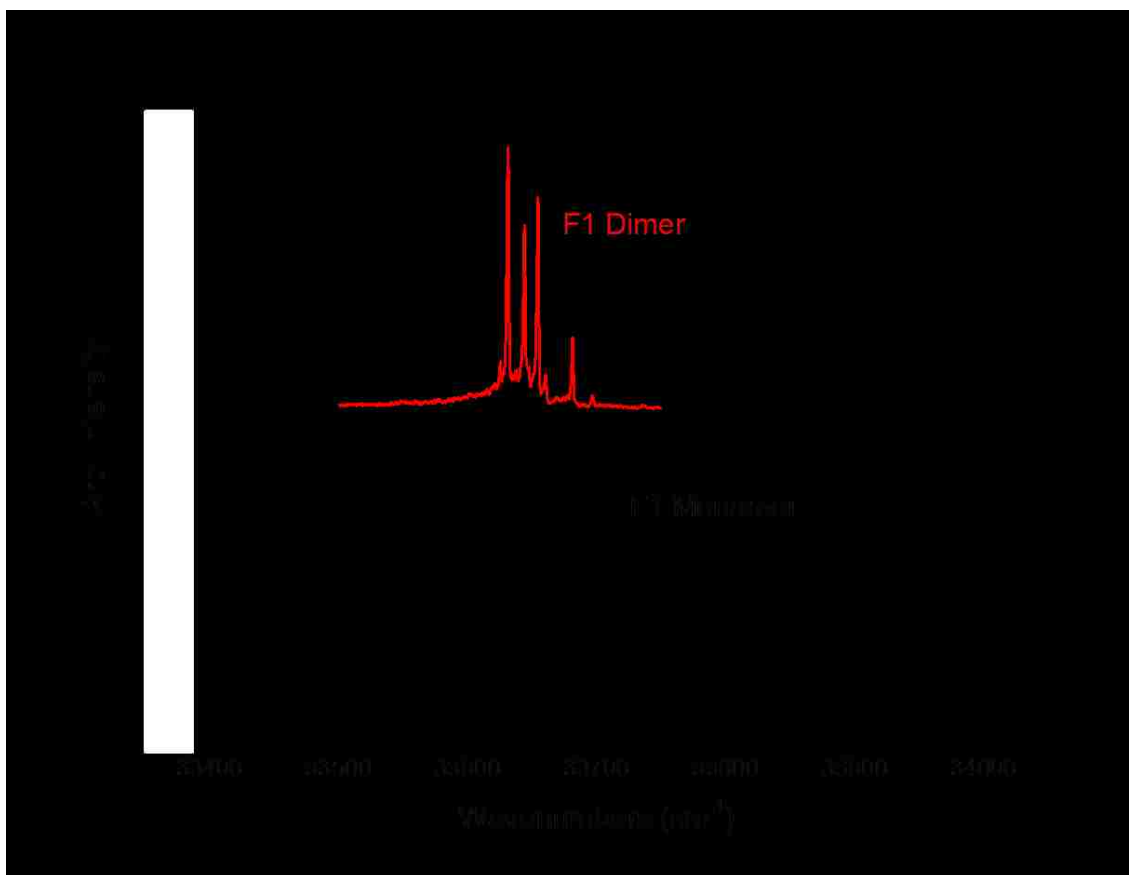
Figure 4.1: The 2CR2PI spectra for the F1 monomer (black trace) and the F1 vdW dimer (red trace). The promotion from monomer to dimer for the F1 molecule results in a small red-shift (~50 cm^{-1}) and a well resolved splitting of the origin band.

The next step in the investigation was to verify whether the splitting pattern reflected a single conformer, as found for the fluorene vdW dimer, or multiple conformers. This was accomplished through the Hole-Burning technique. Fixing the burn laser on the red-most feature in the spectrum (assumed to be the origin band), the spectrum was collected. The results of the experiment can be seen in Figure 4.2. As evident by the hole-burning spectrum, burning the lowest energy feature depletes the entire F1 dimer spectrum. This indicates the presence of a single conformer.
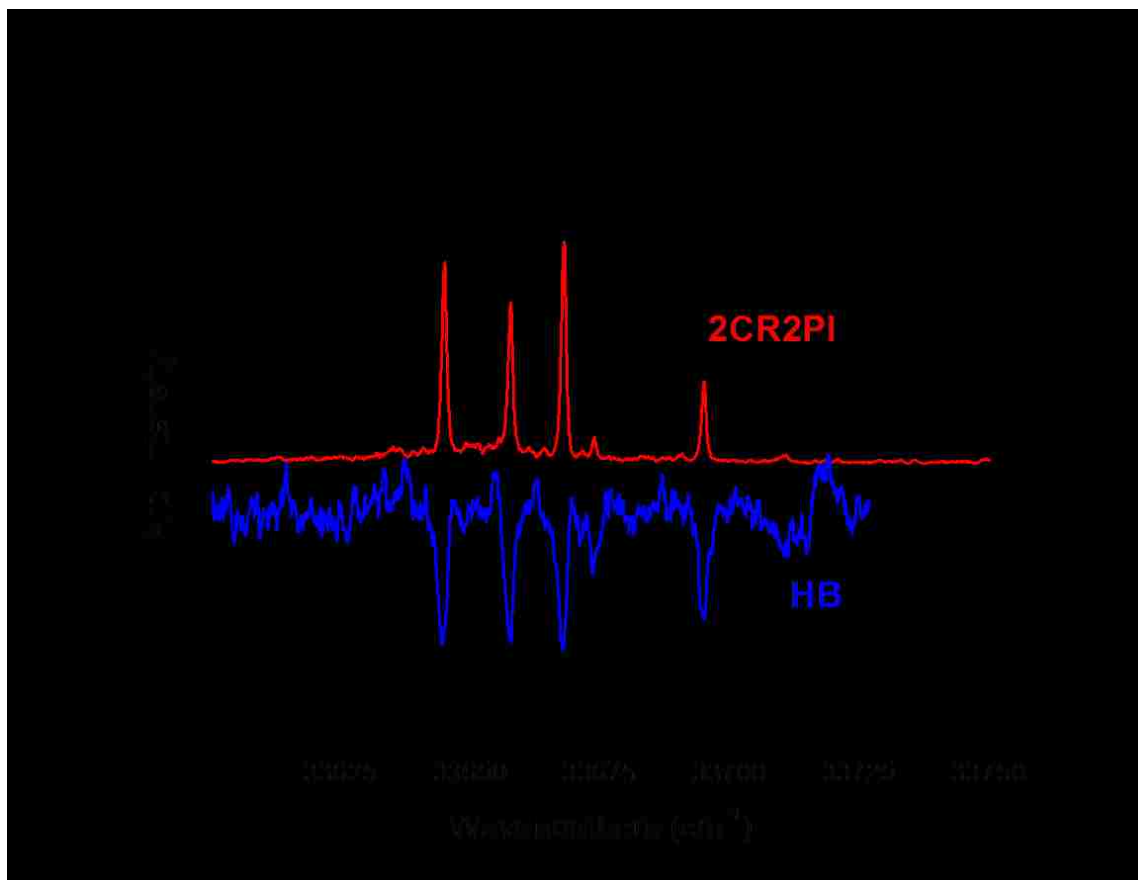
Figure 4.2: Hole-Burning spectrum of the F1 vdW dimer. The burning laser in this case is fixed at the lowest energy feature.

We next measured the ion yield curves of the F1 vdW dimer. Recall that the F1 monomer IP was 7.815 ($\pm$ 0.005) eV, which was lowered to 7.52 ($\pm$ 0.01) eV by linking two F1 molecules together. For the vdW F1 dimer, we also see a lowering of the IP with respect to the monomer, as shown in Figure 4.3. However, the F1 dimers shows a reduction in hole stabilization with respect to F2 or the fluorene vDW dimer, as the IP is lowered by only 0.24 eV, to 7.57 ($\pm$ 0.01) eV. In order to gain further insight into the nature of the F1 vdW dimer, and with the electronic spectrum well in hand, we turned to fluorescence measurements.
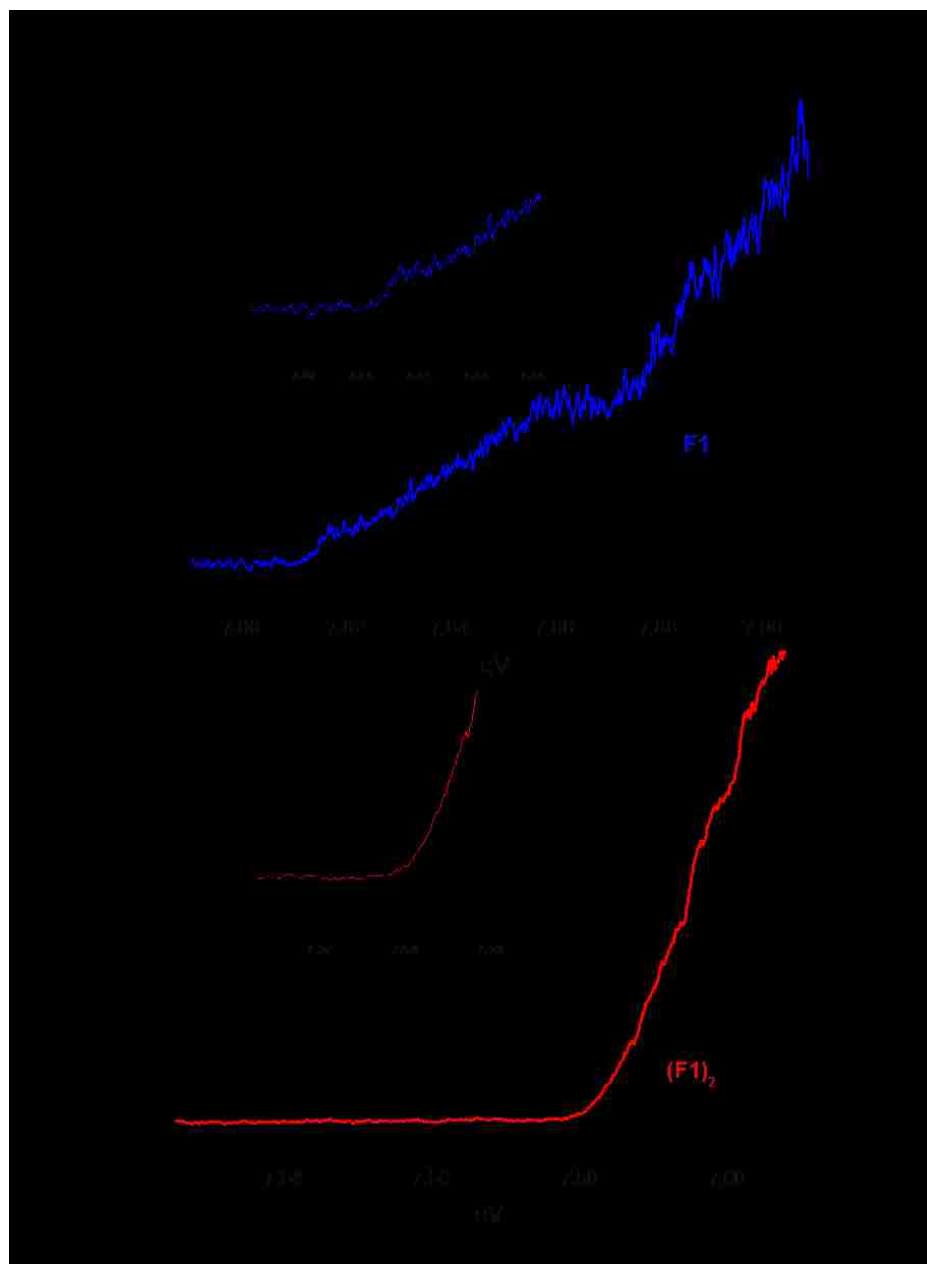
Figure 4.3: The Ionization Potentials of the F1 monomer (red) and the F1 vdW dimer (blue). The IE of the dimer is ~ 0.24 eV lower than that of the monomer.

4.3 LIF and DF Spectra of the F1 vdW Dimer

The 2CR2PI experimental spectrum showed that the electronic origin of the F1 vdW dimer was shifted only about 50 cm^{-1} relative to the monomer. This provided a potential complication to fluorescence measurements. As previously mentioned, Laser-Induced Fluorescence does not have the same mass-selection abilities of the Ionization experiments. Previously, this did not prove to be an issue due to the fact that (F)$_2$ and F2 electronic band systems were red-shifted from their respective monomers by at least 200 cm^{-1}. However, despite the smaller splitting, LIF measurements of the F1 vdW dimer were successful.

The LIF spectrum of the F1 monomer and dimer is shown in Figure 4.4, where they are compared with results from 2CR2PI spectroscopy. From the figure we can see that the F1 monomer and dimer spectrum were both reproduced using LIF techniques. The spectral features did prove to be close to one another; however, their proximity was sorted by adding the corresponding 2CR2PI spectra to the trace for comparison. Once this was done, due to the good resolution of both the monomer and dimer, the LIF spectrum could be separated. The same well-resolved, resonant features that were seen in the ionization experiments are seen in the total LIF experiments. The LIF spectrum is slightly broader than the 2CR2PI spectrum, which may be a result of residual power broadening.
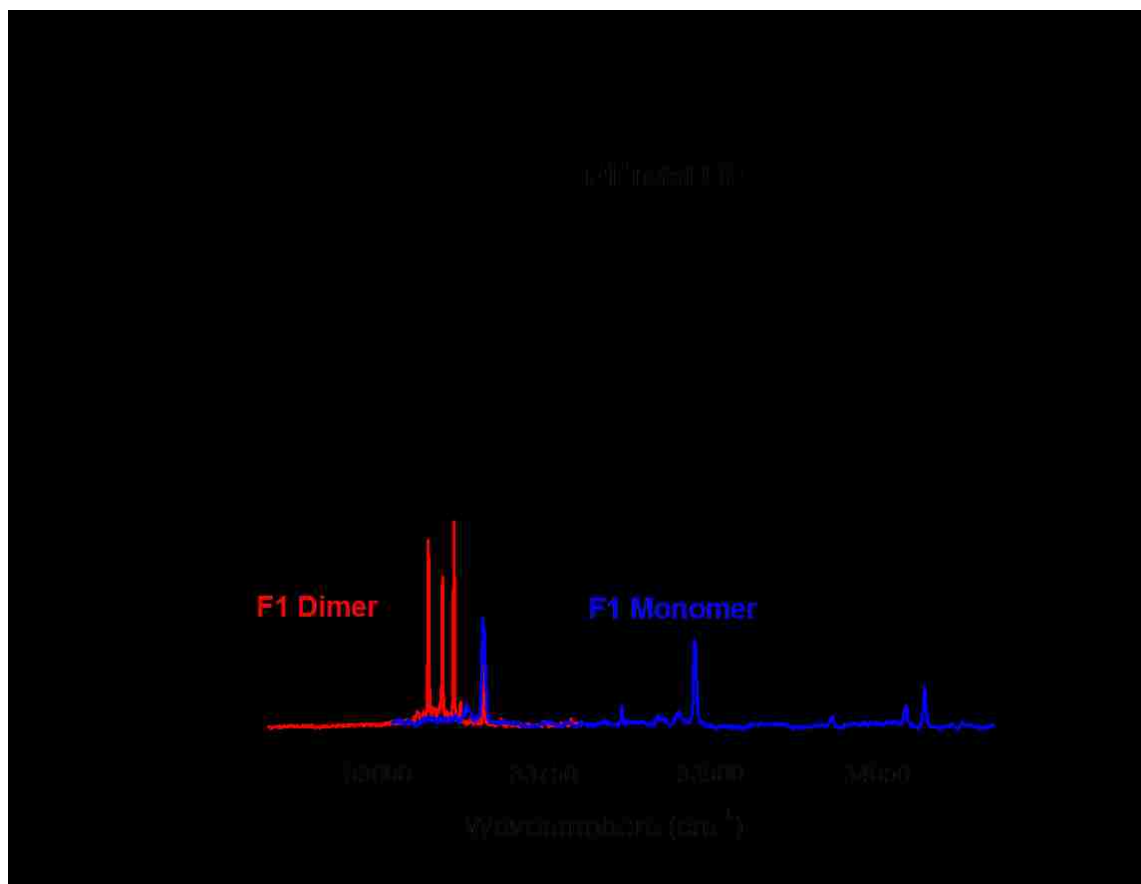
Figure 4.4: The Total LIF spectrum (black trace) of the F1 molecule compared to the monomer (blue trace) and dimer (red trace) 2CR2PI spectra.

In order to probe for possible excimer formation, and also to further explore the assignment of features in the electronic spectrum of the F1 vdW dimer, we turned to DF spectroscopy. First, a high resolution (2400 l/mm grating) DF spectrum was collected using the reddest feature (lowest in energy) of the dimer spectrum as the excitation wavelength, 594.68 nm. The results of the experiment can be seen in Figure 4.5. The corresponding DF for the F1 dimer turns out to exhibit well resolved vibronic structure, with no hint of the broad, red-shifted excimeric emission seen in the cases of $(F)_2$ and F2.

This suggests that, upon electronic excitation, the F1 vdW dimer does <u>not</u> form an excimer. The presence of a highly structured DF spectrum provides a wealth of information on the ground state vibrational energy levels, which will be discussed in more detail below.

A DF spectrum of the low energy region was obtained by narrowing the slits the in the monochromator in the hopes of achieving even better resolution. This revealed extensive torsional structure, which is helpful in two aspects. First, it aids in assigning the conformer, as we describe in further detail below. Second, it aids in assigning the sharp features in the excitation spectrum, as to whether the spectrum reflects a single electronic system or two split excitonic systems. Additional DF's were taken of features to the blue of the putative electronic origin, at excitation wavelengths of 594.45 and 594.27 nm. In each case, as shown in Figure 4.6 and Figure 4.7, the resulting DF's show enhanced Franck-Condon activity in the low frequency vibrational modes. This is consistent with the excitation of vibrationally excited states, as opposed to another electronic origin. Thus, the DF spectra are consistent with an electronic spectrum exhibiting excitations to a single electronic state of a single conformer.
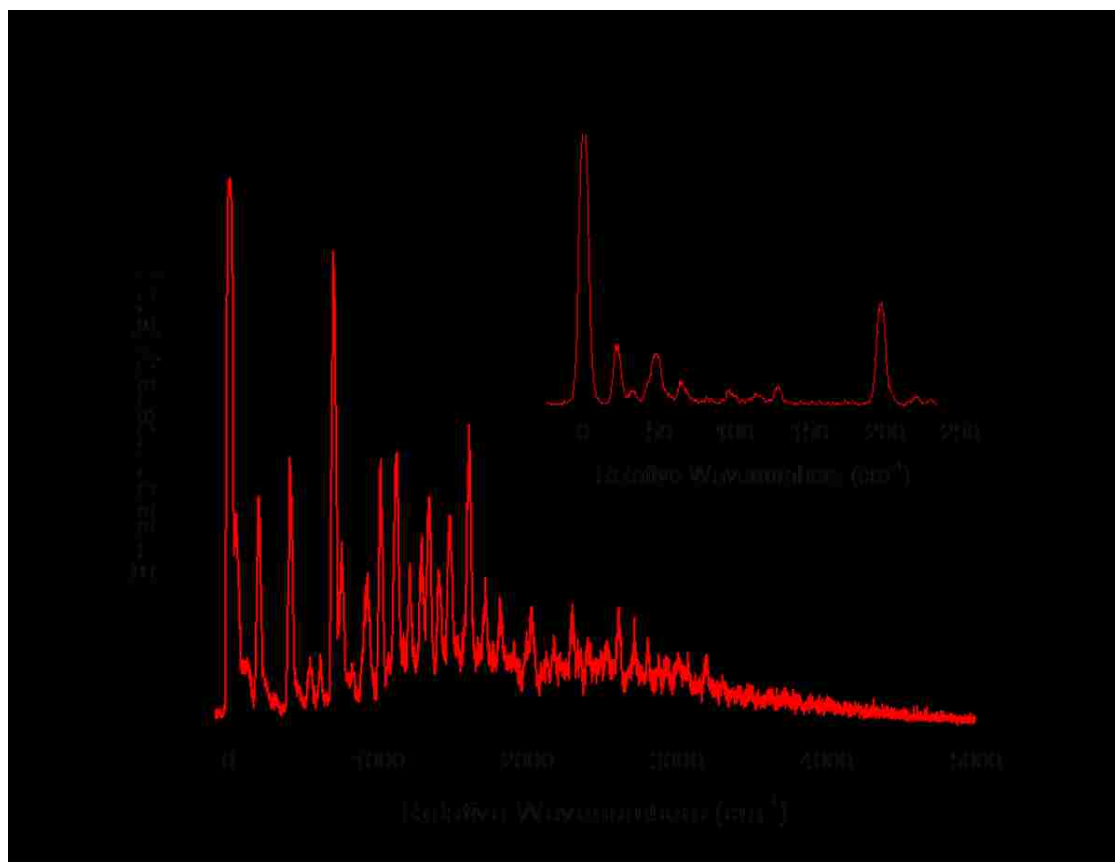
Figure 4.5: Dispersed Fluorescence spectrum of F1 vdW dimer, excited at 594.68 nm.
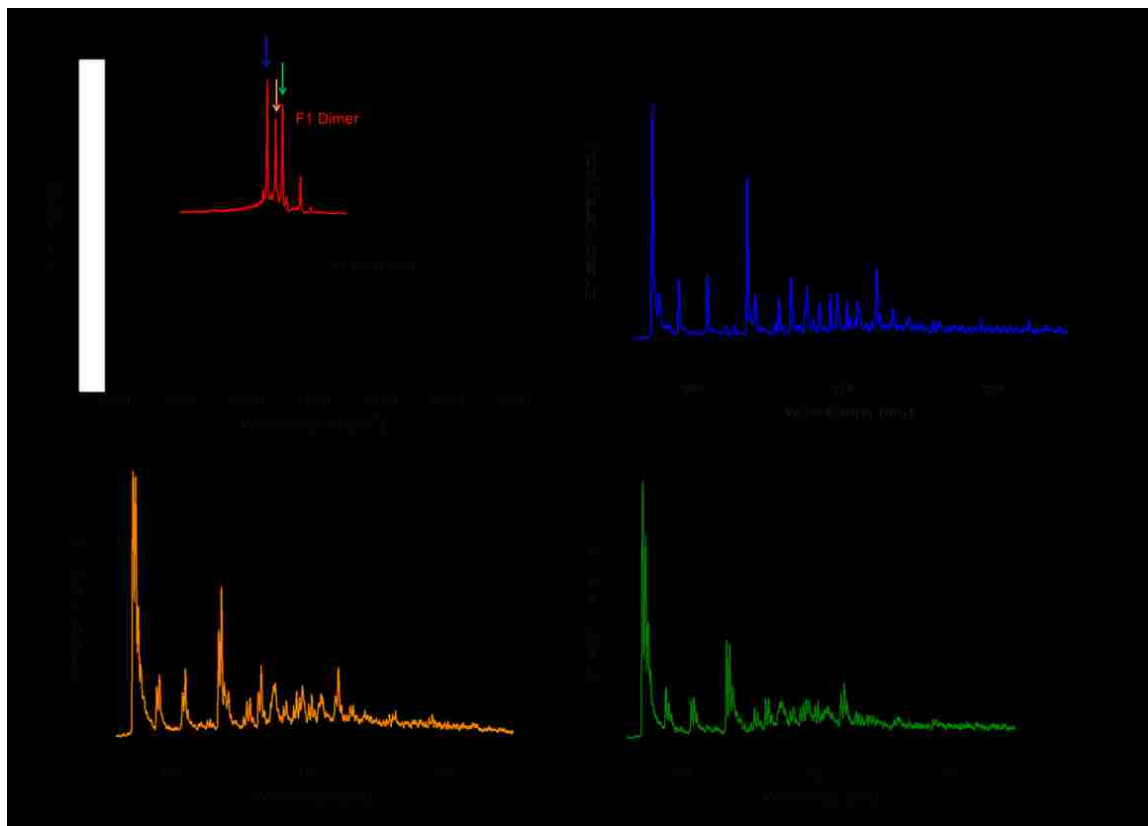
Figure 4.6: Dispersed Fluorescence spectra of all three 'origin peaks' seen in the original 2CR2PI spectrum. Features of specific excitation wavelength are indicated by colored arrows and their corresponding DF spectra.
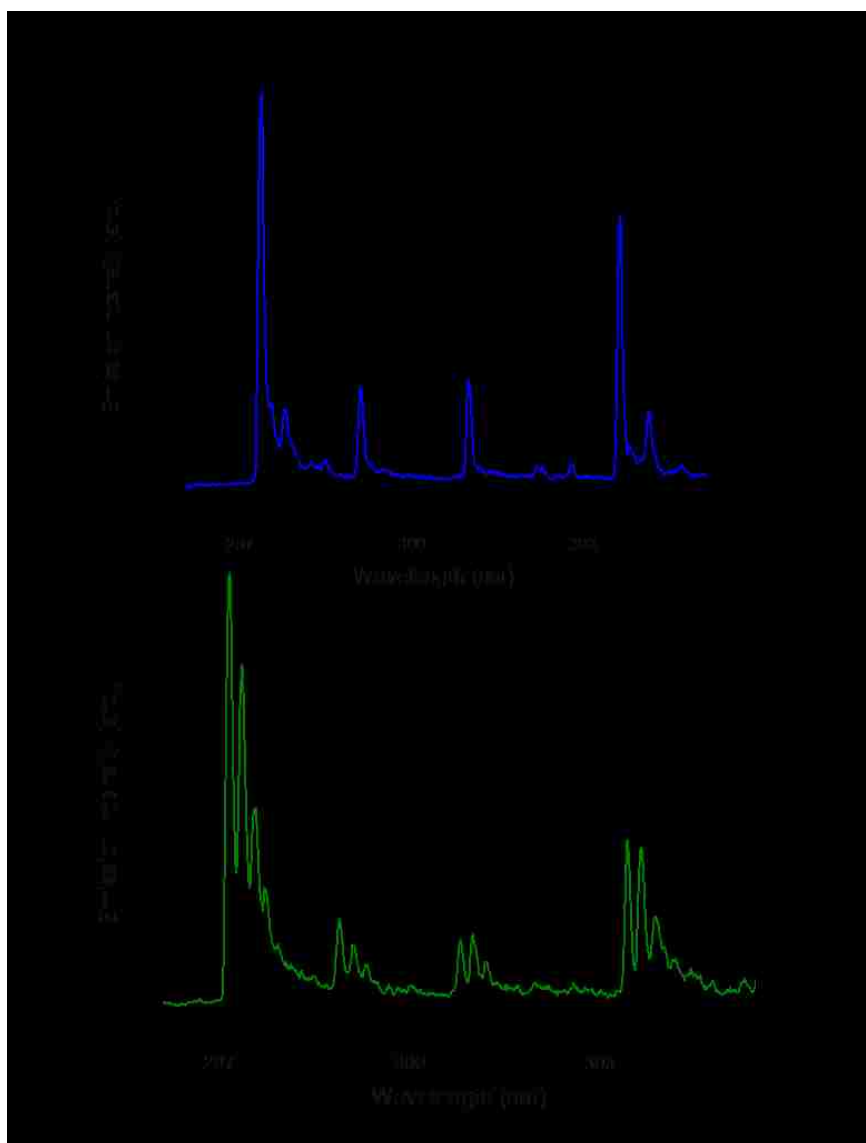
Figure 4.7: Dispersed Fluorescence spectra demonstrating the torsional motion of the methyl groups in F1 dimer.

4.4   Lack of Excimer Formation in the F1 vdW Dimer

The data presented above suggests that the electronic spectrum of the F1 vdW dimer contains transitions corresponding to a single electronic band system of a single conformer. In elucidating the structure of that conformer, several facts are helpful to consider. First, we expect a second excitonic system to be present; however, it must be weak in intensity, which suggests that the alignment of the chromophores in the dimer might be parallel, or nearly so. Second, the lack of excimeric emission suggests that this dimer cannot easily form an excimeric state upon excitation, which may signal either that the excimeric minimum is less pronounced or that a barrier to excimer formation exists which cannot be accessed from the vibrationless level.

To gain further insight, we carried out computational studies of the dimer. Using the same optimization methods as that previously employed for $(F)_2$ and F2, multiple minimum energy structures in the ground state were found for the F1 vdW dimer. Selected minimum energy structures of the F1 dimer and their binding energies are shown in Figure 4.8. In addition to a pi-stacked conformer, conformers displaying significant C-H/pi interaction are found. The conformers with minimal π-interactions have the lowest binding energy and can vary by more than 20 kJ/mol.
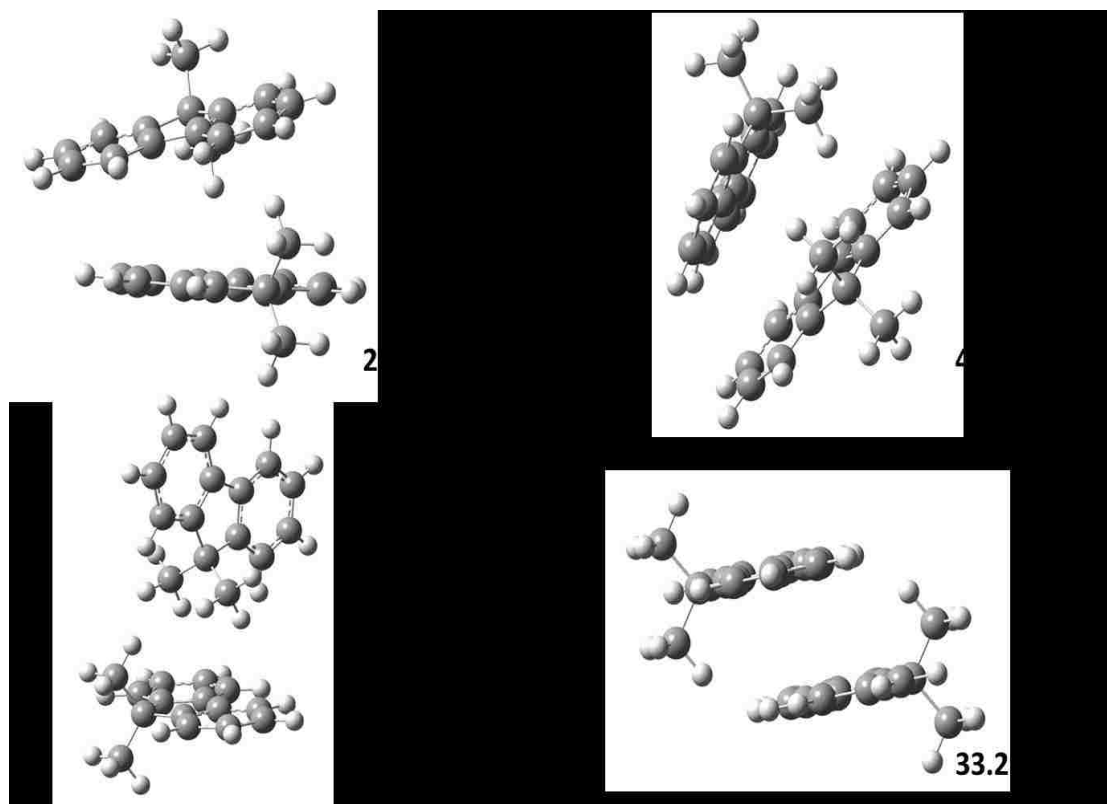
Figure 4.8: Selected minimum energy ground state structures and their binding energies for the F1 vdW dimer. The selection varies from multiple π interactions and CH/π interactions with the stacked conformers being the lowest in energy.

Using the geometries from the minimum energy structure outputs of the F1 dimer, frequency calculations in the ground state were performed to attempt to match the estimated frequency values (Table 4.1) from the high resolution experimental DF spectrum. We can attempt to match the lowest energy vibrational frequencies using the calculated values from the optimized minimum energy structures (Table 4.2). Calculated frequencies are close to experimental but no exact matches occur.

Assignment	Exp. Avg. Freq.
$\omega 1$	22
$\omega 2$	33
$\omega 1 + \omega 1$	44
$\omega 3$	48
$\omega 1 + \omega 2$	56
$\omega 1*3$ or $\omega*2$	65
$\omega 4$	84
$\omega 3 + \omega 3$	97
$\omega 3 + \omega 3 + \omega 1$	115
$\omega 3 + \omega 3 + \omega 2$	129

Table 4.1: Observed frequencies and assignments for the F1 dimer. Observed frequencies are taken from the DF spectrum of $(F1)_2$.
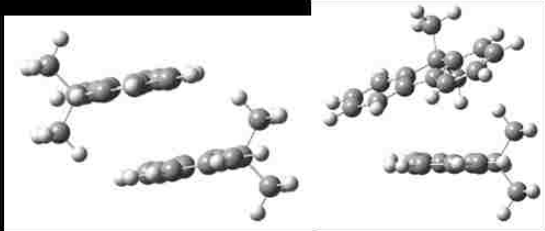
Theo. Freq. 1	Theo. Freq. 2	Theo. Freq. 3	Theo. Freq. 4	Theo. Freq. 5
13	31	8	25	11
20	37	18	32	23
29	47	27	51	35
54	65	43	59	42
59	67	47	77	58
67	84	61	83	72
90	99	88	84	88
95	115	91	118	104

Table 4.2: Theoretical ground state frequencies for F1 vdW dimer.

Despite the fact there are no exact matches, two geometries are very close to the predicted frequency values, shown in Table 4.3. Both the parallel displaced and 'diagonal' F1 dimer structures match the assigned fundamental frequencies fairly well. These two geometries take advantage of π-interactions. In order to determine which conformer is more likely, a TD-DFT treatment similar to prior experiments was completed. Relative energies of the diagonal and parallel displaced were calculated in the ground and excited state (Figure 4.9). Additionally, a more π-stacked geometry was optimized in the excited state, similar to the stacked conformations of $(F)_2$ and F2. In the

ground state, the diagonal conformer is the minimum, while the stacked conformer is the

minimum in the excited state.

Assignment	Experimental Freq.	Theoretical Freq.	Theoretical Freq.
ω1	22	24.86	--
ω2	33	32.04	30.93
ω1 + ω1	44		37.26
ω3	48	50.51	46.77
ω1 + ω2	56	59.22	64.57
ω1*3 or ω*2	65	76.63	67.29
ω4	84	83.03	83.97
ω3 + ω3	97	83.93	98.92
ω3 + ω3 + ω1	115	118.21	115.08
ω3 + ω3 + ω2	129	128.17	126.52

Table 4.3: Experimental frequencies compared to the theoretical frequencies from the stacked and diagonal F1 dimer optimized ground state geometries.

Similar to the relationship between the F2 closed and stacked conformer, the parallel

displaced geometry would seem to serve as the 'pre-excimer' geometry for the stacked

conformer.
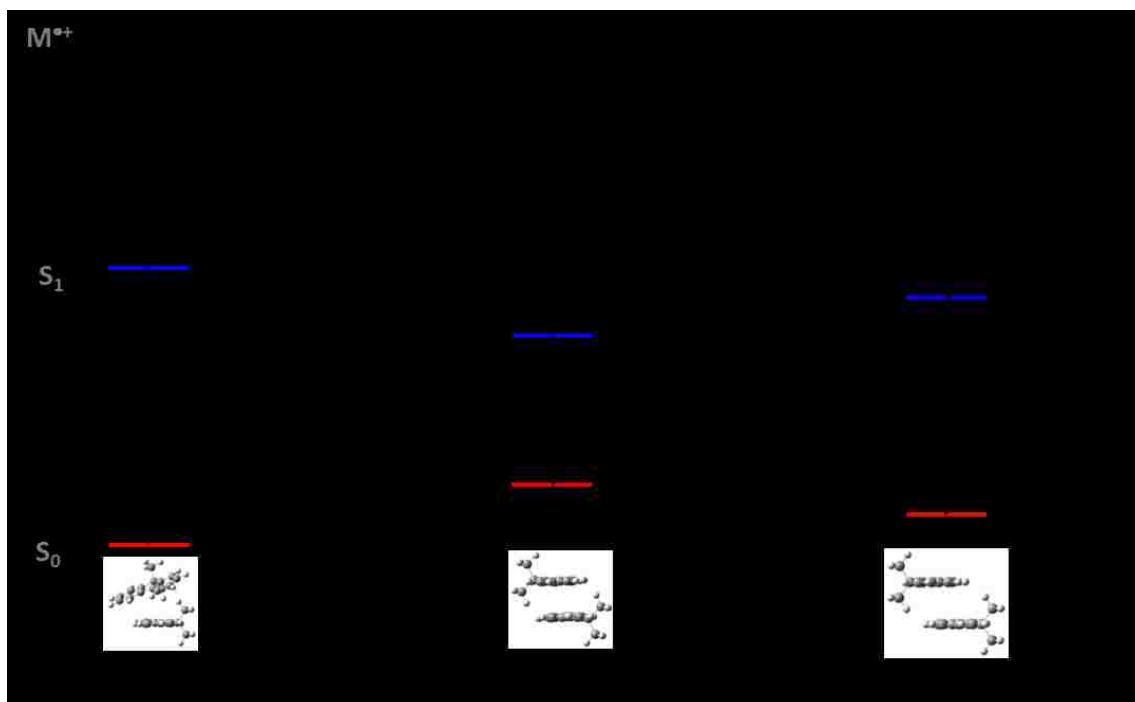
Figure 4.9: Relative energies of the parallel displaced, diagonal, and stacked F1 dimer geometries in the ground, excited, and ionic state.

TD-DFT calculations were also done on the F1 dimer similar to those done on $(F)_2$ and F2. The results are shown in Tables 4.4, 4.5, and 4.6. Shown in the calculations is similar to what was previously observed.

Table 4.4: S_1, S_2, and V_{ab} Coupling Values for F1 Dimer Diagonal Geometry

	E, eV	E, kJ/mol	E, cm^{-1}	transition	coefficient	f
S_1	4.77	460.09	38461.54	99 ->105	-0.10119	0.1218
				101 ->106	-0.11835	
				103 ->106	0.28336	
				104 ->105	0.59544	
S_2	4.85	468.11	39131.29	99 ->106	-0.12273	0.2721
				101 ->105	-0.16572	
				103 ->105	0.49196	
				103 ->107	0.16581	
				104 ->106	0.3467	
				104 ->108	-0.15649	
V_{ab}	0.04	4.01	334.87			

Table 4.5: S_1, S_2, and V_{ab} Coupling Values for F1 Dimer Parallel Displaced Geometry

	E, eV	E, kJ/mol	E, cm^{-1}	transition	coefficient	f
S_1	4.56	439.79	36763.35	103 ->106	0.18983	0.00
				104 ->105	0.65501	
				104 ->108	0.10134	
S_2	4.84	466.55	39001.56	99 ->106	0.14793	0.3121
				100 ->105	-0.18614	
				103 ->105	0.21751	
				103 ->108	0.13647	
				104 ->106	0.50865	
				104 ->107	0.28852	
V_{ab}	0.13	13.38	1119.10			

Table 4.6: S_1, S_2, and V_{ab} Coupling Values for F1 Dimer Stacked Geometry

	E, eV	E, kJ/mol	E, cm^{-1}	transition	coefficient	f
S_1	3.54	341.23	28524.16	104 ->105	0.69846	0.00
S_2	4.16	401.39	33553.67	101 ->105	0.1452	0.0271
				103 ->109	-0.1024	
				104 ->106	0.6063	
				104 ->107	-0.28851	
V_{ab}	0.31	30.08	2514.76			

This scenario is reminiscent of the rearrangement $(F)_2$ can undergo to form an excimer. However, in the case of F1 dimer, there seems to be a barrier that it cannot overcome to rearrange to form an excimer, demonstrated in Figure 4.10. This barrier must be larger than the barrier $(F)_2$ overcomes to form the excimer, and must be due to the steric effects introduced by the addition of the methyl groups.
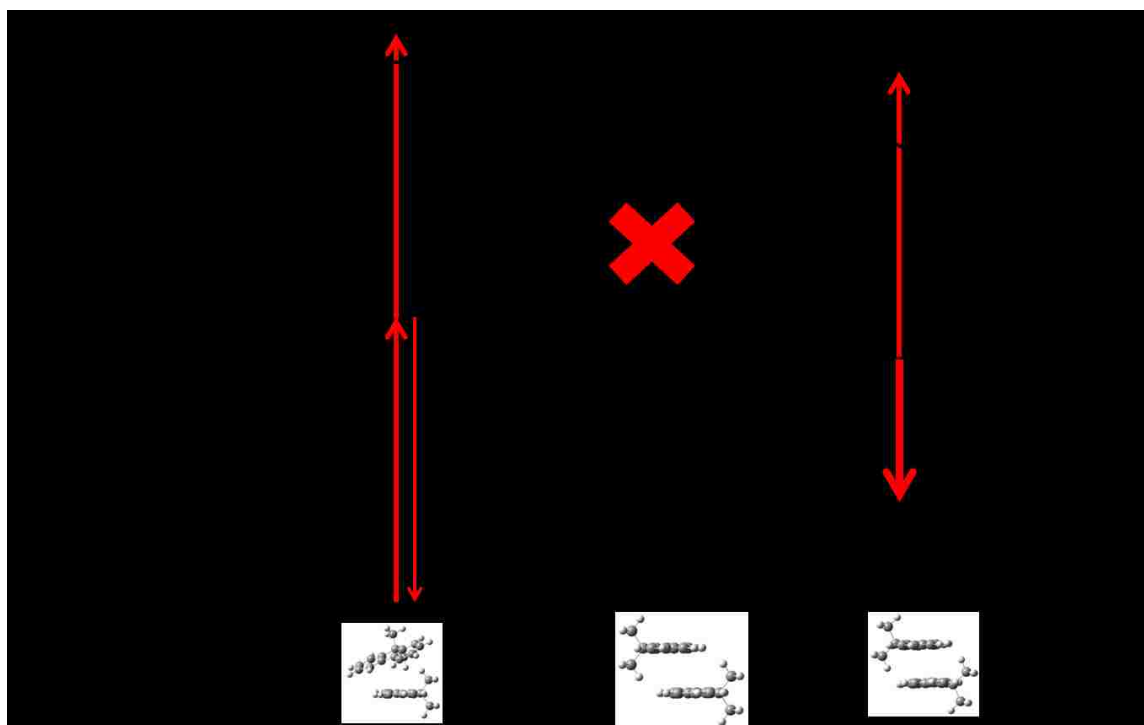
Figure 4.10: Schematic representation of F1 dimer's inability to form an excimer.

4.5   Summary

In the previous chapter, we showed that the geometrical requirements for excimer vs. hole stabilization were more restrictive. The results presented in this chapter for the F1 vdW dimer is consistent with that hypothesis. Here we find that excimer formation does not occur, while hole stabilization still occurs, albeit to a reduced degree. Experimental results show a minimally red-shifted dimer origin, relative to the observed red-shift in $(F)_2$ and F2. Additionally, well-resolved, resonant excited state spectra are observed with both ionization and fluorescence techniques, as well as resolved emission via Dispersed Fluorescence. The experimentally observed frequencies from the DF agree with the theoretical frequencies of multiple optimized structures: the diagonal and parallel displaced conformers. Relative energy and TD-DFT calculation revealed that the parallel displaced conformer is capable of forming an excimer upon excitation, lowering its energy by 43.63 kJ/mol by adopting a more π-stacked conformation. Although it is unclear which may be the contributing conformer, it is apparent that the addition of methyl groups at the 9-H position provides enough steric hindrance to increase the barrier for excimer formation in the excited state, preventing it from occurring.

Chapter 5

More Complex vdW and Covalently Linked Fluorene Clusters

5.1   Exploring More Complex Fluorene Systems

Up to this point, the systems that have been studied have been no larger than two fluorene units. F2, (F)$_2$, and (F1)$_2$ all contain two fluorene or fluorene derived subunits. Previous studies indicated that both F2 and (F)$_2$ show excimer like behavior (with F2 being the better choice of the two), while all three appear to have hole-stabilizing properties when transformed into the cationic state. As a consequence to these studies, one can ask the question, is it possible to stabilize energy and charge even further with clusters of a larger size?[145] Previous studies have shown that this might not necessarily be the case.[146,147] One might assume that covalently linking more fluorene units together would further stabilize the excited state. However, theoretical results show that there might be a phenomena known as a 'reorganization penalty' that presents itself as the systems get larger.[148,149] This penalty increases linearly along with the size of the molecular chain and directly competes with the delocalization of energy across the system. Previous solution phase studies have shown that a red-shift occurs from fluorene monomer to the covalently linked F2, in the same way it does in this gas-phase study, but does not shift by any significant amount up to F6. It would be beneficial to investigate the behavior of these molecules in the gas-phase due to the isolation of the sample. In the gas-phase one does not need worry about packing structures or solvent effects.

Additionally, the geometric uncertainties become larger as cluster sizes increase, especially in non-covalent systems. With the aid of Dr. Rajendra Rathore and his lab, larger and sterically hindered molecules have been synthesized in the hopes that some of these uncertainties can be eliminated. Using F1 as an inspiration, these molecules were designed with the motivation of being able to force clusters into a specific geometry using their own structure as a guide. Additionally, fluorene units have also be covalently linked using cyclohexane as a bridge.[151] This provides a more rigid linker between fluorene subunits, eliminating their ability to change geometry when promoted to the excited or ionic state.

5.2   Increasing complexity in covalently linked systems: F3 vs F2

In previous chapters, it has been demonstrated that $(F)_2$ and F2 can form excimers as well as stabilize electron holes.   However, could it be possible to increase the stabilizations of excimer formation and charge delocalization by adding more fluorene subunits? To test this, larger systems were designed and examined using the same techniques previously described for consistency. Covalently, systems containing more than two subunits were examined, more specifically, F3.[134] Using 2CR2PI, a spectrum was collected for the trichromophoric F3, shown in Figure 5.1. In the figure, the spectrum of F3 is compared with F1 and F2. The F3 spectrum is very similar to that of F2, with the appearance of an additional weaker band at lower energy.

The shoulder on the red side of the most intense feature in the F3 spectrum is roughly 450 cm^{-1} to the red of the most intense F3 feature at about 32990 cm^{-1}. Further experiments were done on these two features to investigate their energetic properties. First, ion yield spectra were measured to obtain the respective IPs . With the excitation laser fixed to their respective wavelengths (~605 nm for the intense feature and ~613 nm for the red-shifted "shoulder") the ion yield curves were collected and are shown in Figure 5.2.
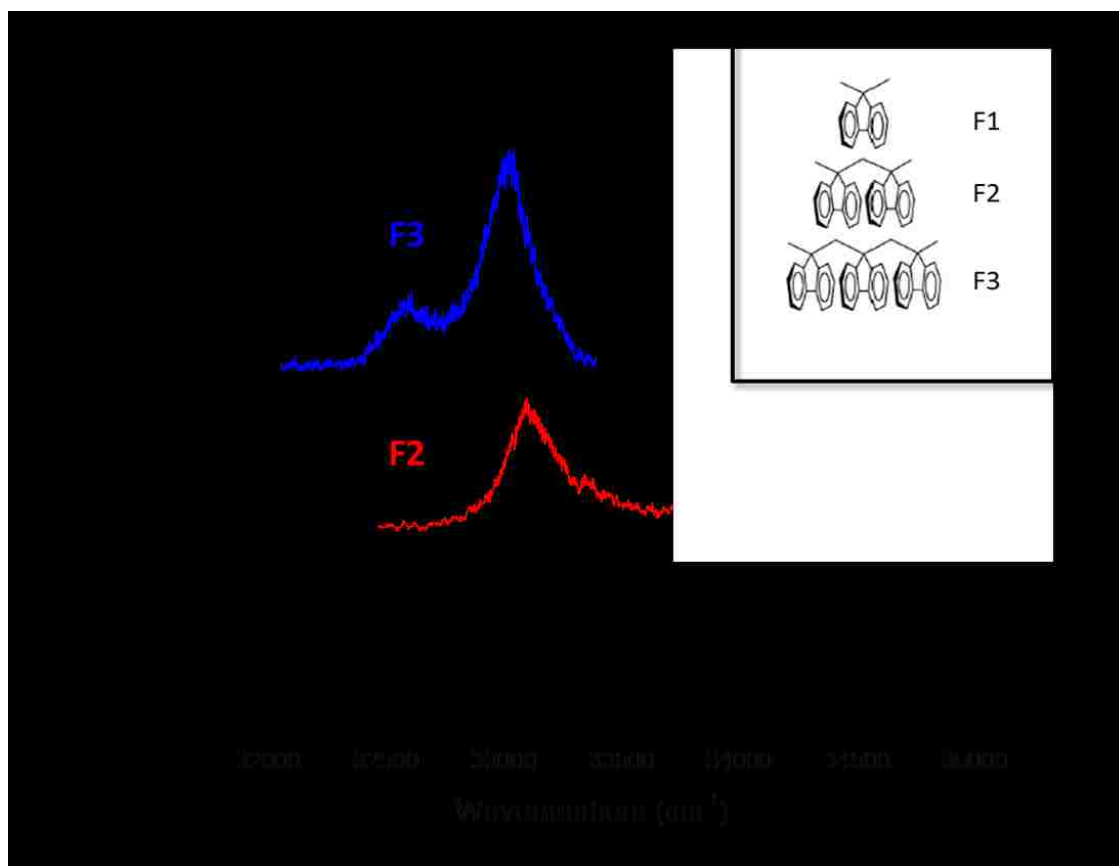
Figure 5.1: 2CR2PI spectra of the F1, F2, and F3 molecules.
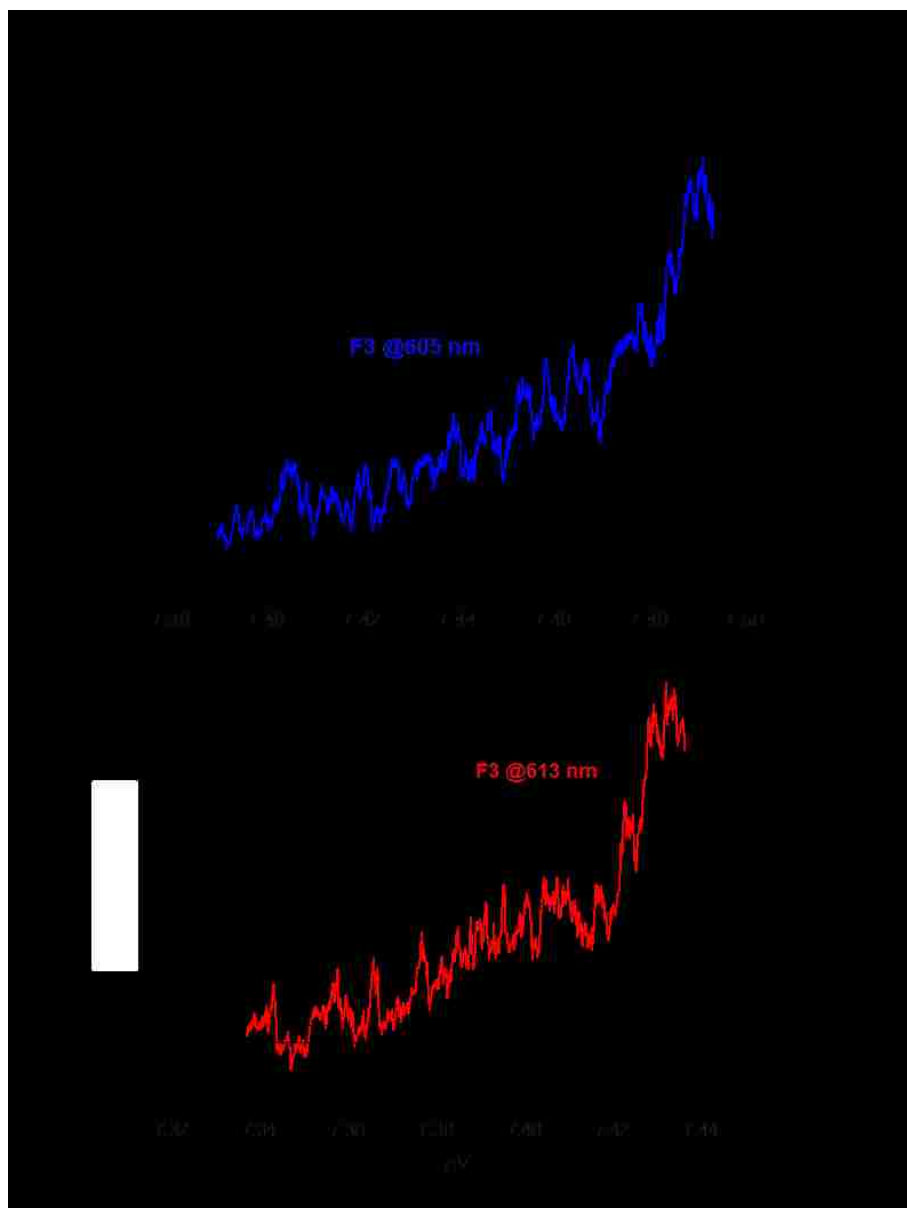
Figure 5.2: The Ionization Potentials for F3 at two different excitation wavelengths, 605 (blue trace) and 613 nm (red trace).

The data in Figure 5.2 shows that there is a small difference between the two ion curves. When fixing the laser to 605 nm, the more intense of the two features in the 2CR2PI spectrum, the IP of the sample is around 7.40 eV. On the other hand, when fixing the excitation laser to 613 nm, the IP of the sample is about 7.34 eV. As multiple conformers are not expected in this system, this difference may be attributed to split excitonic components which access to slightly different regions of the cationic PES. In both cases, however, there is an additional lowering of the IP from the value observed for F2 (7.52 eV).

With the excitation spectrum in hand from the mass-resolved experiments, fluorescence experiments were conducted next. First, an excitation spectrum of F3 was collected using LIF. The resulting spectrum, plotted up against the original 2CR2PI spectrum, is shown Figure 5.3. The same intense feature and red-shifted shoulder can be found in the LIF spectrum; however, here the shoulder was weaker in comparison. As we expect the true intensities to be more accurately reflected in the LIF experiment, this may suggest that the 2CR2PI experiment overestimated the strength of this feature.

Dispersed Fluorescence was then used to investigate the excimer formation and the stabilization of the excimeric state in F3. First, the excitation laser was fixed to the more intense feature at about 605 nm. The resulting DF spectrum is shown in Figure 5.4, plotted against the F2 DF for comparison.
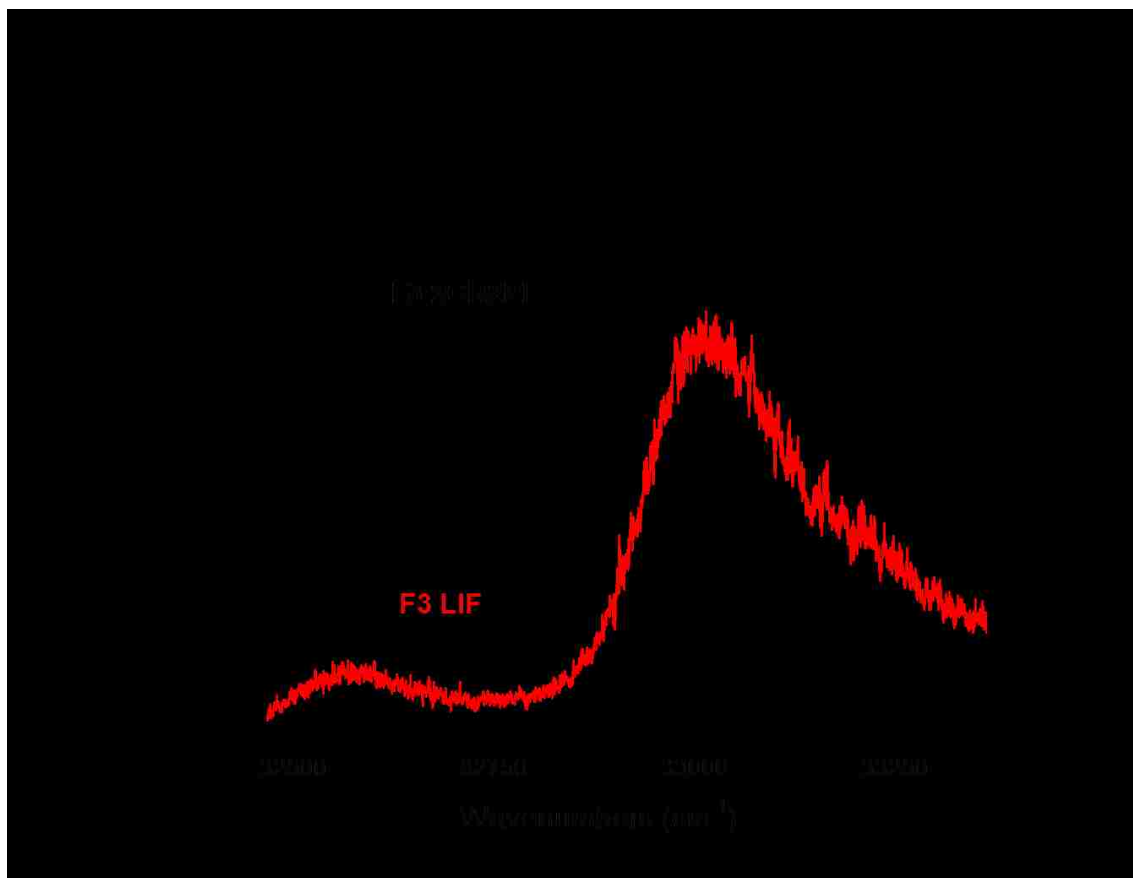
Figure 5.3: A comparison of the 2CR2PI and total LIF spectra of F3.
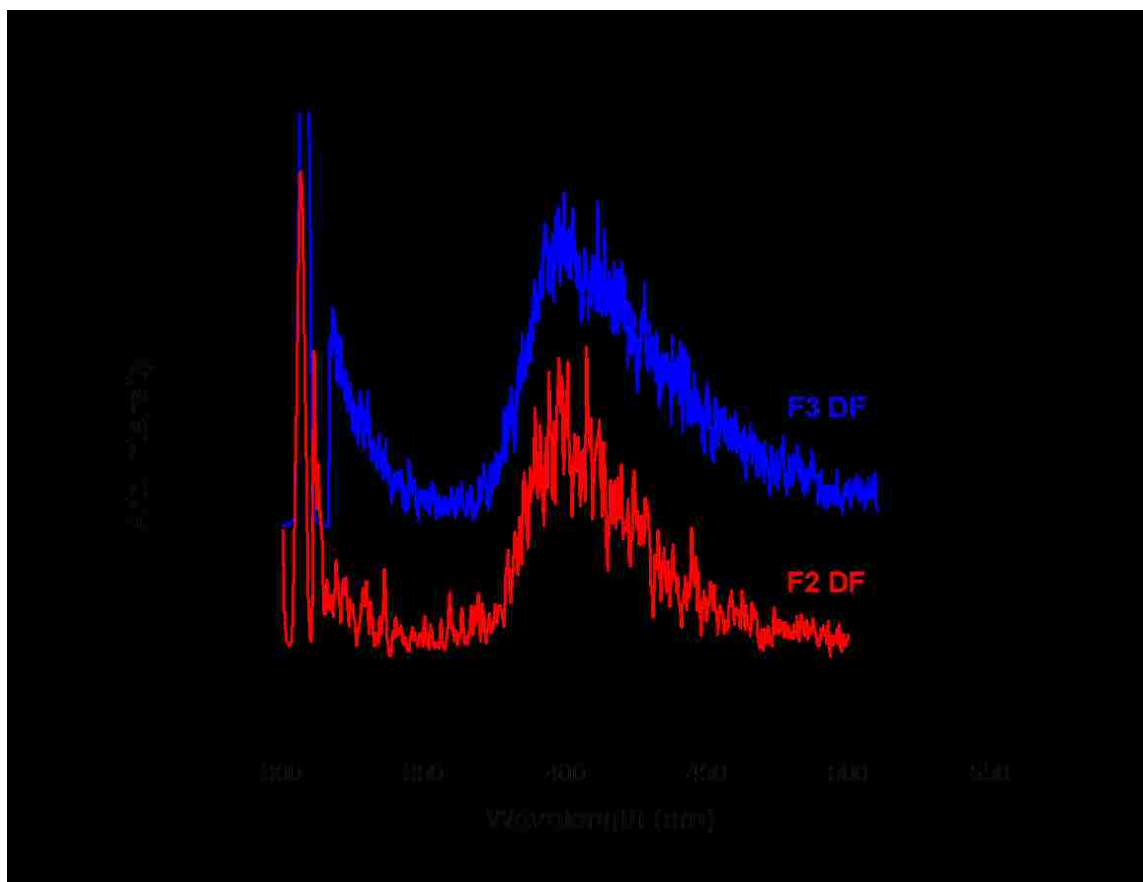
Figure 5.4: The Dispersed Fluorescence spectrum of F3 molecule at 605 nm compared with the previously discussed F2 molecule.

From Figure 5.4, it can be seen that the DF of F3 is essentially identical to that of F2. As discussed earlier, F2 forms an excimer efficiently due to the ability to form a perfect sandwich structure. Therefore, while F3 also forms an excimer upon electronic excitation, the presence of a third fluorene subunit does not assist in further stabilization of the excimeric state.

To investigate further the red-shifted shoulder, a DF was attempted and is shown in Figure 5.5. As the fluorescence appeared with very low intensity, the resulting DF was very noisy; however, the appearance is overall very similar to that obtained following excitation of the higher energy feature.

Experimental results have shown that F3 does not provide any additional stabilization of the excited state; however, a strong excimer is still formed similar to F2. Therefore, even though the π-stacked assembly has been lengthened, and the range over which energy and charge can be delocalized, the 'reorganization penalty' significantly competes with the system and completely offsets it making it no more efficient than F2. Theoretical studies have demonstrated that F3 with the excimer localized on two fluorene subunits is lower in energy than F3 where the excimer is delocalized along all three fluorenes in a completely π-stacked conformation.[146] Additionally, when measurements were taken of F1 and F2, there was a significant lengthening of the lifetime, from about 15 ns to nearly 60 ns. Lifetime measurements of the F3 composite molecule show an excited state lifetime of 50 ns. This is on the order of a lifetime extension similar to that of F2. It has already been demonstrated that F2 forms an excimer, and therefore, it can be concluded that the similarities in DF's and lifetime extensions indicate excimer

formation in F3 as well. This is in good agreement with previous solution-phase

experimental and theoretical studies done.[147]
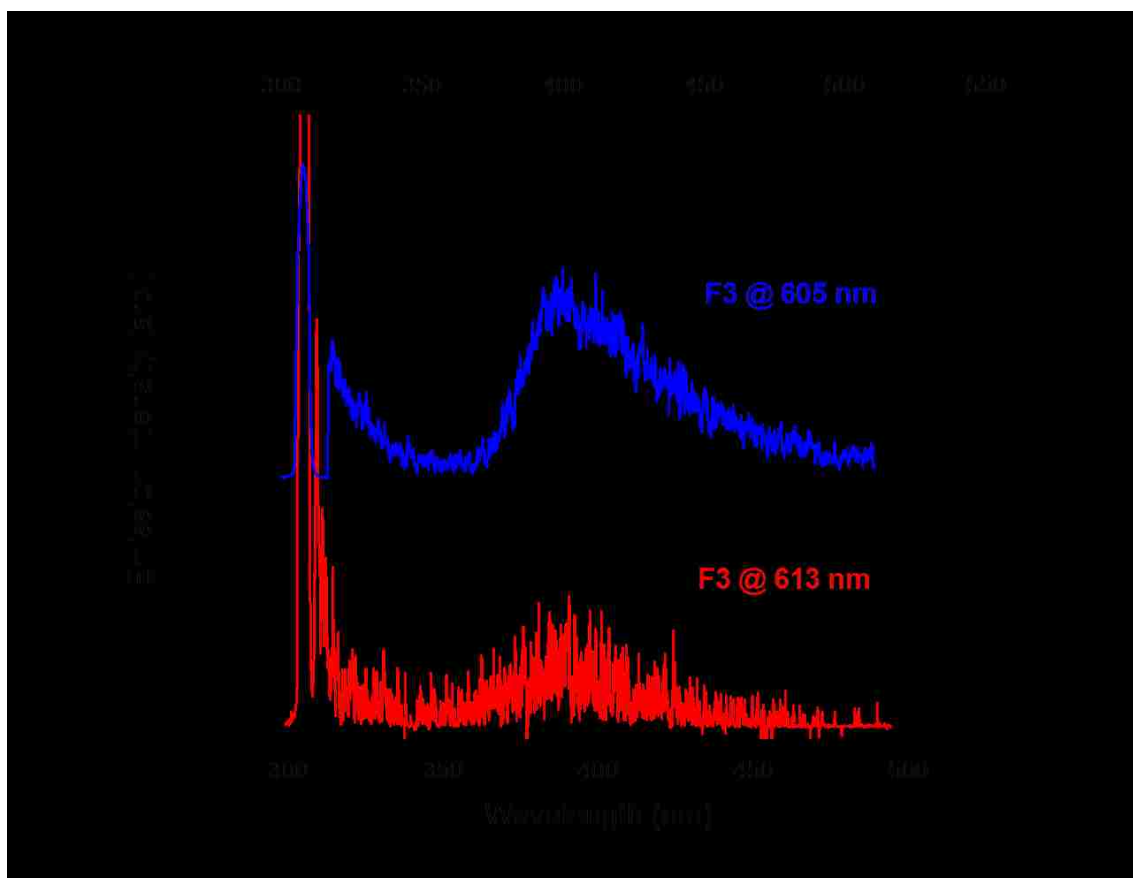
Figure 5.5: Dispersed Fluorescence spectrum of the less intense 613 nm feature.

Calculations were conducted in order to help with analysis of possible structures. Featured in Figure 5.6 are ground-state minimum energy structures that were found using the M06-2X method. Previously, with F2, the choice of structure was either open or closed. With the addition of a third fluorene sub-unit, more conformers are possible with combinations of open and closed geometries. The completely stacked conformer for F3 is the lowest energy relative to all other conformers, similar to what was seen before with F2. Now presented with these results, we cannot rule out the possibility that the lowest energy (reddest) feature represents a second conformer. The ion yield curves showed a slightly lower IP with the feature at about 613 nm. The shoulder, therefore, could resemble the completely π-stacked conformation, while the intense feature at 605 nm could be the hybrid open/closed conformer. This shows that an electron hole could be further stabilized without a reorganization penalty.
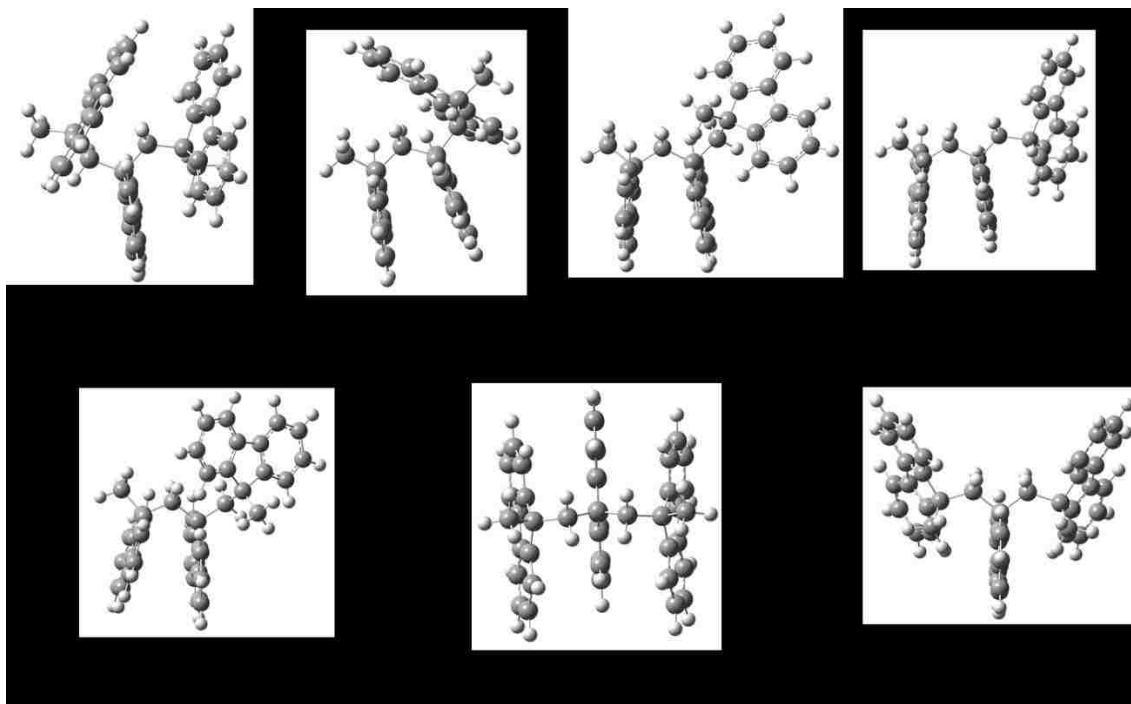
Figure 5.6: Optimized ground state structures of F3 with relative energies.

5.3   Increasing complexity: Fluorene vdW Clusters

After looking at larger covalently linked systems, higher order vdW clusters were investigated. The 2CR2PI spectra of fluorene vdW clusters up to n=6 can be found in Figure 5.7. As discussed earlier, there is a large red-shift from monomer to dimer, about 200 cm^{-1}. Similar to what was seen with F3, there is no significant red-shift of the origin transitions of any of the higher order clusters. As the clusters increase in size, the most intense feature of the spectra continue to shift more to the red, but never by the amount that was seen from monomer to dimer, with the difference between n=2 and n=6 being no more than 50 cm^{-1}. Additionally, it appears that the spectra do not shift at all until the cluster size reaches n=5. At this size, the spectra become very broad with no resolvable features. This is not surprising, as the number of potential conformers is very high.[156] Therefore from the 2CR2PI data, the vdW fluorene clusters seem to follow the same trend as the covalently linked conformers, being unable to stabilize the excited state any further.

Following the 2CR2PI experiments, the Ionization Potentials for cluster up to n=6 were also collected. The most intense features in the spectra were used as the excitation wavelengths for the data collection. Previously stated, there was no additional stabilization of the excited state, however, the IP of the sample was lowered. The vdW fluorene clusters follow a similar trend and are able to lower the IP as well. In Figure 5.8 the IP of the clusters decrease by at least 0.09 eV with every fluorene addition, except from the pentamer and hexamer whose IP's appear to be identical. This is expected due

to the high number of potential conformers, making it likely that the additional fluorenes

are unable form an orientation that can help further delocalize the electron hole.
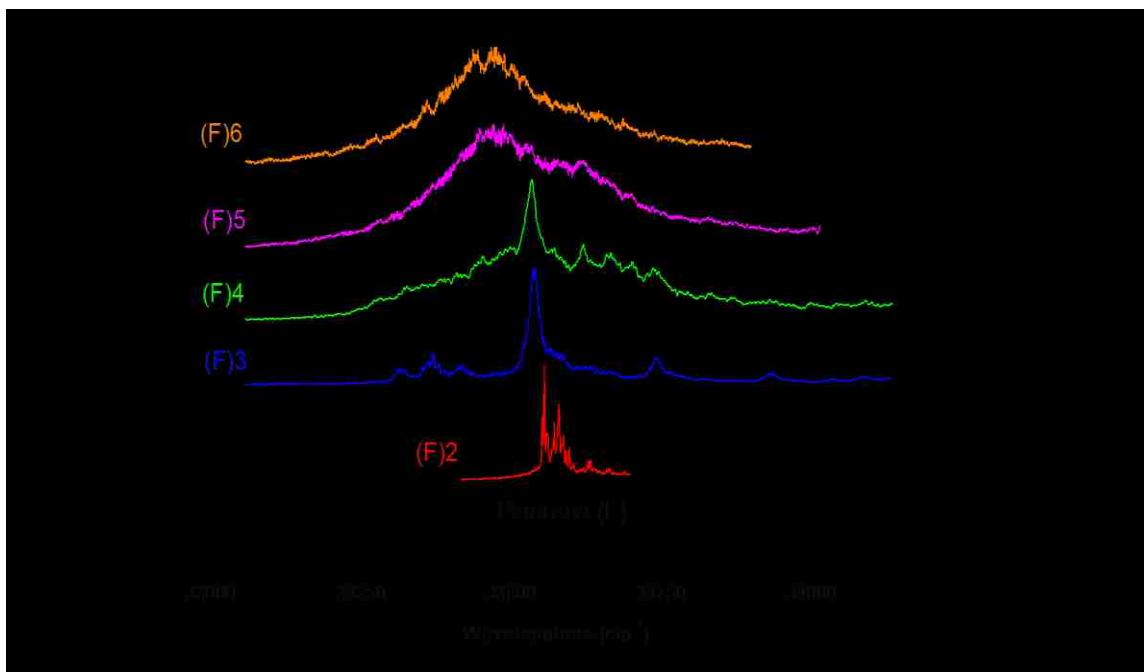
Figure 5.7: The 2CR2PI spectra series for the vdW clusters of fluorene up to n=6, where n is the number of fluorenes present.
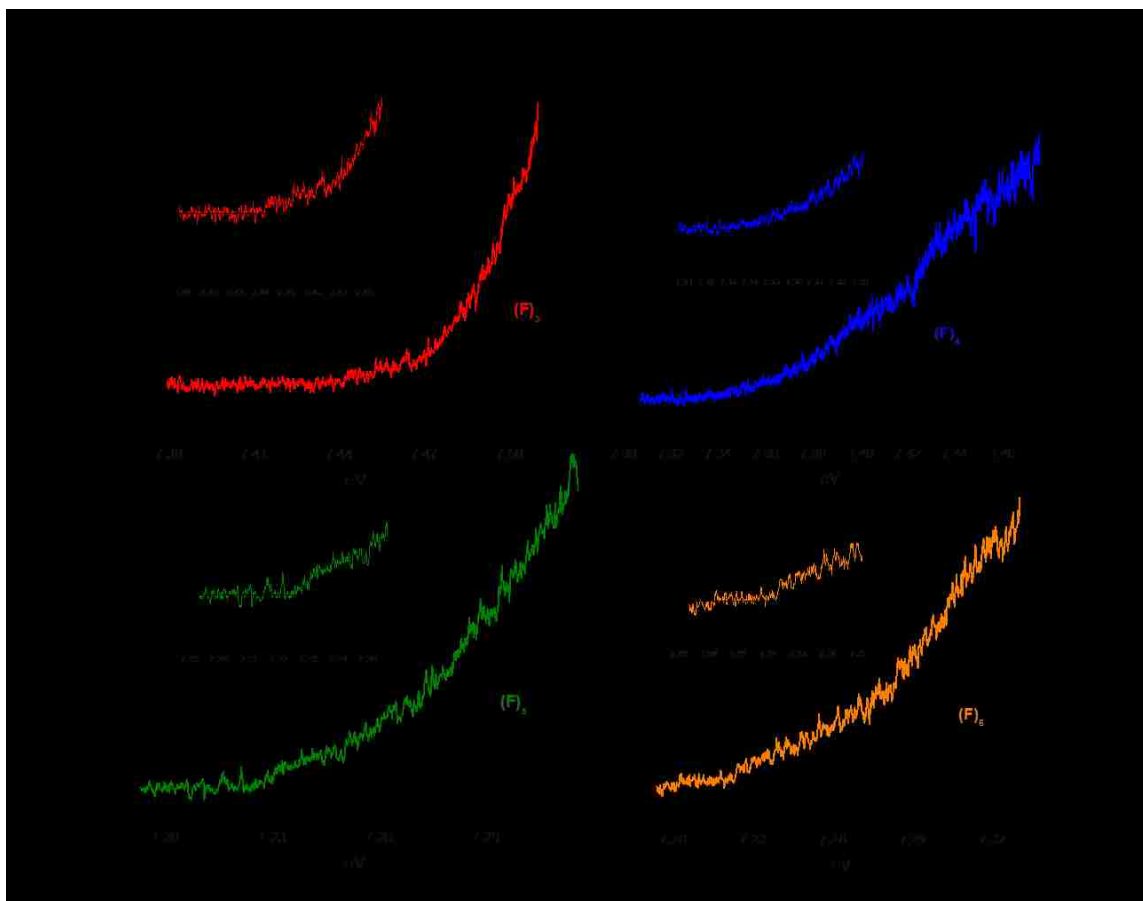
Figure 5.8: Ionization potentials of fluorene vdW clusters n=3-6, where n is the number of fluorenes.
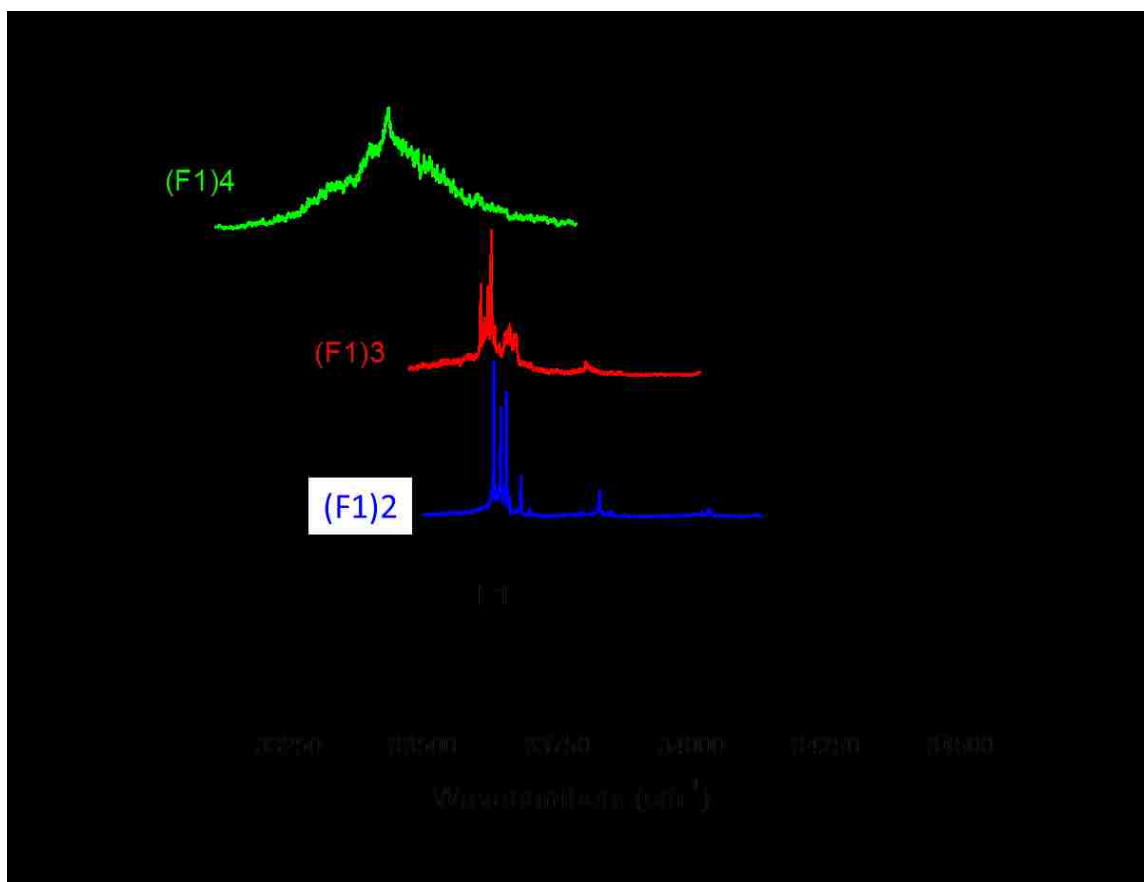
Figure 5.9: 2CR2PI spectra of F1 vdW cluster n=1-4 where n is the number of F1 units present.

Lastly, higher order vdW F1 clusters were examined. It has already been demonstrated that F1 cannot stabilize the excited state due to the steric effects caused by methyl groups at the 9H position. On the other hand, F1 dimer demonstrated that the requirements for electron hole stabilization are more relaxed than the requirements for excimer formation. Figure 5.9 shows the results of the 2CR2PI experiments of cluster size up to n=4. The F1 trimer is very similar to the F1 dimer, showing the same inability to form an excimer. However, when the cluster reaches size n=4, there is a sizeable red-shift relative to the other F1 clusters. Again, many different conformers are possible, giving rise to the overall broadness, but the most intense feature of the spectrum appears about 200 cm^{-1} the red of the dimer and trimer origins.

The Ionization Potentials were collected following 2CR2PI experiments. Figure 5.10 features the IP of the trimer and tetramer, which are lowered as expected. From dimer to trimer, the IP is lowered from 7.58 eV to about 7.41($\pm$0.01) eV. This emphasizes the exclusivity between excimer formation and electron hole stabilization. However, when promoted to tetramer status, the IP does not change significantly, decreasing by only 0.03 eV to 7.38 ($\pm$0.01).

In conclusion, the higher order clusters demonstrate the inability to further stabilize the excited state due to the reorganization penalty. However, there does not appear to be a penalty to electron hole stabilization, as ion yield curves continue to decrease as cluster size grows. However, the limit appears to be clusters greater than n=5. The F1 vdW clusters further demonstrated that the criteria for excimer formation are not the same as electron hole stabilization, as it continued to lower its IP up to a tetramer.
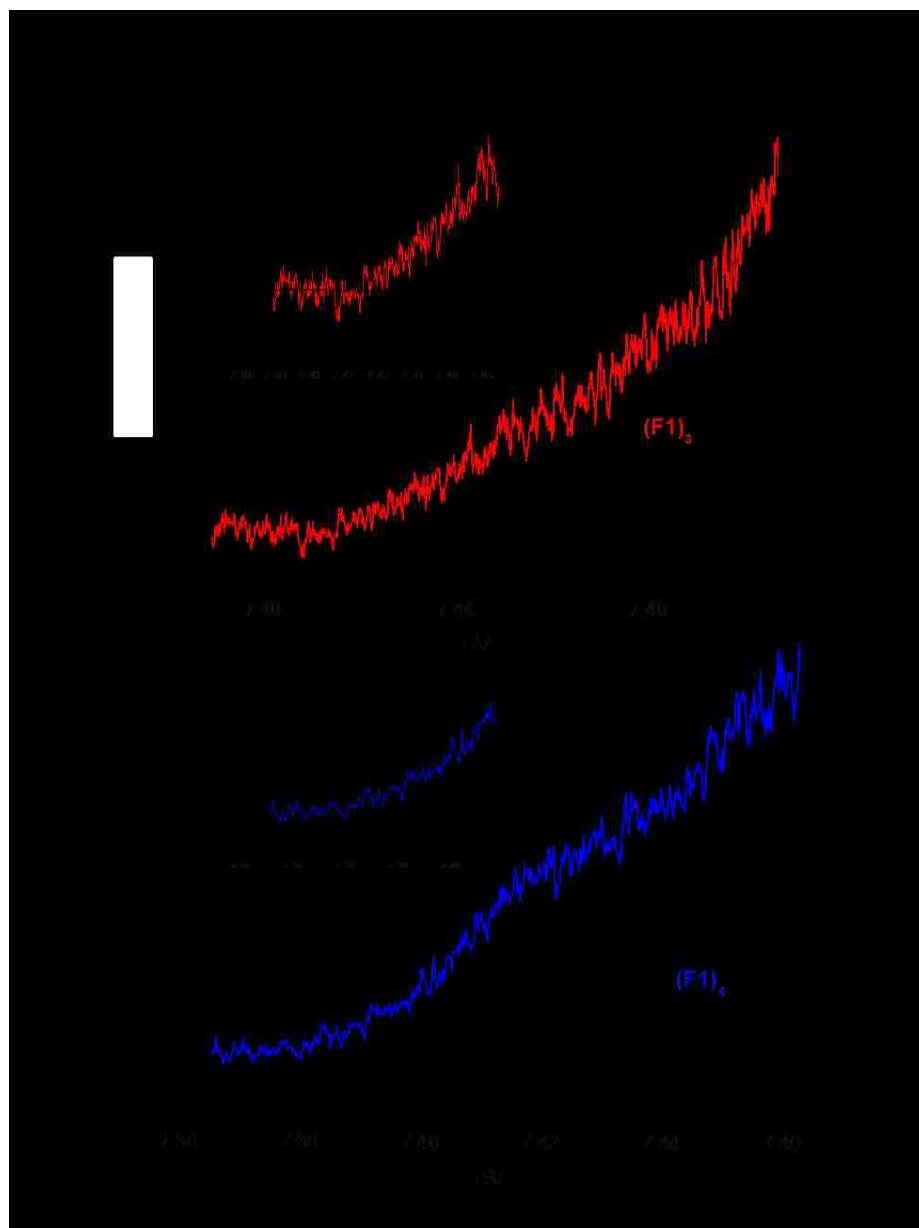
Figure 5.10: Ionization potentials for the vdW F1 trimer and F1 tetramer.

5.4   Examining Steric Effects Using Substituted Fluorenes: Mono and Di-tertbutyl Fluorene

Stemming from the conclusions reached from F1 dimer's inability to form an excimer, an experiment was designed to further investigate the effects of bulky substituents. Therefore, fluorene units containing tert-butyl groups were synthesized by the lab of Dr. Rajendra Rathore. Displayed in Figure 5.11 are the structures these substituted products: a mono-substituted fluorene with a tert-butyl group at the 2H position (TBF), and a di-substituted fluorene with tert-butyl groups at the 2H and 7H positions (DTBF). The di-substituted fluorene sample was designed to ensure the formation of an orthogonal excited state geometry. The dimer was optimized using the M06-2X level of theory and is shown in Figure 5.12. Similar to $(F)_2$, the dimer should form the orthogonal orientation, but, due to the steric effect of the tert-butyl groups, will be unable to undergo rearrangement. Therefore, upon excitation, we predict the dimer will remain in its orthogonal orientation. The mono-substituted fluorene sample will be examined to understand the effect of a single bulky group. Unlike F1, these tert-butyl groups are in-plane with the transition moment.
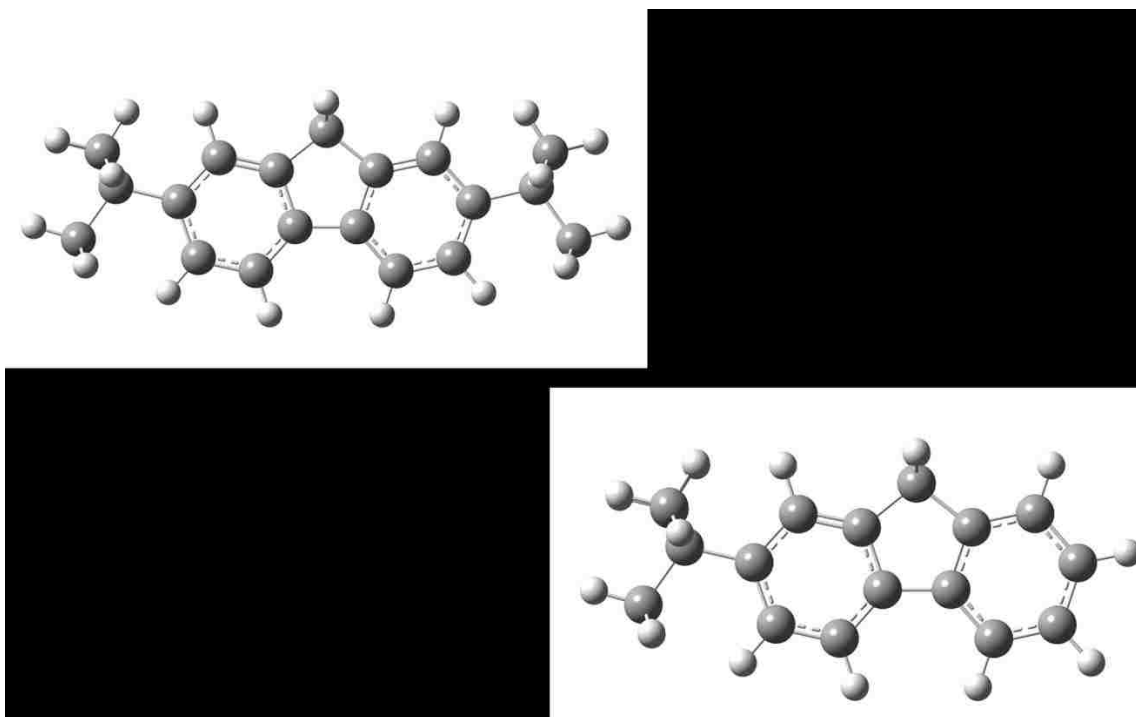
Figure 5.11: Geometry optimized structures of the Mono and Di-Substituted tert-butyl monomers. The steric effects of the tert-butyl groups have the potential to influence the excited state geometry of clusters.

F1 demonstrated that the presence of the methyl groups did not significantly influence the excited state behavior showing a very similar monomer spectrum to that of fluorene. The TBF will be examined to see the influence of a single tert-butyl group while maintaining more degrees of freedom than DTBF.

2CR2PI methods were carried out on TBF first. TBF proved to be very difficult to ionize, often yielding very little signal. This became even more apparent when spectra were gathered for high order clusters. The resulting 2CR2PI spectra are shown in Figure 5.13 for the TBF monomer and dimer. The monomer is well resolved with the most intense peak appearing at 33429 cm^{-1} and the lowest energy feature appearing at 33382 cm^{-1}. Additionally, the dimer is red-shifted relative to the monomer by nearly 300 cm^{-1} and has a very broad, unresolved profile. Also, shown in Figure 5.13, are the LIF spectra for the TBF monomer and dimer.
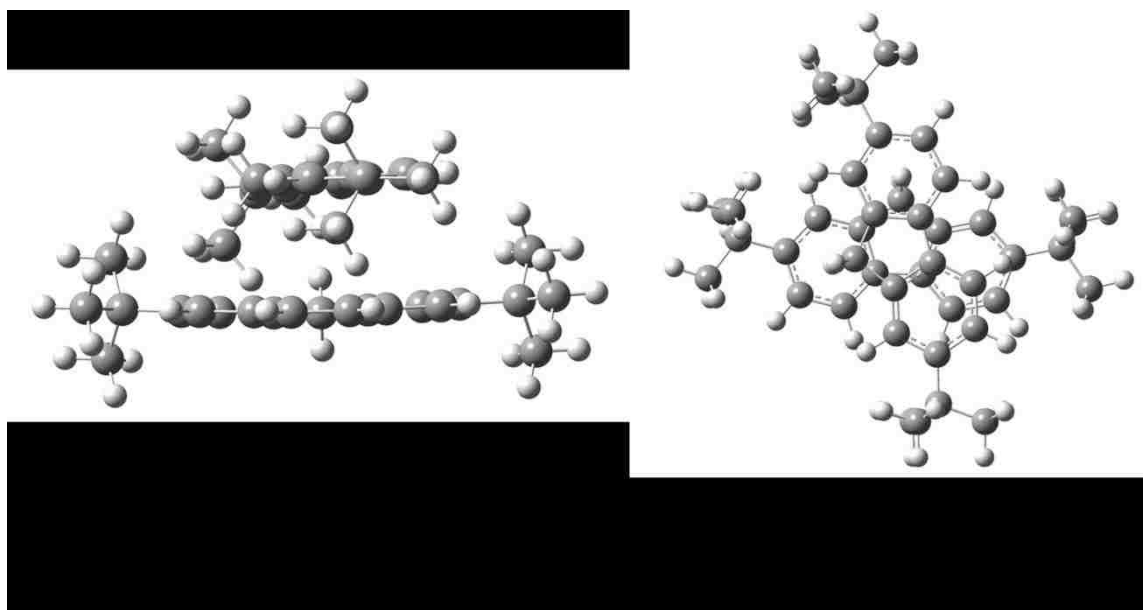
Figure 5.12:   The ground state geometry optimized structure for Di-Substituted tert-butyl Fluorene Dimer with its estimated binding energy.
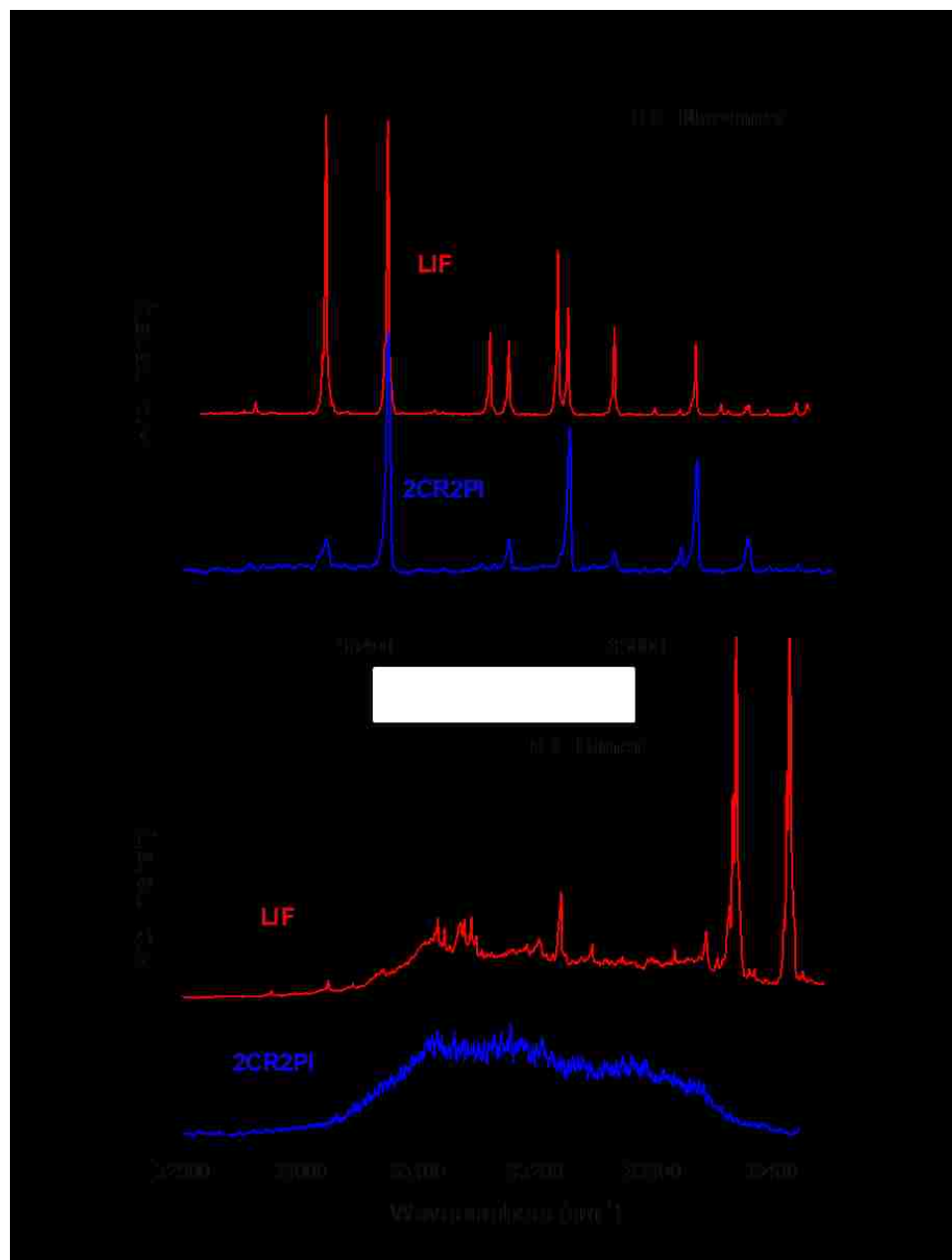
Figure 5.13: 2CR2PI and LIF spectra of the Mono-Substituted tert-butyl fluorene monomer and vdW dimer.

The LIF shows similarities to the 2CR2PI monomer and dimer spectra, but they are not identical. The intensity and number of features are different. The LIF spectrum achieves better resolution in both cases. As mentioned before, signal in the 2CR2PI experiment was very small. However, in the LIF experiment, signal was never an issue. Therefore, TBF has a difficult time ionizing, but not fluorescing. This might be due to the fact that there is better overlap of the transition from the ground to the excited state than the overlap of the transition from the excited to ionic state.

In addition to the excited state spectra, IP of the TBF monomer and dimer were successfully collected. The ion yield curves, shown in Figure 5.14, gave an interesting result. The IP was lowered by just 0.06 eV. A similar result was seen with the results of the higher order F1 clusters. The F1 tetramer was the only system with a significant red-shift; however, it also had the smallest decrease in IP. The red-shift from monomer to dimer for TBF is significant: 256 cm^{-1}. Therefore, there is stabilization in the excited state as a result of its geometry.

Dispersed Fluorescence experiments were conducted to investigate the ground state. The excitation wavelength was fixed to 599.12 nm for TBF monomer, while the excitation wavelength for the dimer was done at several of the slightly resolved features seen in the LIF spectra, all yielding the same spectra. The spectra of the monomer and dimer, shown in Figure 5.15, have very different profiles. The dimer shows a very broad and unresolved peak similar to what was seen in the DF spectra of $(F)_2$ and F2. However, the location of most intense part of the feature is not shifted far to the red. Instead, it is found close to the laser peak, at about 325 nm.
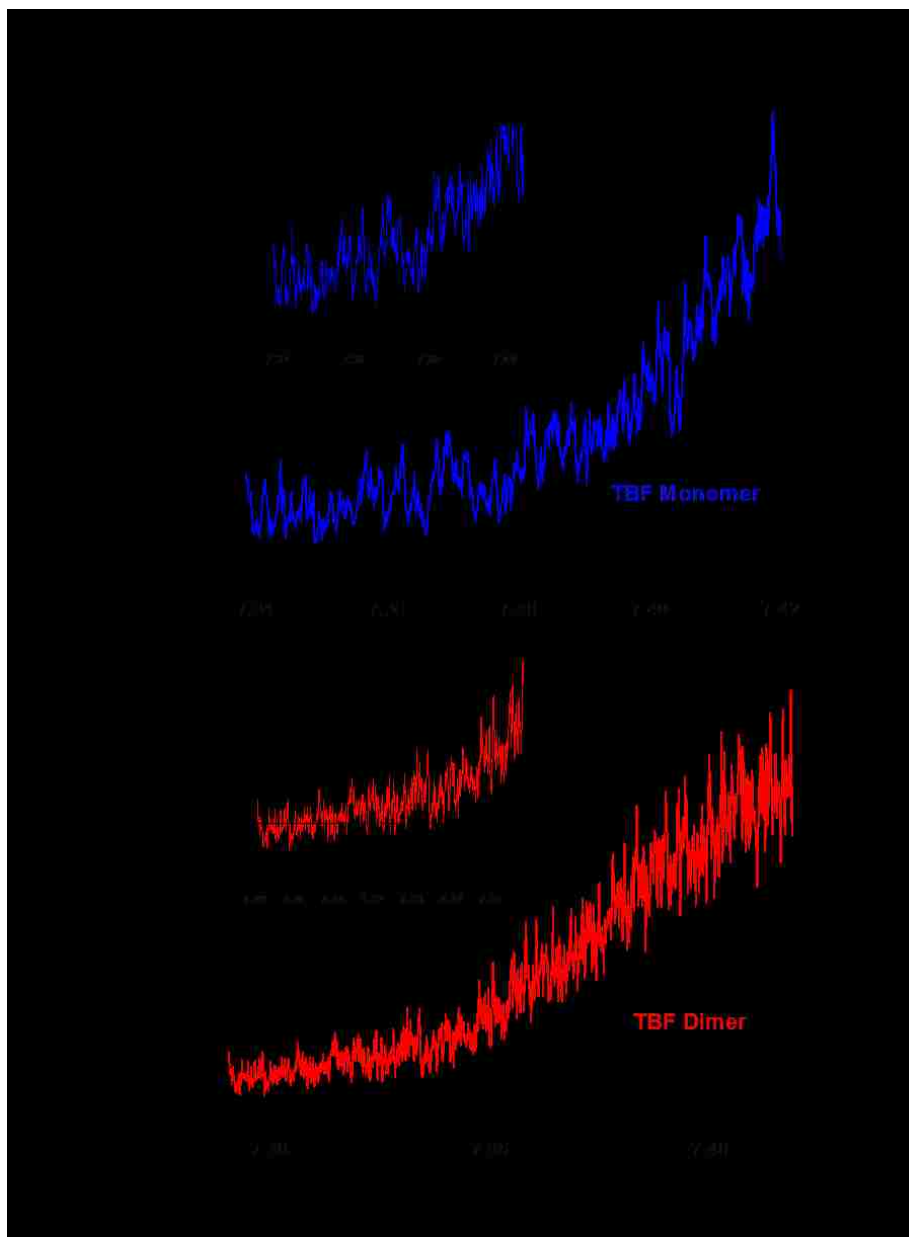
Figure 5.14: Ion potentials for the TBF Monomer and Dimer. The curves show a decrease of only about 0.6 eV, from 7.38 to 7.32 eV.

This broad profile bearing resemblance to $(F)_2$ and F2 is potential evidence for excimer formation. However, $(F)_2$ and F2's features were located at 360 and 400 nm, respectively. Therefore, excimer formation is very weak in the excited state of TBF. To

investigate this potential weak excimer formation, computations were done to optimize possible conformers for the TBF dimer.

Two geometries successfully converged for the TBF dimer. The geometries are featured in Figure 5.16 and are described as diagonal stacked and parallel displaced. In the ground state, the diagonal stacked geometry has a lower binding energy by almost 10 kJ/mol. Comparing this to calculations done with $(F)_2$, the same trend was seen. Relative energies and excited state calculations were completed on these structures, as well and a π-stacked conformation. Shown in Figure 5.17, the energies cohere to the trends seen in previous chapters showing a favorable excimer formation as a result of a π-stacked geometry upon excitation. Information derived from $(F)_2$'s dimer spectrum cannot be derived from this dimer spectrum due to its poor resolution in the 2CR2PI and LIF experiments. Similar to $(F)_2$, however, measurements of TBF revealed a lengthening of the excited state lifetime; 19 ns for the monomer and 30 ns for the dimer. Lengthening of the excited state lifetime is a characteristic of excimer formation and was also observed with $(F)_2$ and F2, albeit to a larger degree. Optimizations were also done in TBF dimer's cationic state to explain why it lacks a significant lowering of the IP. Figure 5.18 shows that when the tert-butyl groups are rotated while in the π-stacked conformation, the center-to-center distance between chromophores increases, thus minimizing the system's ability to delocalize the electron hole.
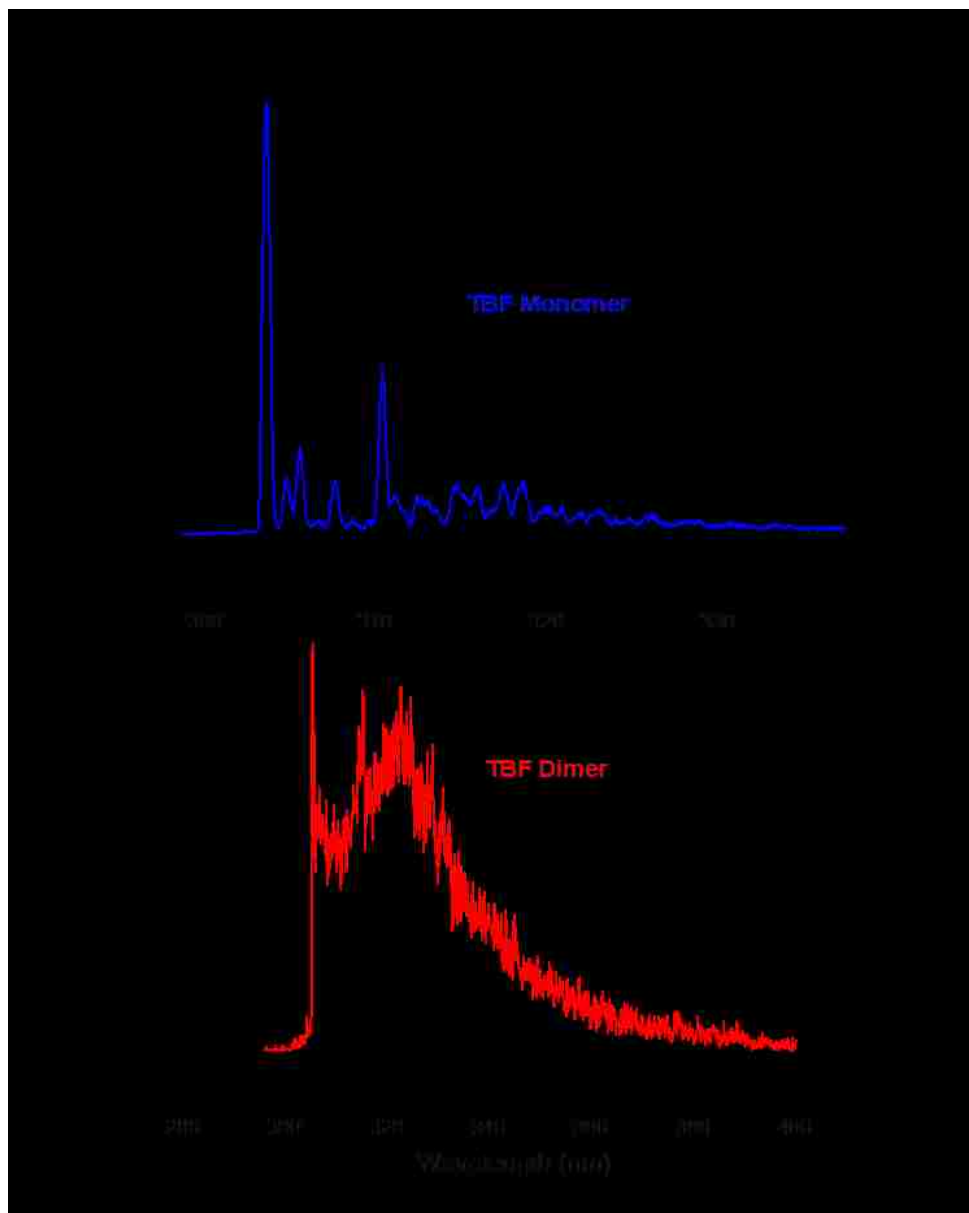
Figure 5.15: Dispersed Fluorescence spectra of the TBF Monomer and Dimer.
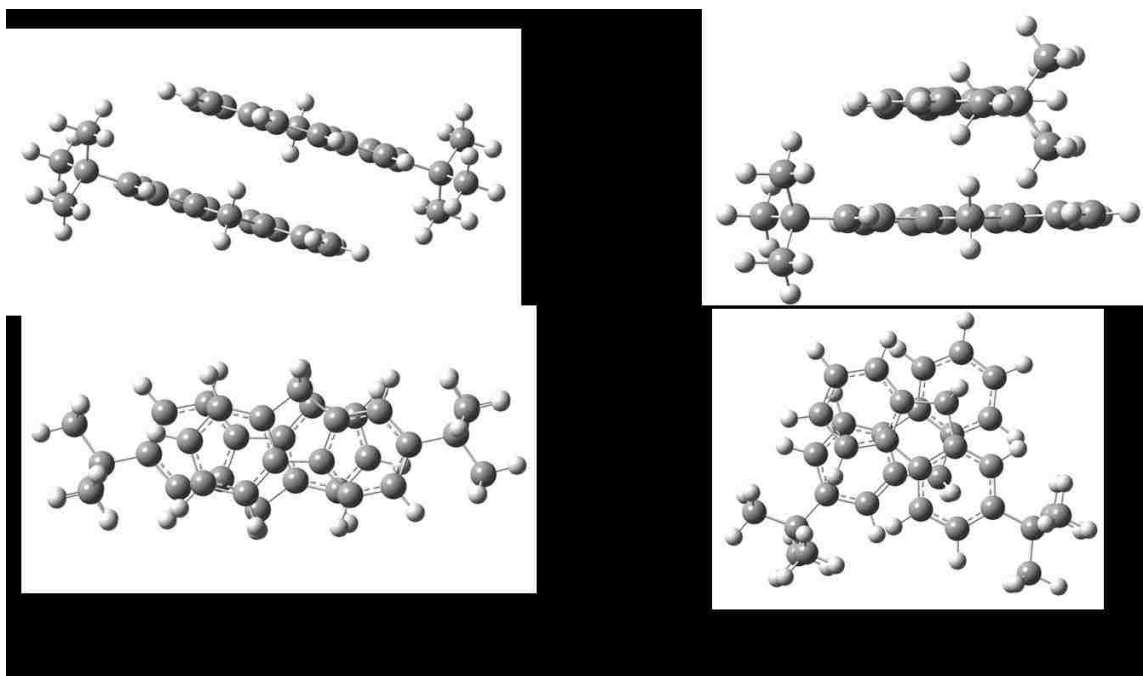
Figure 5.16: Mono-Substituted tert-butyl Fluorene Dimer ground state geometries of stacked orientation (left) and diagonal orientation (right) listed with their estimated binding energies.
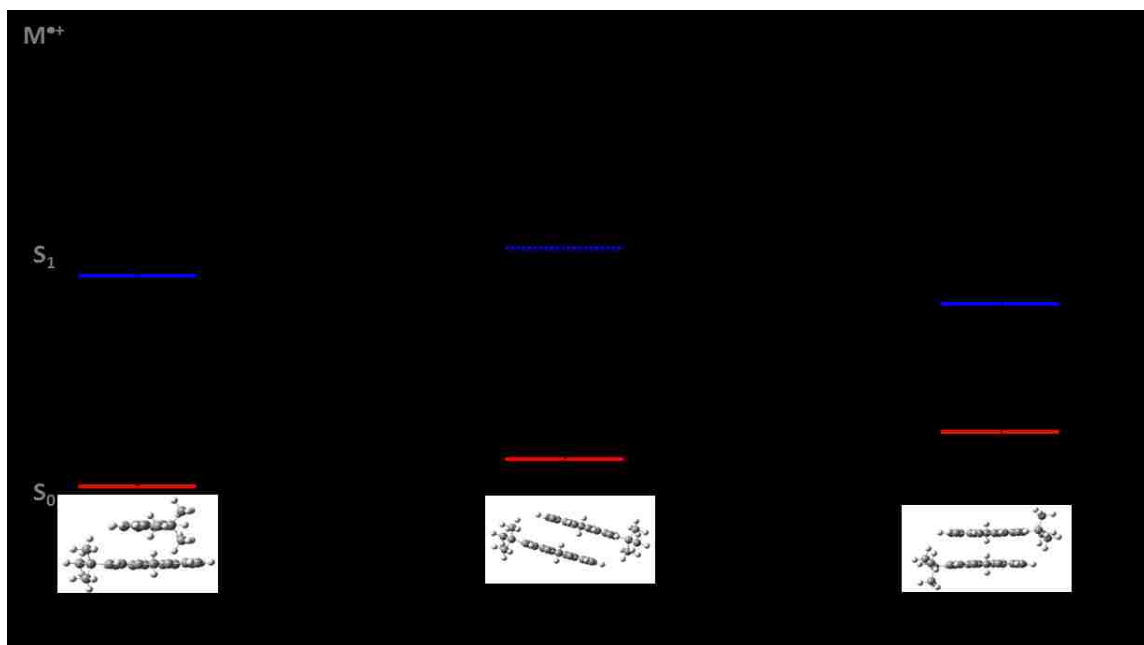
Figure 5.17: Relative energies of TBF Dimer geometries in the S_0, S_1, and Ionic state.

Table 5.1: S_1, S_2, and V_{ab} Coupling Values for TBF Dimer Parallel Displaced Geometry

	E, eV	E, kJ/mol	E, cm^{-1}	transition	coefficient	f
S_1	4.66	449.36	37564.33	117 ->122	0.12133	0.00
				119 ->122	-0.29021	
				119 ->123	0.16598	
				120 ->121	0.58259	
S_2	4.80	463.29	38728.17	115 ->122	0.12728	0.4042
				117 ->121	-0.16577	
				117 ->124	-0.10018	
				119 ->121	0.5098	
				119 ->124	-0.19519	
				120 ->122	-0.1822	
				120 ->123	0.28276	
V_{ab}	0.07	6.97	581.92			

Table 5.2: S_1, S_2, and V_{ab} Coupling Values for TBF Dimer Diagonal Geometry

	E, eV	E, kJ/mol	E, cm^{-1}	transition	coefficient	f
S_1	4.73	456.81	38186.89	115 ->122	-0.10656	0.1929
				117 ->121	0.11548	
				119 ->121	-0.17127	
				119 ->122	0.2313	
				119 ->124	-0.16705	
				120 ->121	0.54607	
				120 ->122	0.1155	
S_2	4.77	460.08	38460.06	117 ->122	0.13294	0.2725
				119 ->121	0.53685	
				119 ->123	0.13596	
				120 ->121	0.15926	
				120 ->122	0.2086	
				120 ->124	-0.17357	
V_{ab}	0.017	1.64	136.59			

Table 5.3: S_1, S_2, and V_{ab} Coupling Values for TBF Dimer Stacked Geometry

	E, eV	E, kJ/mol	E, cm^{-1}	transition	coefficient	f
S_1	3.42	329.67	27558.84	120 ->121	0.69936	0.00
S_2	4.18	402.87	33677.97	117 ->121	0.17198	0.0763
				120 ->122	-0.5994	
				120 ->123	0.28826	
V_{ab}	0.38	36.6	3059.57			
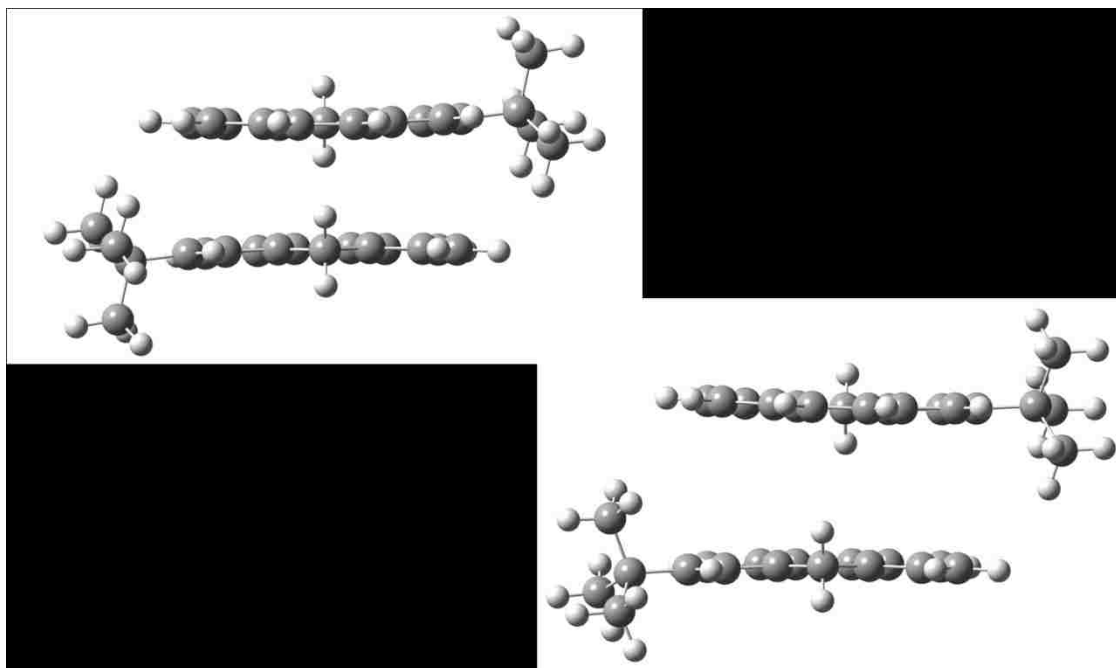
Figure 5.18: TBF Dimer cation structures. The bottom structure's tert-butyl groups have been rotated and have destabilized the conformer as a consequence.

DTBF was examined following studies on the TBF system. 2CR2PI and LIF excitation spectra were collected for the DTBF monomer and are shown in Figure 5.19. The two spectra match up well, with LIF able to provide better resolution due to better signal sensitivity. Additionally, the monomer spectrum is similar to the TBF monomer spectrum, but contains more features. This is most likely due to the addition of a second tert-butyl group.

DTBF dimer spectra were also collected using 2CR2PI and LIF techniques. The excitation spectra, Figure 5.20, shows a broadened feature stretching out over a wide range. The dimer, at its highest intensity, is red-shifted from the monomer by 290 cm^{-1}.

This red-shift is indication of a stabilization of the excited state, but the extent of stabilization is not clear from the excitation spectra alone. Therefore, following the 2CR2PI experiments, Ionization Potentials were collected for the DTBF monomer and dimer (Figure 5.21). DTBF monomer's IP is 7.38 eV, while the dimer IP is lowered to 7.14 eV. This is a lowering of about 0.24 eV from monomer to dimer and is identical to the IP lowering that was seen with F1 dimer. This is expected as this experiment was designed under the assumption that DTBF would not be able to form an excimer as a result of the tert-butyl groups. Additionally, similar to F1, the excited state lifetime of DTBF remained unchanged upon the formation of a dimer (16 ns).
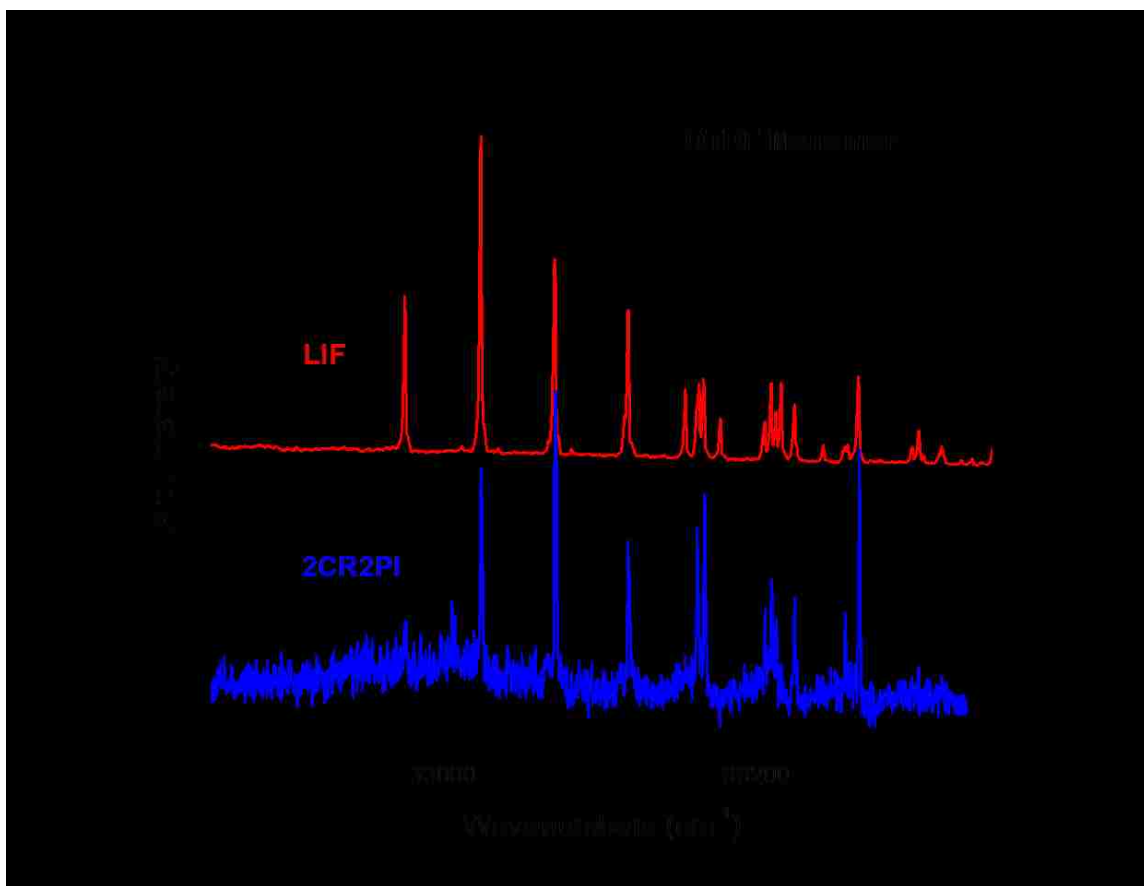
Figure 5.19: 2CR2PI and LIF spectra of the Di-Substituted tert-butyl fluorene Monomer.
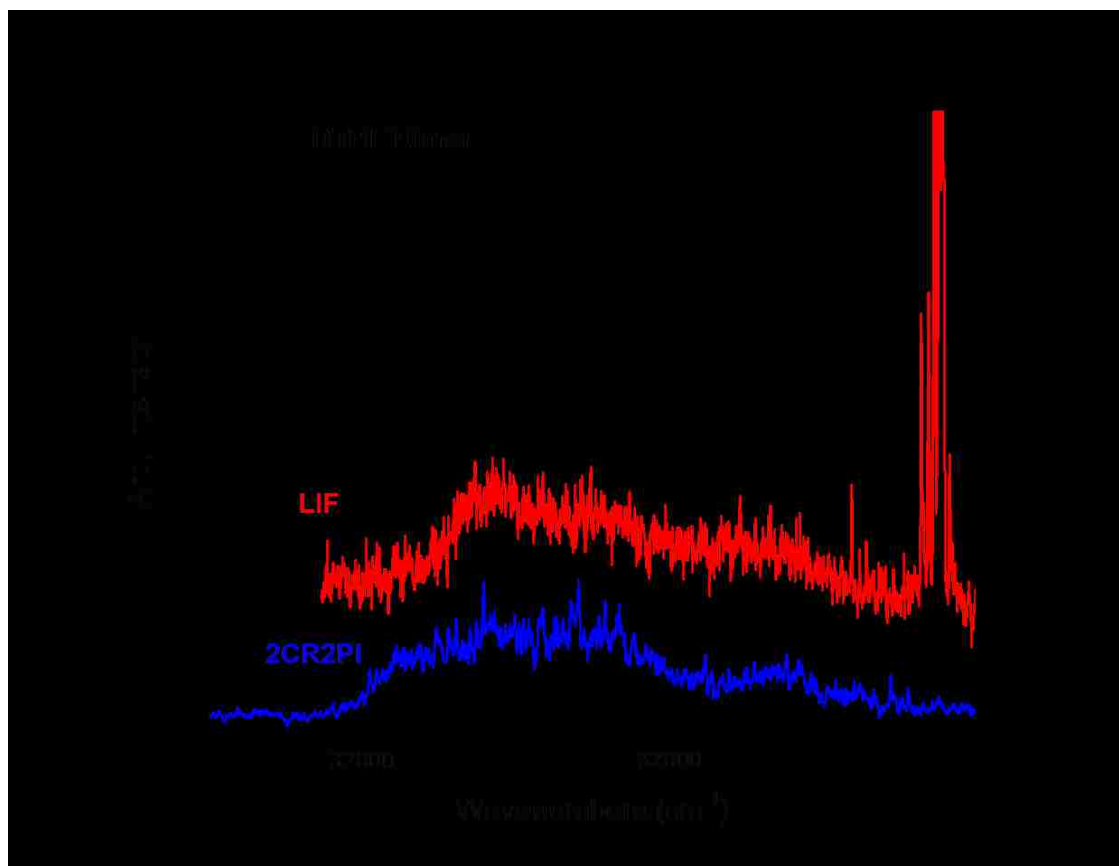
Figure 5.20: 2CR2PI and LIF spectra of the Di-Substituted tert-butyl fluorene Dimer. The intense feature to the far right in the LIF spectrum is activity from the monomer and it used as reference.
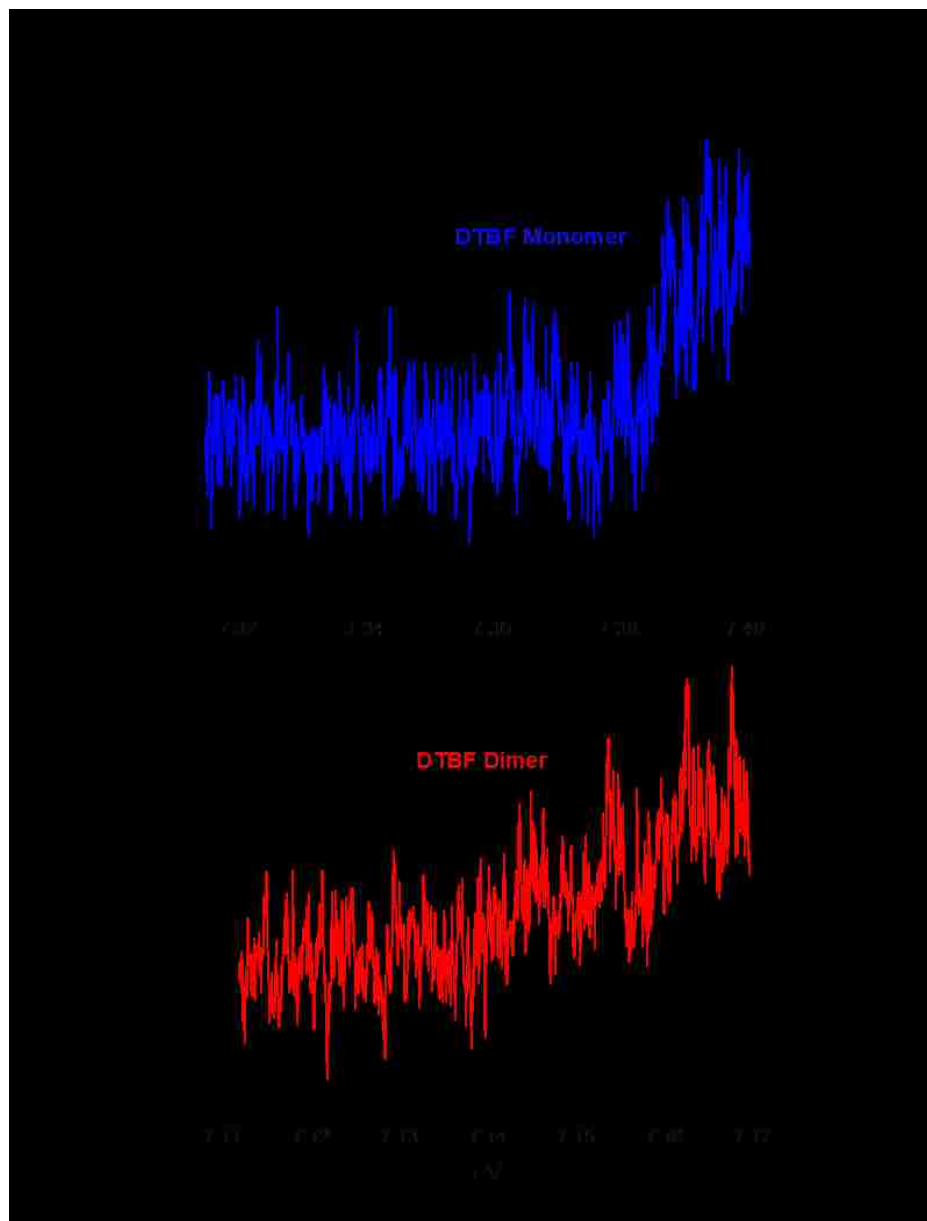
Figure 5.21: Ionization potentials of the DTBF Monomer and Dimer. The IP of the dimer is lowered by 0.24 eV, from 7.38 to 7.14 eV.
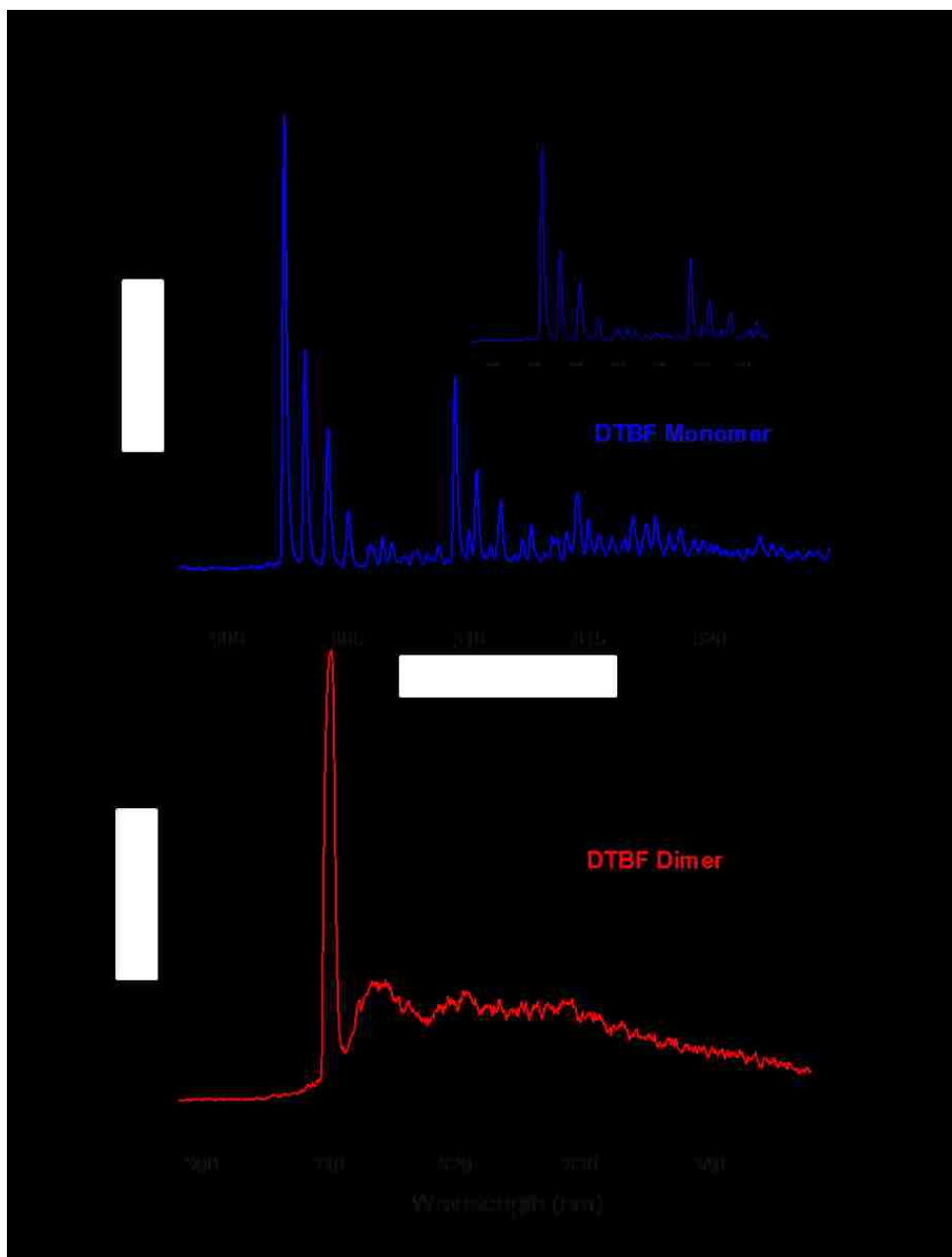
Figure 5.22: Dispersed Fluorescence spectra for the Di-Substituted tert-butyl monomer (blue trace) and dimer (red trace).

Lastly, the Dispersed Fluorescence of DTBF was collected for both the monomer and dimer (Figure 5.22). As with TBF, the monomer and dimer profiles change. However, the dimer profile for DTBF does not resemble broad Gaussian type features like (F)$_2$, F2, and TBF dimer. Rather it appears to be an unresolved version of the monomer spectrum. The broadness can be attributed to a high number of active vibrational modes as a result of dimerization, <u>not</u> excimer formation.

5.5   'Geometry Fixing' of Fluorene Systems

Introducing bulky substituents proved to be an effective way to influence the geometry of the excited state, however, there will always remain a small degree of uncertainty with vdW clusters of molecular in a supersonic beam expansion. Using the covalently linked fluorene systems as inspiration, molecules were designed to completely limit the degrees of freedom by essentially 'fixing' their geometry. Previous studies have been conducted on covalently linked bichromophores that have fixed geometries.[76,149] Spiro-F2, pictured in Figure 5.23, is an example.

Spiro-F2 is a bichromophore made up of two fluorene subunits, connected to each other in an orthogonal orientation at the 9H position. Conducting Ionization and Fluorescence experiments on this molecule yielded a spectrum nearly identical to fluorene monomer. Applying an excitonic model analysis, this result is expected due to the transition dipoles being oriented perfectly perpendicular to one another. The consequence of this conformation is zero excitonic splitting of the spectrum. Our own 2CR2PI spectrum of Spiro-F2 is displayed in Figure 5.24.
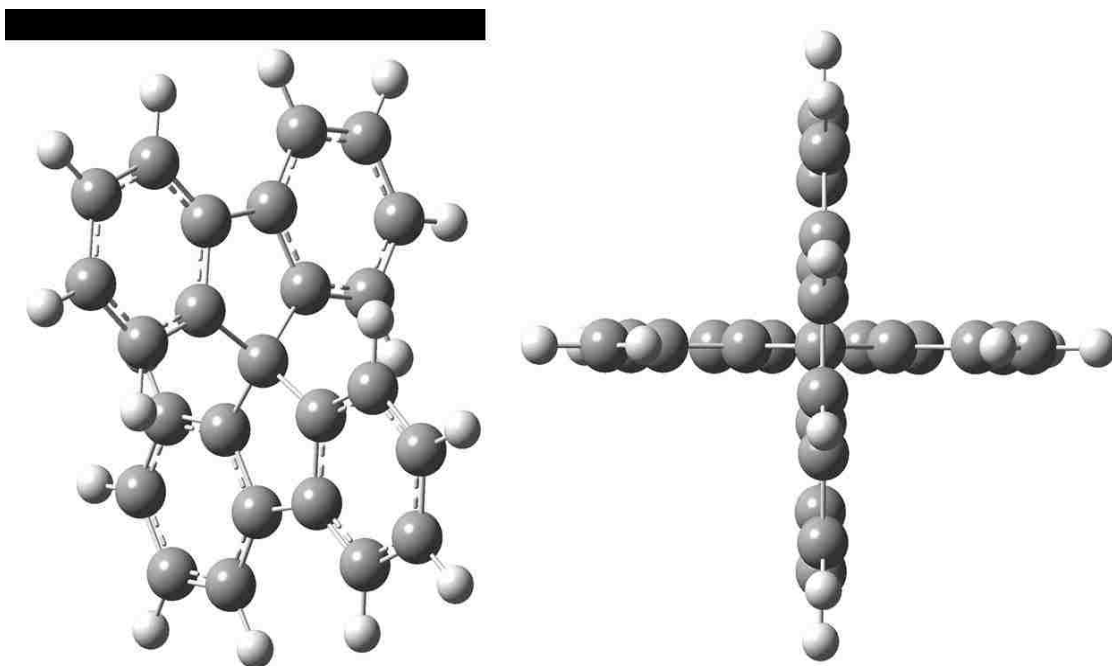
Figure 5.23: The Spiro-F2 composite fluorene molecule. Only one configuration of the molecule is possible and therefore is classified as a "fixed" geometry in this study.
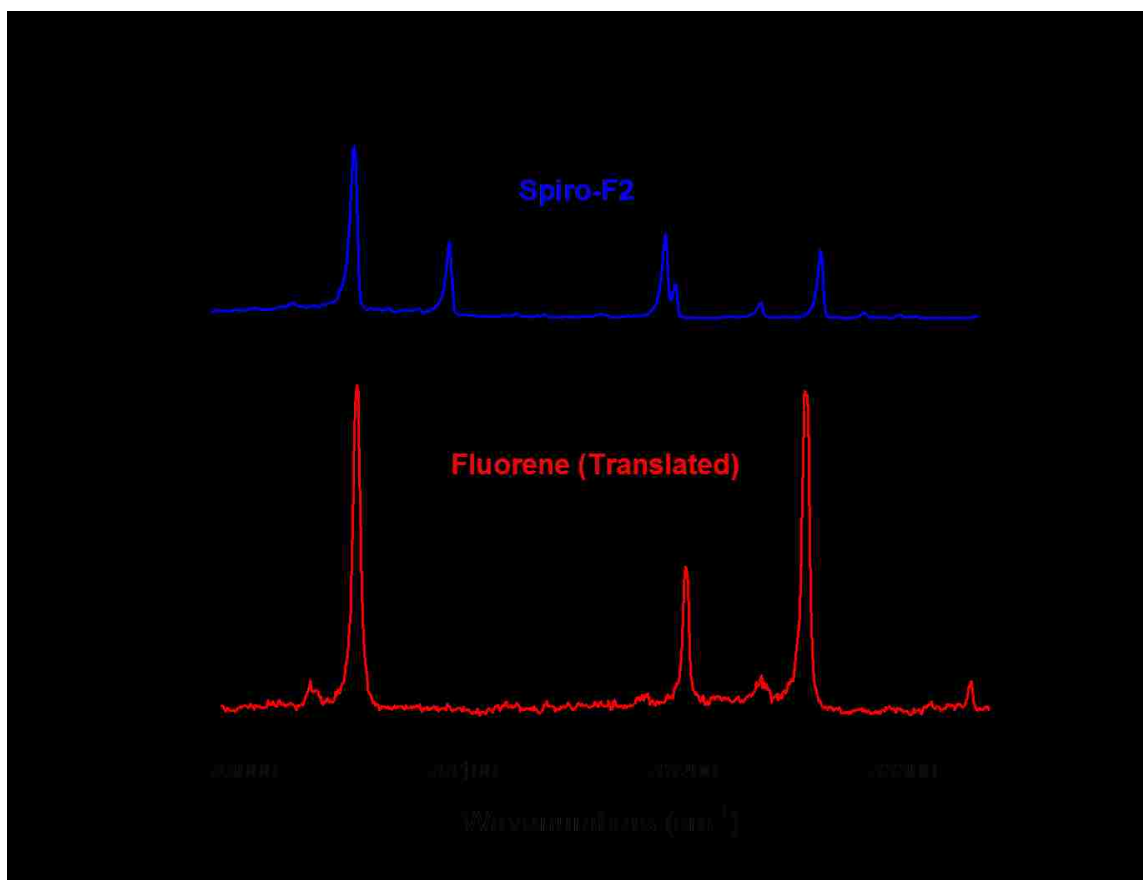
Figure 5.24: 2CR2PI spectrum of Spiro-F2 compared with the fluorene monomer spectrum. The spectrum of fluorene has been horizontally translated to the red in order to better compare with the features of Spiro-F2.

In addition to Spiro-F2, another molecule that has been examined is 9,9'-bifluorenyl.[74,75,95,150] The structure, Figure 5.25, is comprised of two fluorene units linked directly to one another at the 9H position. The linkage resembles F2, however, there is no methylene bridge. This is considered as a fixed geometry molecule because it has been found to adopt only one conformer. Due to the proximity of fluorene units, it cannot π-stack. Instead it adopts primarily a CH/π interaction. This molecule serves as a good model for demonstration of excitonic splitting. An LIF spectrum of the 9,9' molecule was collected, Figure 5.26, and is in agreement with previous studies.[74] In the spectrum there are two intense peaks at 33307 cm^{-1} and 33364 cm^{-1}. These peaks are an excitonically split origin transition.

This was investigated using Dispersed Fluorescence. Two spectra were collected, fixing the excitation laser at 600.46 nm and 599.44 nm (33307 and 33364 cm^{-1}). The results, in Figure 5.27, show two identical spectra. This is evident of transitions originating from a single system. The orientation of the transition moments along the fluorene subunits create the unique splitting, as discussed before with the exciton model.
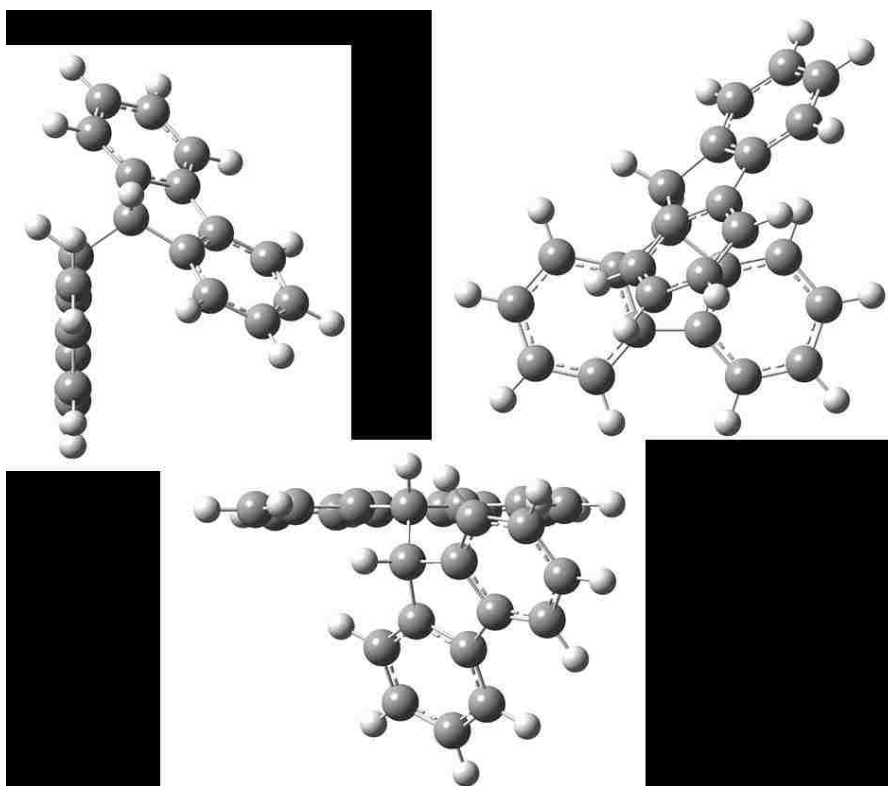
Figure 5.25: The optimized ground state structure of 9,9'-bifluorenyl. The geometry makes use of a CH-π interaction.
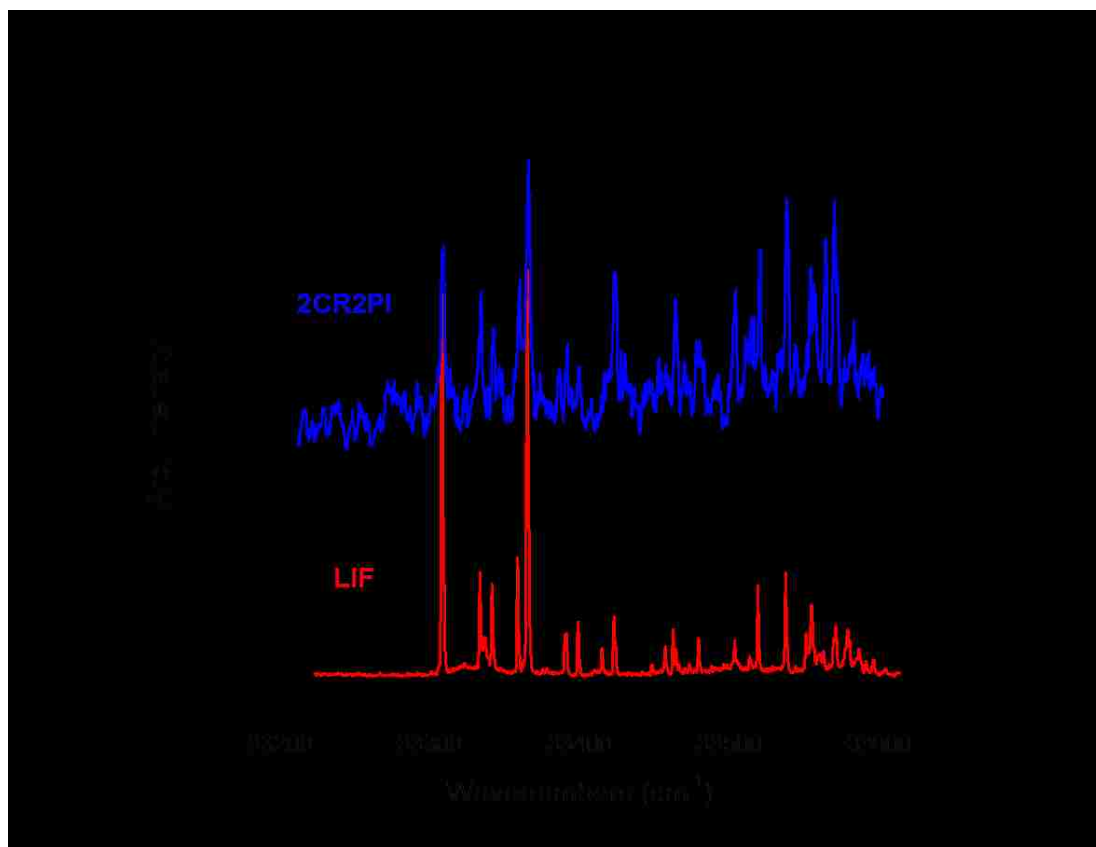
Figure 5.26: The 2CR2PI and LIF excitation spectra of 9,9'-bifluorenyl compound. The transition origin of the compound is split via excitonic interaction by about 57 cm^{-1}.
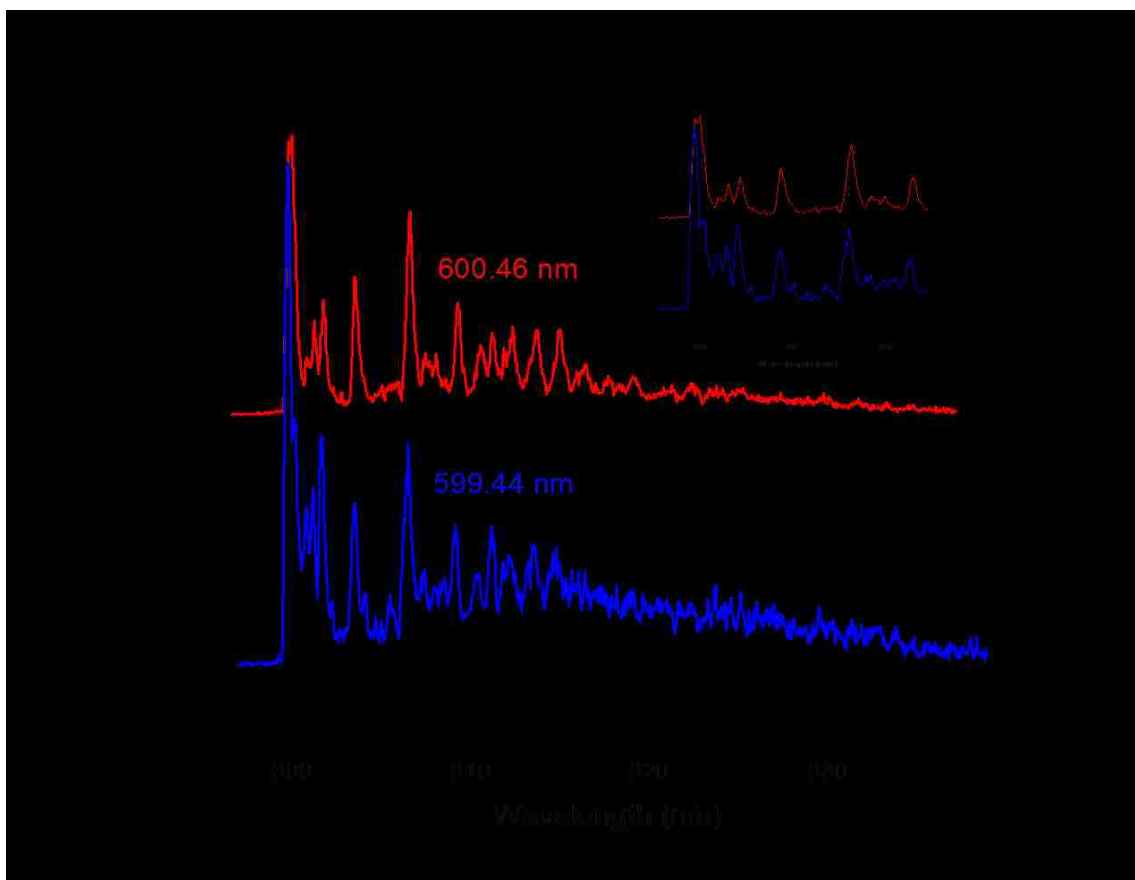
Figure 5.27: Dispersed Fluorescence spectra of the split origin transition of the 9,9'-bifluorenyl compound.

For this experiment, molecules were designed to be 'fixed' like Spiro-F2. Eliminating geometric uncertainty serves as the motivation for this portion of the study. Therefore, it is much easier to analyze resulting data, and molecules can be designed to resemble potential geometries that were calculated for the $(F)_2$ and F2 dimers. Spiro-F2 serves as a good model system, but is not sufficient in demonstrating stacking interactions.

Attention was then given to fluorene dimers that are covalently linked together using cyclohexane bridges. The rigidity of the cyclohexane bridge is used to prevent the fluorene subunits from adopting multiple geometries and therefore will eliminate geometrical uncertainties associated with earlier systems examined. The meta-substituted sample (1,3-DFC)[151] was examined. The excited state spectrum was collected using 2CR2PI techniques and is shown in Figure 5.28. The results show a well resolved spectrum with complex splitting located at the origin band. The resolution and splitting pattern is reminiscent of the origin band profile of F1 dimer. However, the appearance of 1,3-DFC's origin occurs further to the red than F1 dimer and cannot be directly compared to fluorene or F1. This well-resolved structure is evidence for no excimer formation with this geometry. The Ionization Potential, therefore, was also collected. The results of the experiment, in Figure 5.29, indicate an IP of 7.725 eV. Using previous dimer IP's as a reference point, this is the highest IP observed, appearing 0.16 eV lower than fluorene monomer and more than 0.2 eV higher than $(F)_2$. While this is evidence of electron hole stabilization, it is clear that it is less effective than previous dimers studied.

Figure 5.28: 2CR2PI spectrum of 1,3-di-fluorenylcyclohexane.
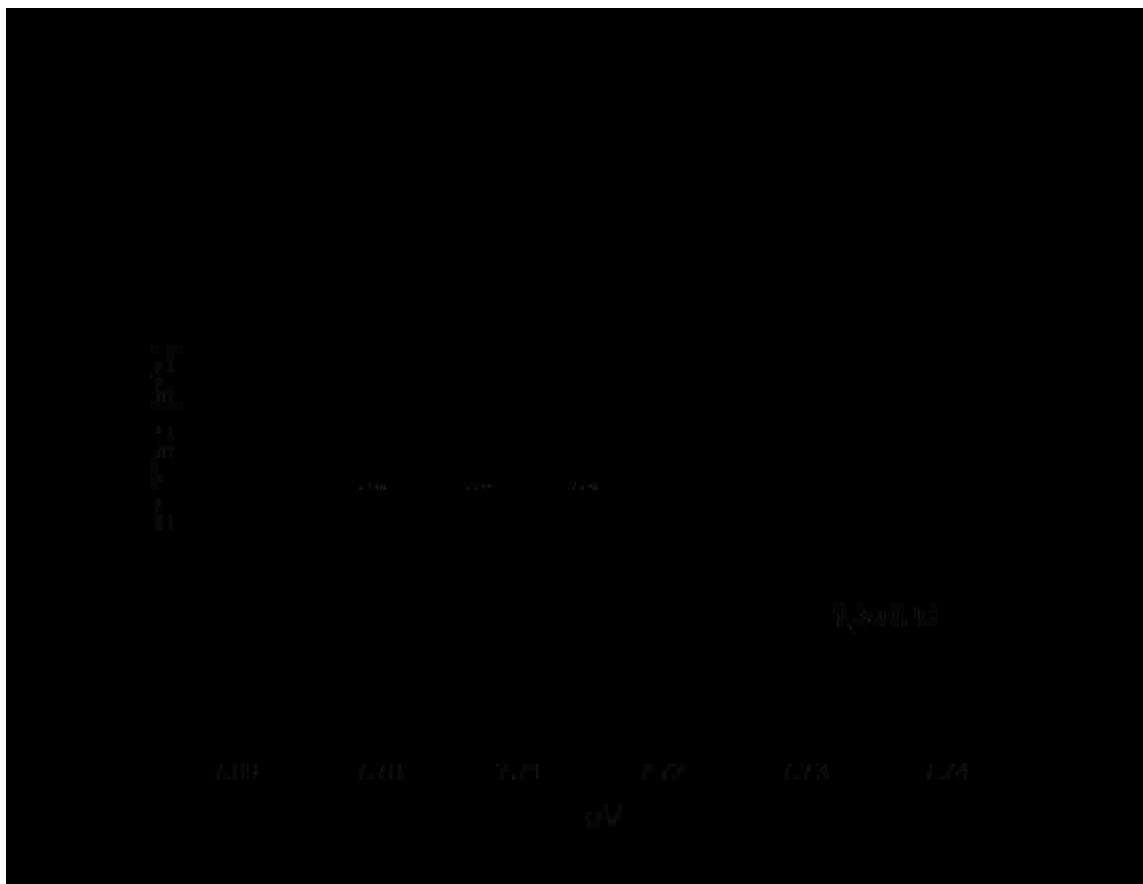
Figure 5.29: Ionization potential of 1,3-di-fluorenylcyclohexane. The IP is a sharp onset and appears at 7.725 eV.

Additionally, ortho-substituted cyclohexane (1,2-DFC) was examined. In this system, the fluorene subunits are much closer to one another than the 1,3 substituted system. Using the 2CR2PI and LIF techniques, excited state spectra of the system was collected and is displayed in Figure 5.30. The 2CR2PI spectrum appears broad and completely unresolved, often yielding little to no signal during the experiment. However, LIF proved to be effective, yielded a high amount of signal. The 1,2 and 1,3-substituted molecules contain the exact same mass, but the excitation spectra confirm that the signals are not the same due to differences in the location of their 'origin transitions.' 1,3-DFC is located at 33398 cm^{-1} and 1,2-DFC at 33300 cm^{-1}.

The Ionization Potential for 1,2-DFC was attempted, but a reliable signal was unable to be obtained. The low signal produced a high signal to noise ratio, and a reproducible ion yield curve has not been collected as a consequence.
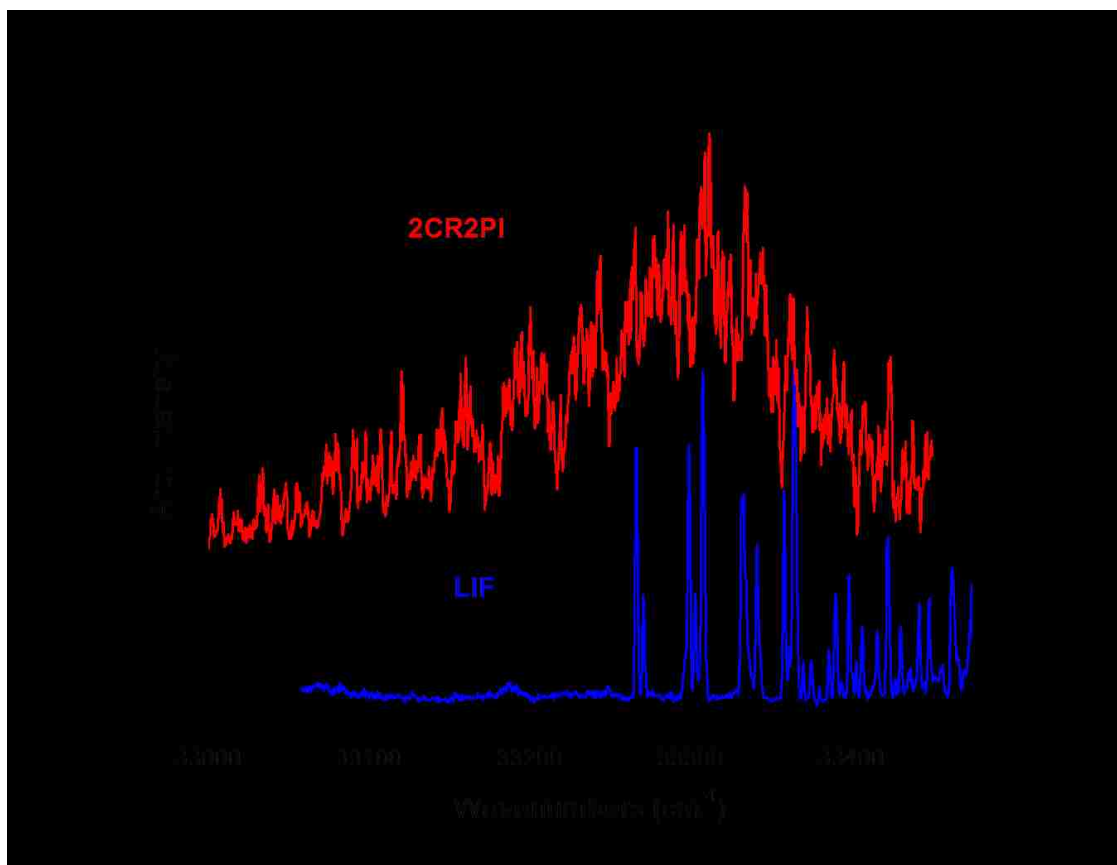
Figure 5.30: 2CR2PI and LIF spectra of 1,2-di-fluorenylcyclohexane.

A Dispersed Fluorescence spectrum of 1,2-DFC was successfully collected. As seen in Figure 5.31, the DF has a large amount of resolved activity that appears over a broad range. The potential cause for 1,2-DFC's inefficiency to ionize and highly active emission spectrum is the geometry of the molecule, specifically the orientation and proximity of the fluorene subunits. To fully understand the results of the experiment on the cyclohexane linked molecules, computations were done in order to find the minimum energy structures. Multiple structures are not expected due to the rigidity of the linker; however, they are still possible because of cyclohexane's affinity for multiple arrangements (chair, twist-boat, boat, half-chair). 1,2-DFC was optimized and yielded two conformers in Figure 5.32. Both successfully converged but one conformer is higher in energy by 573 kJ/mol. This energy difference makes it highly unlikely to be found in the gas phase. Therefore, we will only consider one conformer. The fluorenes in the considered geometry are staggered and in very close proximity. The proximity is an important point here as it is could be the cause of its lack of stabilization. Cyclohexane has a bond length of 1.51 Å when it contains no substituents. When fluorenes are attached, those bonds lengths are modified to account for those additions. Bond lengths in the 1,2-DFC structure range from 1.52 to 1.54 Å, with an exception at the 1,2 carbon-carbon in the ring being 1.59 Å. Optimizations have also been done on 1,3 and 1,4-DFC and are found in Figures 5.33 and 5.34. 1,3-DFC yielded one structure with the fluorenes spaced more than 4.0 Å for their center-to-center distance. The distance and orientations do not provide an optimal geometry for π-interactions.
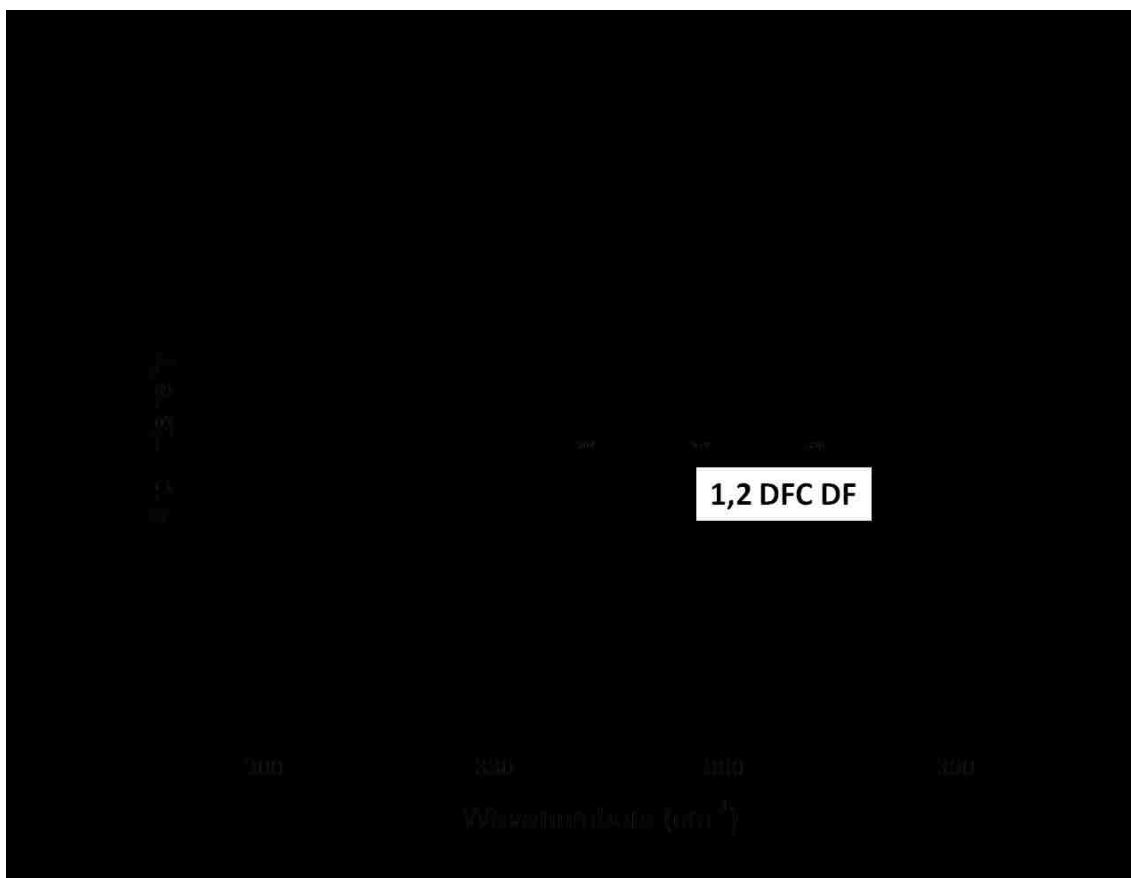
Figure 5.31: Dispersed Fluorescence spectrum of 1,2-di-fluorenylcyclohexane.

The bond lengths for 1,3-DFC range from 1.52-1.56 Å. 1,4-DFC minimum energy structures were calculated for comparison purposes, but was never looked at experimentally. Two possible conformers were found. One geometry contains the fluorenes in plane with each other (chair) while the other has them staggered (twist-boat).

The two conformations are separated by 16 kJ/mol. This is due to the cyclohexane being lower in energy in its chair conformation. The bond lengths of the cyclohexane ring in 1,4-DFC range from 1.52 to 1.54 Å. All the molecules have a very similar range of bond lengths with the exception of the 1.59 Å carbon-carbon bond in 1,2-DFC. Additionally, this can be compared to the carbon-carbon bond length of the linked carbons at the 9H position in 9,9'-bifluorenyl. This bond length was calculated as 1.55 Å. Upon ionization, the bond length of 1,2-DFC lengthens slightly to 1.60 Å, while the 9,9'-bifluorenyl bond length also increases, to 1.56 Å. The excited state lifetime of 1,2-DFC was measured as well and was 21.9 (±0.11) ns. This compares very well to the excited state lifetime of 9,9'-bifluorenyl, which has been reported to be 21.7 ns.[74] In this same study, the C-C bond length at the 9 position was reported as 1.54 Å. This is in good agreement with the completed calculations. A summary of how all the calculated energies compare to one another for all cyclohexane-linked systems can be found in Table 5.4. The lowest energy conformer is the in-plane 1,4-DFC molecule.
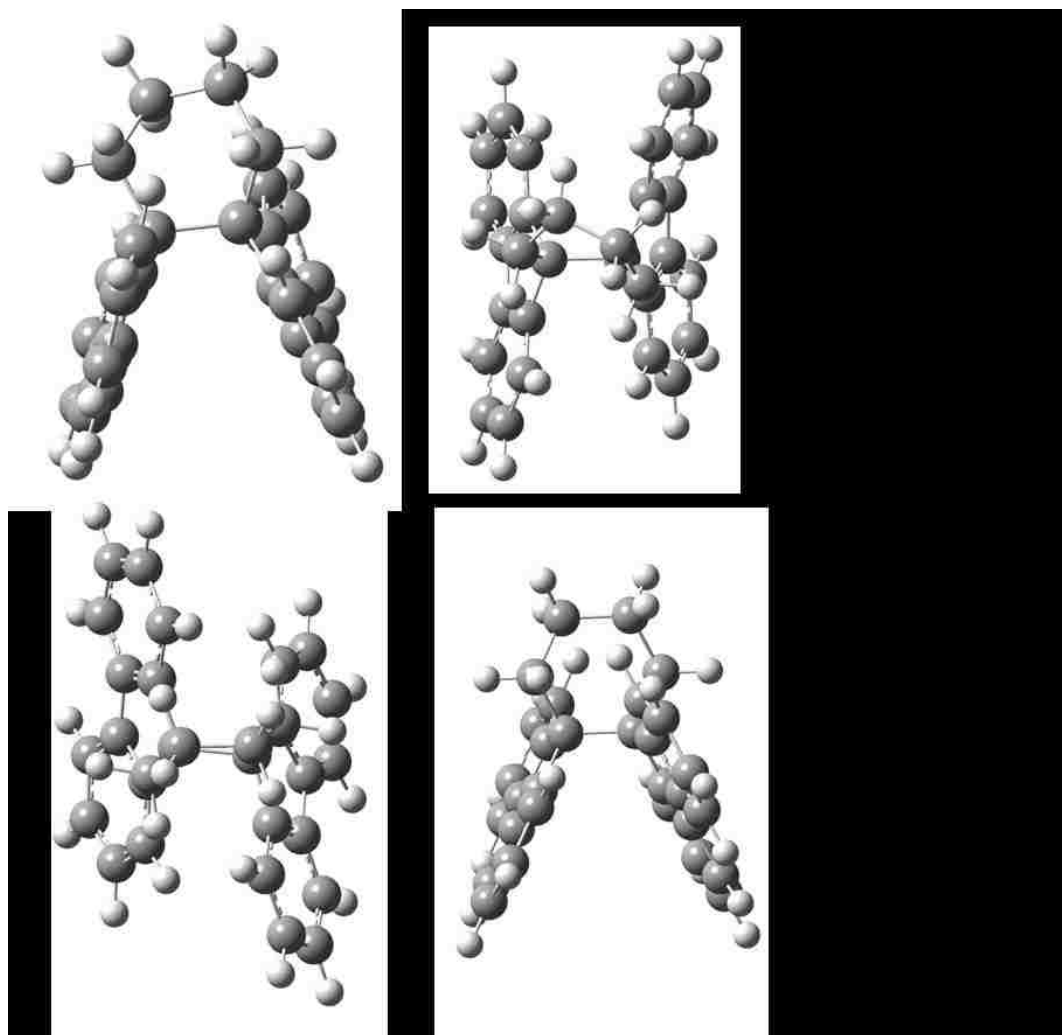
Figure 5.32: The minimized ground state conformers for 1,2-di-fluorenylcyclohexane.
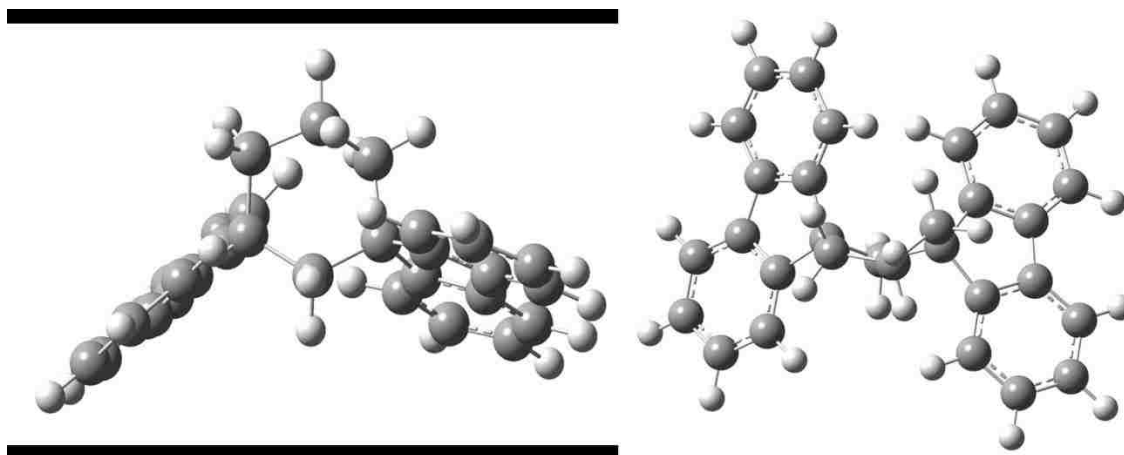
Figure 5.33: The minimized ground state conformers for 1,3-di-fluorenylcyclohexane.
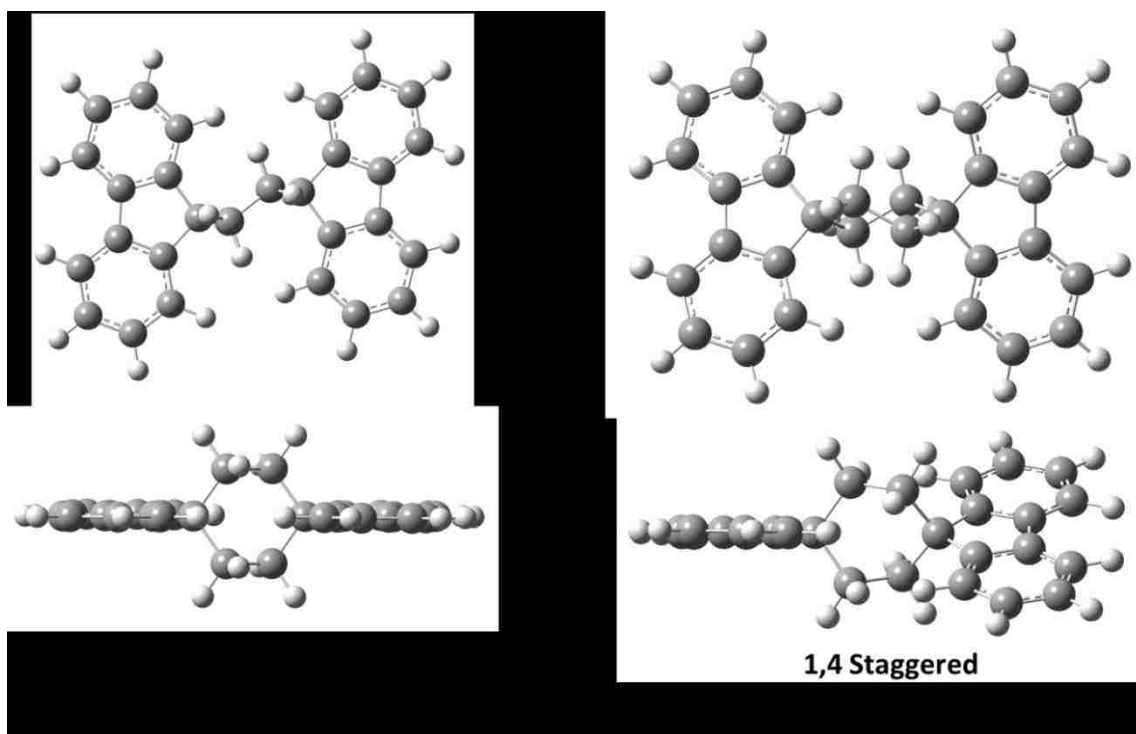
Figure 5.34: The minimized ground state conformers for 1,4-di-fluorenylcyclohexane.

Molecule Type	Relative Energies
1,2 Substituted (1)	584 kJ/mol
1,2 Substituted (2)	10.67 kJ/mol
1,3 Substituted	43.4 kJ/mol
1,4 In-Plane	0 kJ/mol
1,4 Staggered	16.4 kJ/mol

Table 5.4: Relative energies of the various fluorene substituted cyclohexane composite systems.

5.6   Summary

Following the investigation of higher order fluorene clusters, both covalent and non-covalent, additional information about the interactions of chromophores was uncovered.   With F3 and the higher order F1 clusters, there was no additional stabilization of the excited state. F3 DF was identical to the F2 DF, and the excited state lifetime did not lengthen. The F1 clusters repeated that same trend. F1 dimer already doesn't form an excimer, but the case remained constant as cluster size grew.   The excited state lifetime remains unchanged from the monomer, at 15 ns. However, both systems showed that electron hole stabilization can continue to increase as cluster size increases. Fluorene van der Waals clusters showed a slightly different trend. The trimer and tetramer spectra resemble each other, as well as the pentamer and hexamer. After the promotion from tetramer to pentamer, however, the origin appears to shift about 81 cm^{-1} with a small potential increase in excited state lifetime.   The pentamer and hexamer spectra are also broad and completely unresolved unlike the slightly resolved trimer and tetramer.   The continuation of IP lowering also occurred with fluorene vdW clusters, eventually stopping after the cluster size had reached six units.

Steric hindrance, inspired by the vdW F1 dimer, was also explored further using TBF and DTBF model systems. DTBF showed very similar behavior to the F1 dimer, with the exception of an unresolved DF. The lowering of the IP, 0.24 eV, and unchanged lifetime from monomer to dimer, 16 ns, was in great agreement.   This served as verification that even with the inability to form an excimer, a molecular system can still efficiently delocalize an electron hole. TBF proved to be a unique case, possible showing

very weak excimer, drawing comparisons to $(F)_2$. In spite of this TBF was unable to delocalize an electron hole as efficiently as DTBF.

Spiro-F2 and 9,9'-bifluorenyl were both examined and compared to previous studies, showing great agreement. These two molecules served as good model systems for the goal of the experiment. The geometry of Spiro-F2 and 9,9'-bifluorenyl are well documented, showing how chromophores can be covalently linked together in order to effectively freeze or fix their geometries. However, these molecules did not serve as great model systems for understanding π-π interactions. Fluorene units linked together with a cyclohexane bridge were then used to understand the distance relationship between π-ring interactions. Experimental and theoretical treatments were applied to 1,2 and 1,3-DFC, while 1,4-DFC has not yet been experimentally investigated. All three proved to be beneficial in demonstrating the distance relationship between chromophores, specifically cases where the π rings are too far or too close for efficient interaction.

Chapter 6

Future Work and Conclusions

6.1   The Study Moving Forward

F2 served as an excellent model system in helping understand the geometric requirements for excimer formation and hole stabilization.   F2H2 is another model system that is similar to F2, shown in Figure 6.1, which could help investigate excited state processes.
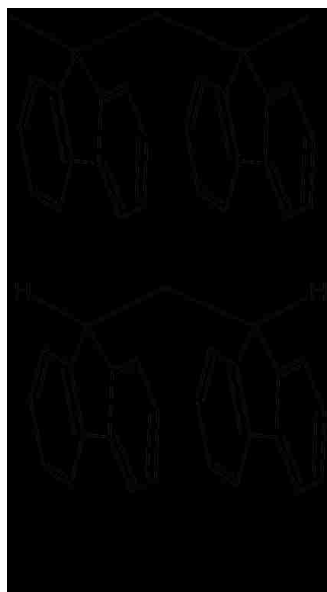
Figure 6.1:   A qualitative representation of F2 and F2H2 that demonstrates the structural difference that determines how each composite molecule is labeled.

F2H2, like F2, is comprised of two fluorene subunits linked together by a methylene

bridge. However, instead of the methyl groups that cap the 9H position in F2, F2H2 has

hydrogens. Preliminary studies on F2H2 in the solid a liquid phase has shown that it

adopts an open conformation, unlike F2. This might be due to the lack of methyl groups

creating steric hindrance as a consequence of adopting on open conformation. F2H2,

therefore, generates interest as a gas-phase system. Through excitation or ionization, it is

possible that it can undergo a rearrangement to the closed conformer, acting as a

molecular switch. Figure 6.2 is a general representation of this process.
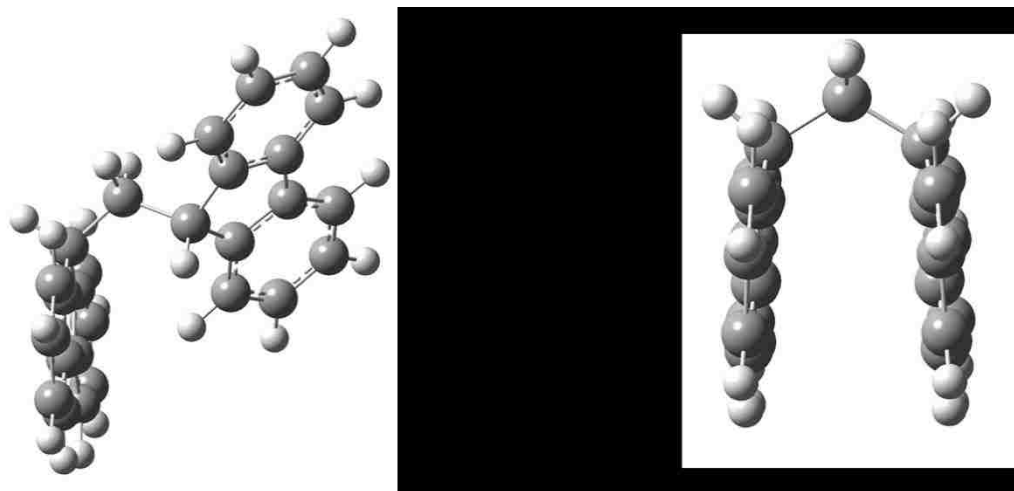
Figure 6.2: Proposed mechanism of conformational closing to create π-stacking as a result of ionization.

Gas-phase methods would be able to distinguish one conformation from the other based

on its spectral behavior. In Chapter 3, data revealed that F2 forms an excimer and

stabilizes electron holes very efficiently. One could assume that F2H2 would be able to

do the same in its closed conformation. Its open conformation, however, would not show

excimer-type emission. In its open conformation, the dominant forces present are CH/π

interactions. Therefore, gas-phase ionization and fluorescence techniques are able to

tease out whether the open conformer, closed conformer, or a combination of the two is present.

1CR2PI and 2CR2PI techniques were used to collect the excitation spectrum of F2H2. The same results were observed in both setups. The spectrum, which is pictured in Figure 6.3 as a black trace, yielded origin features of equal intensity separated by 94 cm^{-1}. Additionally, the spectrum had an overall broadness over a wide range.
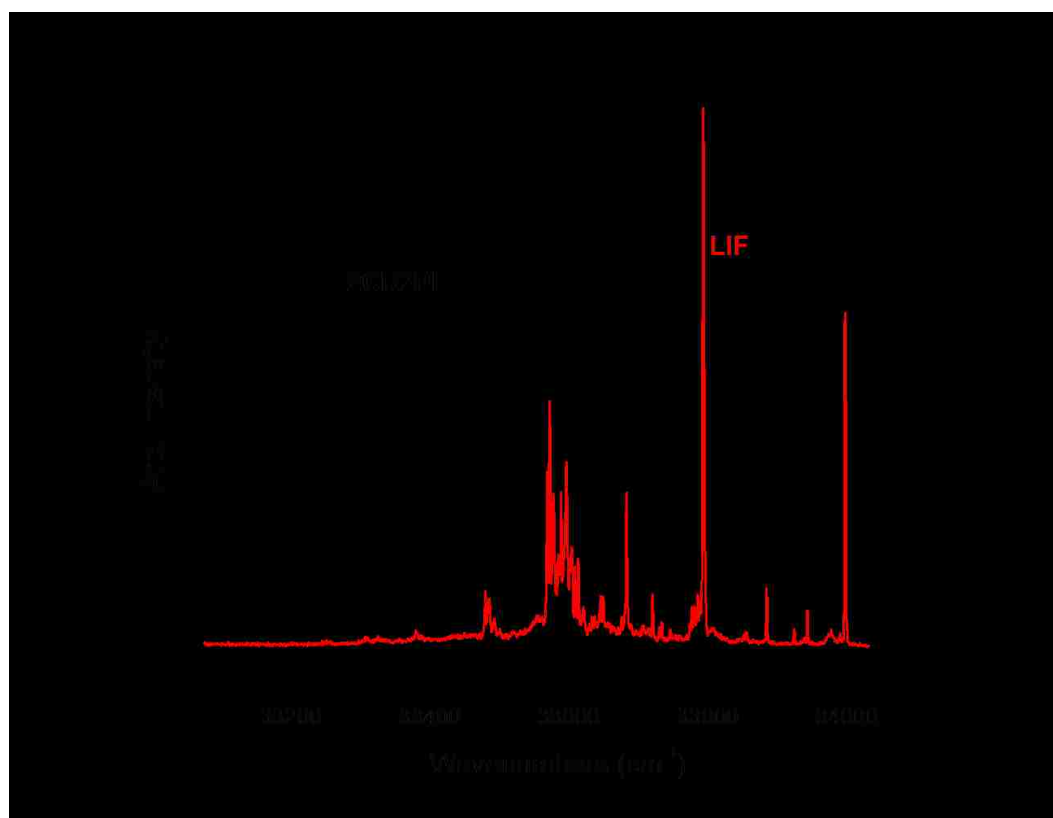
Figure 6.3: The 2CR2PI and LIF excited state spectra for the F2H2 composite molecule.

An LIF spectrum was also collected on the F2H2 system. This yielded a spectrum with improved resolution with the same features of varying intensities. A mass spectrum of F2H2 (Figure 6.4) was collected via the R2PI setup yielded an unexpected result.
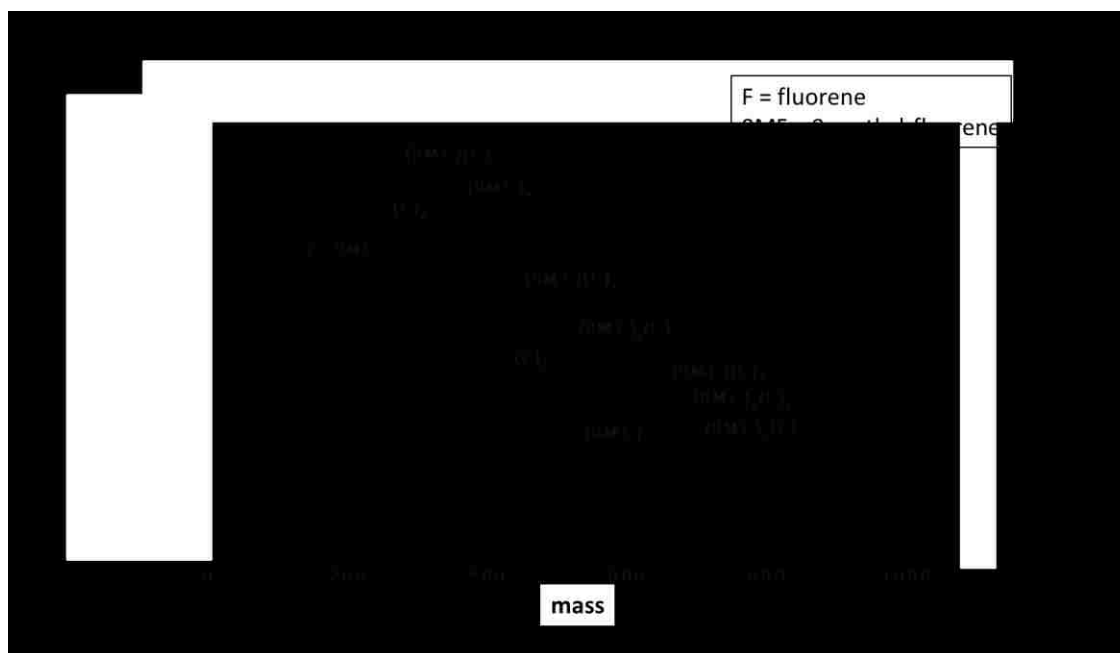
Figure 6.4: Mass spectrum gated at the mass of F2H2 composite molecule.

The mass spectrum indicated that F2H2 was dissociating during the experiment. Using weight to identify the fragments, it showed that fluorene, 9-methylfluorene, and associated homogeneous and heterogeneous clusters were present and the measured spectrum is comprised of fluorene dimer, 9-methylfluorene dimer and the mixed dimer. A potential cause is thermal dissociation; however a rough melting temperature test revealed that F2H2's melting point range is above 185 °C. Photolysis might also be possible, but due to the lack of dissociation with all other similar systems, this is also unlikely. A third possibility, and most probably culprit, is exposure to metal surfaces in both the sample holder and pulsed nozzle assembly. It is unclear what causes dissociation, however it is certain that F2H2 cannot be viewed with the current setup and therefore will be modified for future experiments on the system.

Additionally, F3H2 was also examined using 1CR2PI techniques. The resulting spectrum is featured in Figure 6.5. The spectrum is reminiscent of F2H2, showing a general broadness and multiple 'origins' of varying intensity. The process by which this spectrum is formed has not been fully investigated and joins F2H2 as a system to be investigated in the future with a modified experimental setup.
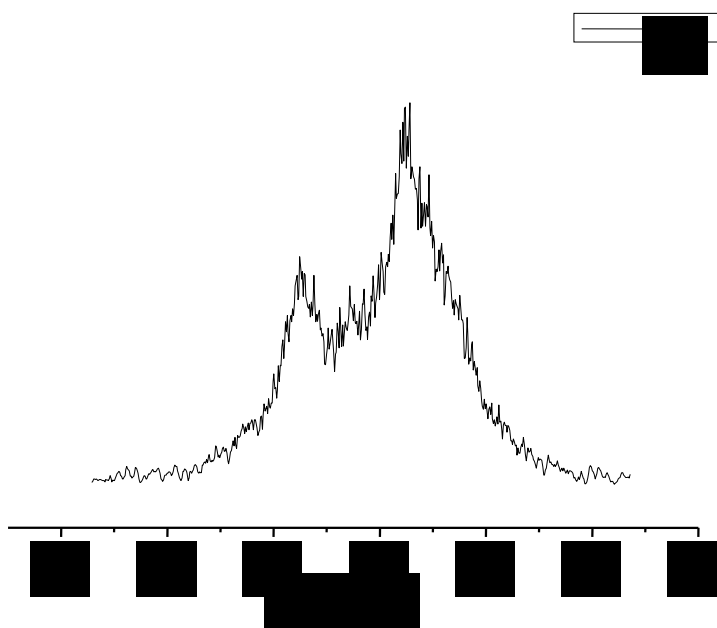
Figure 6.5: The R2PI spectrum of F3H2 composite molecule.

A modification that has been recently to the experimental setup was to the in-house LABVIEW program used for digital data collection. Previously, spectra were collected using a 'gated range' in which data points would be recorded only if the feel within the range of the gate. This was used to selected ions of a specific mass in the

2CR2PI setup, or fluorescence of a certain lifetime in the LIF setup. With Dr. Damian

Kokkin, all LABVIEW programs have been modified to make data collection more

efficient by creating 2-dimersional spectra. Plotted in Figure 6.6 is an example of a 2-D

LIF spectrum collected with DTBF. The program negates the need of a 'gate' by

collecting snapshot signal profile displayed on the oscilloscope at all steps of the laser

through the experiment. The result is a 2-dimesional graph with laser wavelength as the

x-axis and either the fluorescence profile or mass spectrum as the y-axis.   This will make

data collection much more efficient for future experiments.

164
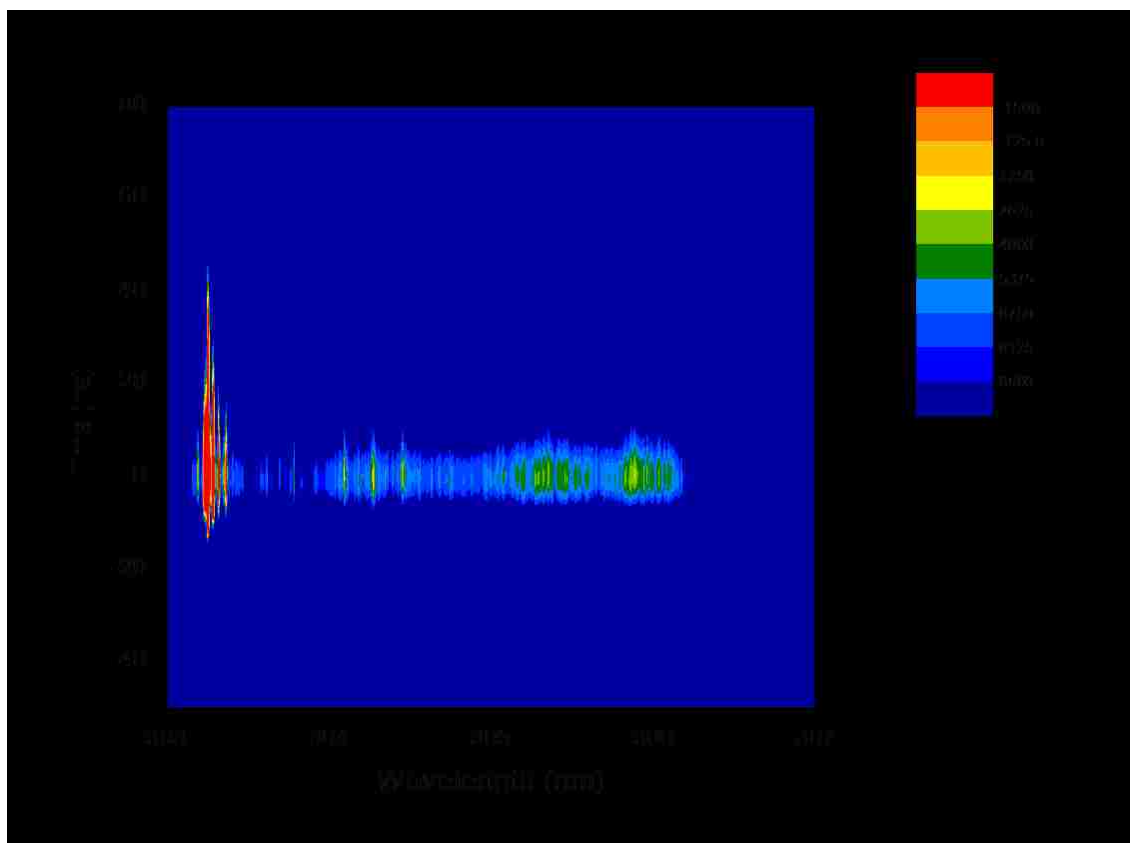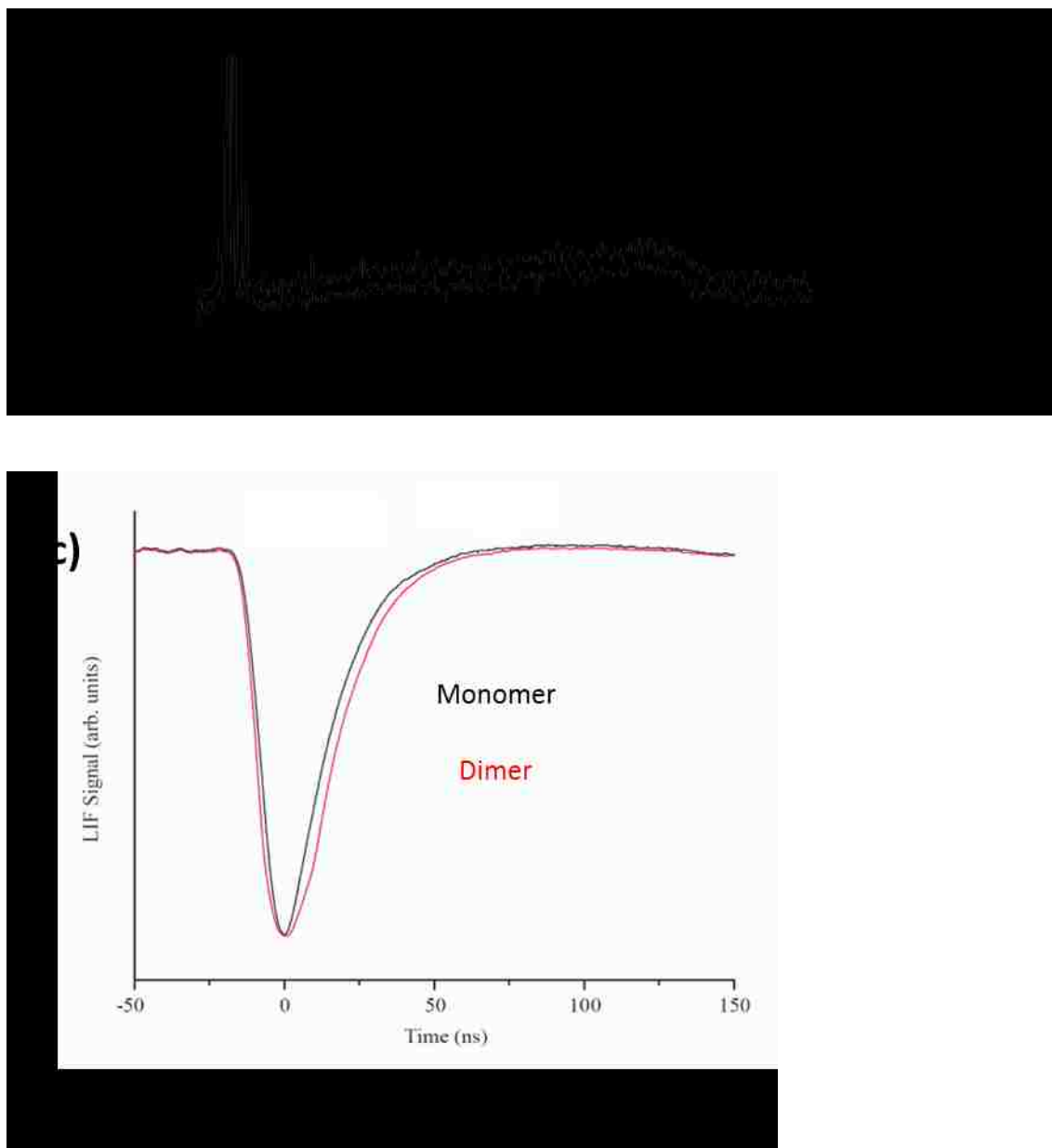
Figure 6.6: (a)2-D LIF Excitation Spectra of DTBF. The (b) x-axis is made up of slices of the excitation spectra, and the (c) y-axis consists of slices of the fluorescence signal imaged on the oscilloscope.

6.2   Conclusion

In this dissertation the formation of an excimer involving fluorene as a model system was investigated to form the criteria necessary for excited state stabilization and electron hole delocalization. The experiment was motivated by the diverse roles that non-covalent forces play in various systems. Non-covalent forces influence many biological processes and are significant contributors to organic electronics and photovoltaics, while fluorene more recently has proven to be an effective system to transport energy and for electron transport. Although fluorene is well studied, the geometrical requirements to efficiently transport energy and charge remained unclear. Gas-phase ionization and fluorescence experiments to probe the molecular states created an opportunity to achieve the goals of the experiment and proved to be an effective tool in the study.

Chapter 3 was the starting point of the experiment. The goal was to provide a better understanding of fluorene's excimer formation. This phenomenon has been well documented but not well understood. The fluorene van der Waals dimer was used as the initial model system with previous results to compare to. Following collection of excitation spectra that matched well with other literature results, the F2 composite dimer was examined to compare with $(F)_2$. $(F)_2$ and F2 showed excimer-like emission as well as a significant lowering of their Ionization Potentials. A computational investigation was necessary and proved useful as it helped discover the geometrical properties necessary to accomplish such phenomena. Minimum energy structures and their relative energies were used to identify the geometries most likely to be found in the gas phase.

F2 showed a high affinity for a π-stacked geometry by forming a 'pre-excimer' in the ground state, ultimately providing direct access to the excimer well in the excited state of the system. $(F)_2$ showed similar excimer emission, albeit not as strong as F2. It was discovered that $(F)_2$ did not form a 'pre-excimer' in the ground phase, forcing it to undergo a fast geometric rearrangement and overcome a barrier upon excitation in order to form an excimer. Although F2 was able to form an excimer more efficiently than $(F)_2$, their ability to stabilize electron hole remained equal. This gave way to the idea that the requirements for excimer formation and electron hole stabilization are not the same.

The aim of Chapter 4 was to investigate the difference between excimer and ion stabilization requirements. Using F1 as a model vdW system proved to be effective because of its slight structural modification. Experimental results showed that it did not have excimer-type emission. This was demonstrated through a lack of significant red-shift in the excitation spectra and from its well-resolved Dispersed Fluorescence spectrum. Calculations were conducted to find possible minimum energy structures of the F1 dimer. The results showed that, due to the steric effects created by the addition of methyl groups at the 9H position of fluorene, ideal π-stacking could not be achieved, thus preventing any significant stabilization of the excited state. Ionization Potentials, however, showed that F1 dimer was able to stabilize an electron hole. Although the IP was lowered less than $(F)2$ and F2, it remained a significant decrease. This reiterated the fact that the geometric requirements for excimer formation and electron hole stabilization are not the same, with hole stabilization requirements being more relaxed.

After demonstrating the exclusivity between geometric requirements, the goals of Chapter 5 served as an appropriate follow up investigation. F2 showed that the use of a

covalent linker was an effective way to influence the excited state of a system, as well as the steric effects demonstrated by F1 dimer. Multiple systems were designed with the goal of improving upon the understanding of these requirements. Tert-butyl and Di-tertbutyl fluorene molecules would serve as model systems in an attempt to further investigate the effects of bulky, steric substituents. 1,2 and 1,3-di-fluorenylcyclohexane were designed to serve as model systems that take advantage of the covalent linker's ability to fix excited state geometries. TBF showed the influence that one bulky group had on fluorene stabilization effects. Although it appeared to possible form a very weak excimer, evidenced by a broad, Gaussian-type emission spectrum and a slight lengthening of the excited state lifetime, it was unable to efficiently stabilize an electron hole, due to its bulky substituent. DTBF showed the opposite trend and strongly resembled the results of F1 dimer. The lifetime did not change from monomer to dimer, nor did it show excimer-like emission in its DF. (However, the dimer profile in the DF was very broad and unresolved but did not resemble a Gaussian profile.)

1,2 and 1,3-DFC were able to demonstrate the distance effects of the π-rings. 1,3-DFC showed a well resolved excitation spectrum with complex, weak splitting patterns and an IP higher than F2 and (F)$_2$. Optimization calculations were completed and showed that the fluorene subunits were too far away from each other to efficiently π-stack, leading to no excimer formation and a moderate lowering of the IP relative to fluorene monomer. 1,2-DFC served as an effective model that demonstrated the effects of π-rings being in close proximity. The excitation spectrum was collected via very small signal, showing a broad, unresolved feature in the 2CR2PI setup. In the LIF setup, however, 1,2-DFC showed a resolved and highly active excitation spectrum; a

consequence of the proximity of the rings. Lifetime measurements revealed a similar excited state lifetime to 9,9'-bifluorenyl, suggesting 1,2-DFC was comparable to the covalently linked dimer. Calculations showed that the carbon-carbon bond that directly links the fluorene subunits was elongated to about 1.59 Å, while the similar system with a carbon-carbon linker, 9,9'-bifluorenyl was estimated to be slightly shorter at 1.55 Å.

This study has successfully contributed to the understanding of π-interactions and the effect it has on chromophoric systems. This study was also successful in demonstrating the effectiveness supersonic pulsed-valve gas-phase experimental techniques. Using fluorene as an inspiration, a diverse roster of model systems have been developed to explore non-covalent interactions and what influences their efficiency. F2H2 and F3H2 have been examined and discussed briefly and will prove to be effective models in understanding π-interactions as a potential driving force for molecular motion, i.e. the opening and closing of molecular structures in the future.

BIBLIOGRAPHY

1) Schalley, C. A.; Introduction, in Analytical Methods in Supramolecular Chemistry (ed C. Schalley), *Wiley-VCH Verlag GmbH & Co. KGaA*, Weinheim, Germany, **2006**

2) A.) Carey, F. A.; Sundberg, R. J.; Advanced Organic Chemistry Part A: Structure and Mechanics, 3rd Ed., *Plenum Press, New York*, **1990.** B.) Brown, T. L.; LeMay, H. E.; Bursten, B. E.; Murphy, C. J.; Chemistry: The Central Science, 11th Ed., *Pearson Education, New Jersey*, **2009**

3) Williams, L. D.; Molecular Interactions (Noncovalent Interactions), *Georgia* Tech, rev. 2016,
http://ww2.chemistry.gatech.edu/~lw26/structure/molecular_interactions/mol_int.html#AD

4) Hobza, P.; Müller-Dethlefs, K.; Non-Covalent Interactions: Theory and Experiment; *RSC Theoretical and Computational Chemistry Series* (RSC Publishing), **2010**

5) Jeffrey, G. A.; An Introduction to Hydrogen Bonding, *Oxford University Press*, Oxford, **1997**

6) Grabowski, S.; What is the Covalency of Hydrogen Bonding?, *J. Chem. Rev*., **2011**, 111, 2597

7) Legon, A. C.; Millen, D.; The Nature of the Hydrogen Bond to Water in the Gas-Phase, *J. Chem. Soc. Rev*., **1992**, 12, 71

8) Hobza, P. A. Z., R. Ed.; Weak Intermolecular Interactions in Chemistry and Biology, **1980**, Elsevier: Amsterdam

9) Sun, S.; Bernstein, E. R.; Aromatic van der Waals Clusters: Structure and Non-rigidity, *J. Phys. Chem.*, **1996**, 100, 13348-13366

10) Hunter, C.A.; Sanders, J. K. M.; The Nature of Pi-Pi Interactions, *J. Am. Chem. Soc*., **1990**, 112, 5525-5534

11) Burley, S. K.; Petsko, G. A.; Dimerization Energetics of Benzene and Amino Acid Side Chains, *J. Am. Chem. Soc*., 108, **1986**, 7995-8001

12) Gross, E. K. U. and Kohn, W.; Time-Dependent Density Function Theory, *Advanced Quantum Chem* **1990,** 21

13) Yamakawa, M.; Yamada, I.; Noyori, R.; CH/pi Attraction: The Origin of Enantioselectivity in Transfer Hydrogenation of Aromatic Carbonyl Compounds Catalyzed by Chiral eta(6)-Arene-Ruthenium(II) Complexes, *Angew Chem Int Edit*, **2001**, 40, 2818

14) Nishio, M.; CH/Pi Hydrogen Bonds in Organic Reactions, *Tetrahedron* **2005**, 61, 6923

15) Bertani, R.; Sgarbossa, P.; Venzo, A.; Lelj, F.; Amati, M.; Resnati, G.; Pilati, T.; Metrangolo, P.; Terraneo, G.; Halogen bonding in metal–organic–supramolecular networks, *Coord. Chem. Rev*. **2010**, 254, 677

16) Nishio, M.; The CH/PiHydrogen Bond: Implication in Chemistry, *J. Mol. Struct*., **2012**, 1018, 2-7

17) Del Bene, J. E.; Jordan, M. J. T.; Vibrational Spectroscopy of the Hydrogen Bond: An ab initio Quantum-Chemical Perspective, *Int. Rev. Phys. Chem*., **1999**, 18, 119

18) Schuster, P.; Zundel, G.; Sandorfy, C. The hydrogen bond : recent developments in theory and experiments; *North-Holland Publishing Company*: Amsterdam ; New York, **1976**

19) American Chemical Society. Meeting (206th : 1993 : Chicago Ill.); Smith, D. A.; American Chemical Society. Division of Computers in Chemistry. Modeling the hydrogen bond; *American Chemical Society*: Washington, DC, **1994**

20) Thanthiriwatte, K. S.; Hohenstein, E. G.; Burns, L. A.; Sherrill, C. D.; Assessment of the Performance of DFT and DFT-D Methods for Describing Distance Dependence of Hydrogen-Bonded Interactions, *J. Chem. Theory Comput*., **2011**, 7, 88

21) Nishio, M.; Tsuboyama, S.; Umezawa, Y.; Takahasi, H.; CH/Pi Interaction in the Conformation of Organic Compounds, *Tetrahedron*, **1999**, 55, 10047-10056

22) Auffinger, P.; Hays, F. A.; Westhof, E.; Ho, P. S. *Proceedings of the National Academy of Sciences of the United States of America* **2004**, 101, 16789

23) Voth, A. R.; Hays, F. A.; Ho, P. S. *Proceedings of the National Academy of Sciences of the United States of America* **2007**, 104, 6188

24) Nishio, M.; Hirota, M.; Umezawa, Y. The CH/Pi interaction : Evidence, Nature, and Consequences; *Wiley*: New York, **1998**

25) Desiraju, G. R.; Steiner, T. The weak hydrogen bond : in structural chemistry and biology; *Oxford University Press*: Oxford ; New York, **1999**

26) Muraki, M.; The Importance of CH/Pi Interactions to the Function of Carbohydrate Binding Proteins, *Protein Pept. Lett*., **2002**, 9, 195

27) Nakagawa, Y.; Irie, K.; Yanagita, R. C.; Ohigashi, H.; Tsuda, K.; Indolactam-V is Involved in the CH/Pi Interaction with Pro-11 of the PKCδ C1B Domain: Application for the Structural Optimization of the PKCδ Ligand, *J. Am. Chem. Soc.*, **2005**, 127, 5746

28) Ramirez-Gualito, K.; Alonso-Rios, R.; Quiroz-Garcia, B.; Rojas-Aguilar, A.; Diaz, D.; Jimenez-Barbero, J.; Cuevas, G.; Enthalpic Nature of the CH/Pi Interaction Involved in the Recognition of Carbohydrates by Aromatic Compounds, Confirmed by a Novel Interplay of NMR, Calorimetry, and Theoretical Calculations, *J. Am. Chem. Soc*., **2009**, 131, 18129

29) Nishio, M.; The CH/Pi Hydrogen Bond in Chemistry. Conformation, Supramolecules, Optical Resolution and Interactions Involving Carbohydrates, *Phys. Chem. Chem. Phys*., **2011**, 13, 13873

30) Amendola, V.; Fabbrizzi, L.; Mosca, L.; Anion Recognition by Hydrogen Bonding: Urea-Based Receptors, *Chem. Soc. Rev*., **2010**, 39, 3889

31) Zhang, Y.; Ji, B. M.; Tian, A. M.; Wang, W. Z.; Competition between Pi-Pi Interaction and Halogen Bond in Solution: A Combined 13C NMR and Density Functional Theory Study, *J. Chem. Phys*., **2012**, 136, 141101

32) Arunan, E.; Desiraju, G. R.; Klein, R. A.; Sadlej, J.; Scheiner, S.; Alkorta, I.; Clary, D. C.; Crabtree, R. H.; Dannenberg, J. J.; Hobza, P.; Kjaergaard, H. G.; Legon, A. C.; Mennucci, B.; Nesbitt, D. J.; Defining the Hydrogen Bond: An Account (IUPAC Technical Report), *Pure Appl. Chem*., **2011**, 83, 1619-1636

33) Sredojevic, D.; Bogdanovic, G. A.; Tomic, Z. D.; Zaric, S. D.; Stacking vs. CH–Pi Interactions between Chelate and Aryl Rings in Crystal Structures of Square-Planar Transition Metal Complexes, *Cryst. Eng. Comm*., **2007**, 9, 793-798

34) Zhu, S.; Xing, C.; Xu, W.; Jin, G.; Li, Z.; Halogen Bonding and Hydrogen Bonding Coexist in Driving Self-Assembly Process, *Crystal Growth and Design* **2004**, 4, 53-56

35) Balle, T. J.; Flygare, W. H.; Fabry–Perot Cavity Pulsed Fourier Transform Microwave Spectrometer with a Pulsed Nozzle Particle Source, *Rev. Sci. Instrum.* **1981**, 52, 33

36) Gutowsky, H. S.; Emilsson, T.; Arunan, E.; Low-*J* Rotational Spectra, Internal Rotation, and Structures of Several Benzene–Water Dimers, *J. Chem. Phys.* **1993**, 99, 4883

37) Suzuki, S.; Green, P. G.; Bumgarner, R. E.; Dasgupta, S.; Goddard, W. A., III; Blake, G. A.; Benzene Forms Hydrogen Bonds with Water, *Science* **1992**, 157, 942

38) Schlag, E. W.; Müller-Dethlefs, K.; High-Resolution Zero Kinetic Energy(ZEKE) Photoelectron Spectroscopy of Molecular Systems, *Annu. Rev. Phys. Chem*. **1991**, 42, 109-136

39) Wright, T.; Panov, S. I.; Miller, T. A.; Vibrational Spectroscopy of the Chlorobenzene Cation Using Zero Kinetic Energy Photoelectron Spectroscopy, *J. Chem. Phys*., 102, 4793, (**1995**)

40) Riese, M.; Altug, Z.; Grotemeyer, J.; Mass-Analyzed Threshold Ionization Spectroscopy of Pyridine. Structural Distortion in the First Excited State, *Phys. Chem. Chem. Phys*., **2006**, 8, 4441-4448

41) Brutschy, B.; Ion-Molecule Reactions with Molecular Clusters, *Chem. Rev*., **1992**, 92, 1567-1587

42) Sinnokrot, M. O.; Valeev, E.F.; Sherrill, C.D.; Estimates of the ab initio Limit for Pi-Pi Interactions: the Benzene Dimer, *J. Am. Chem. Soc*. **2002**, 124, 10887-10893

43) Güthe, F.; Ding, H.; Pino, T.; Maier, J. P.; Diagnosis of a Benzene Discharge with a Mass-Selective Spectroscopic Technique, *Chem. Phys*., 269, (**2001**), 347-355

44) Karlström, G.; Linse, P.; Wallqvist, A.; Jönsson, B.; Intermolecular Potentials for the H_2O-C_6H_6 and the C_6H_6-C_6H_6 Systems Calculated in an ab initio SCF CI Approximation, *J. Am. Chem. Soc*., **1983**, 105, 3777-3782

45) Sinnokrot, M. O.; Sherrill, C. D.; Highly Accurate Coupled Cluster Potential Energy Curves for the Benzene Dimer: Sandwich, T-Shaped, and Parallel-Displaced Configurations, *J. Phys. Chem. A*, **2004**, 108, 10200-10207

46) Ferguson, J.; Absorption and Emission Spectra of the Perylene Dimer, *J. Chem. Phys*., 44, 2677, **1966**

47) Saigusa, H.; and Morohoshi, M.; Tsuchiya, S.; Excimer and Exciplex Formation in van der Waals Dimers of Toluene and Benzene, *J. Phys. Chem. A*, **2001**, 105, 7334-7340

48) Rogers, D. M.; Hirst, J. D.; Lee, E. P. F.; Wright, T. G.; Ab initio Study of the Toluene Dimer, *Chemical Physics Letters*, 427, (**2006**), 410-413

49) Yeh, J.; Shen, T.; Nocera, D. G.; Leroi, G. E.; and Suzuka, I; Ozawa, H.; Namuta, Y.; Resonance Two-Photon Ionization Spectroscopy of the Aniline Dimer, *J. Phys. Chem*., **1996**, 100, 4385-4389

50) Ringer, A. L.; Sinnokrot, M. O.; Lively, R. P.; Sherrill, C. D.; The Effect of Multiple Substituents on Sandwich and T-Shaped Pi-Pi Interactions, *Chem. Eur. J*., **2006**, 12, 3821-3828

51) Motohiro, N.; Minoru, H.; Yoji, U. Ed.; The C-H/π Interaction: Evidence, Nature, and Consequences, **1998**, *Wiley-VCH*: USA

52) Chipot, C.; Jaffe, R.; Maigret, B.; Pearlman, D. A.; Kollman, P. A.; Benzene Dimer: A Good Model for Pi-Pi Interactions in Proteins? A Comparison between the Benzene and the Toluene Dimers in the Gas Phase and in an Aqueous Solution, *J. Am. Chem. Soc*., **1996**, 118, 11217-11224

53) Jaffe, R. L.; Smith, G. D.; A Quantum Chemistry Study of Benzene Dimer, *J. Chem. Phys*., 105, 2780, **1996**

54) Sinnokrot, M. O.; Sherrill, C. D.; High-Accuracy Quantum Mechanical Studies of Pi-Pi Interactions in Benzene Dimers, *J. Phys. Chem*. A, **2006**, 110, 10656-10668

55) Law, K. S.; Schauer, M.; Bernstein, R.; Dimers of Aromatic Molecules: (Benzene)2, (toluene)2, and Benzene-Toluene, *J. Chem. Phys*., 81, 4871-4882, **1984**

56) Squire, D. W.; Bernstein, R. B.; Multiphoton Ionization Mass Spectrometric Study of Toluene Clusters in a Pulsed Nozzle Beam Time-of-Flight Apparatus, *J. Phys. Chem*., **1984**, 88, 4944-4952

57) Ishikawa, S.; Ebata, T.; Ishikawa, H.; Inoue, T.; Mikami, N.; Hole-Burning and Stimulated Rama-UV Double Resonance Spectroscopies of Jet-Cooled Toluene Dimer *J. Phys. Chem*. **1996**, 100, 10531-10535

58) Musgrave, A.; Wright, T. G.; Electronic Spectroscopy of Small Toluene Clusters, *J. Chem. Phys*., 122 074312, **2005**

59) Di Palma, T. M.; Bende, A.; Borghese, A.; Photoionisation and Structures of Jet-Formed Toluene Clusters, *Chemical Physics Letters* 495, (**2010**), 17-23

60) Bloom, J. W. G.; Wheeler, S. E.; Toward a More Complete Understanding of Noncovalent Interactions Involving Aromatic Rings, *J. Phys. Chem. A*, **2014**, 118, 6133-6147

61) Wheeler, S. E.; Understanding Substituent Effects in Noncovalent Interactions Involving Aromatic Rings, *Acc. Chem. Res.*, 46, **2013**, 1029-1038

62) Wheeler, S. E.; Local Nature of Substituent Effectsin Stacking Interactions, *J. Am. Chem. Soc.*, **2011**, 133, 10262-10274

63) Imhof, P.; Kleinermanns, K.; Dispersed Fluorescence Spectra of Chlorobenzene, *Chem. Phys*., 270, (**2001**), 277-236

64) Bergeron, D. E.; Ayles, V. L.; Richards, O. J.; Wright, T. G.; Electronic Spectroscopy of para-fluorotoluene Clusters, *Chemical Physics Letters*, 430, (**2006**), 282-286

65) Lu, W. Y.; Hu, Y. H.; Lin, Z. Y.; Yang, S. H.; Two-Photon Ionization Studies of Binary Aromatic van der Waals Clusters: Benzene…Chlorobenzene and (Chlorobenzene)2, *J. Chem. Phys*., 104, 8843, **1996**

66) Liu, B.; Wang, B.; Wang, Y.; Wang, L.; Ultrafast Dynamics of Chlorobenzene Clusters, *Chemical Physics Letters*, 477 (**2009**) 266–270

67) Reid, S. A.; Muzangwa, L.; Nyambo, S.; Uhler, B.; On Pi-stacking, C-H/Pi, and Halogen Bonding Interactions in Halobenzene Clusters: Resonant Two-Photon Ionization Studies of Chlorobenzene, *J. Chem. Phys*., **2012**, 137, 184307

68) Reid, S. A.; Nyambo, S.; Muzangwa, L.; Uhler, B.; Pi-Stacking, C-H/Pi, and Halogen Bonding Interactions in Bromobenzene and Mixed Bromobenzene-Benzene Clusters, *J. Phys. Chem. A*, **2013**, 117, 13556-13563

69) House, J. E.; Fundamentals of Quantum Mechanics, *Academic Press*, San Diego, California, **1998**

70) Franck, J.; Dymond, E. G.; Elementary Processes of Photochemical Reactions, *Trans. Faraday Soc*. **1926**, 21, 536-542

71) A. S. Davydov; Theory of Molecular Excitons (translated by M. Kasha and M. Oppenheimer, Jr.) *McGraw-Hill*, New York (**1962**)

72) D. S. McClure; Electronic Spectra of Molecules and Ions in Crystals; *Academic Press,* New York (**1959**)

73) Kasha, M.; Rawls, H. R.; Ashraf El-Bayoumi, M.; The Exciton Model in Molecular Spectroscopy, *Butterworth's London*, **1965**, Vol. 11, pp. 371-92

74) Smith, P. G.; Gnanakaran, S.; Kaziska, A. J.; Motyka, A. L.; Hong, S. M.; Hochstasser, R. M.; Topp, M. R.; Electronic Coupling and Conformational Barrier Crossing of 9,9'-bifluorenyl Studied in a Supersonic Jet, *J. Chem Phys*. 100 (5), **1994**

75) Troxler, T.; Pryor, B.; Topp, M. R.; Rotational Coherence Spectroscopy of 9,9'-bifluorenyl: Assignment of Exciton Components, *Chem. Phys. Lett*., 239,(**1995**), 44-50

76) Dantzig, N.; Levy, D. H.; Vigo, C.; Piotrowiak, P.; Vibronic Coupling and Energy Transfer in Bichromophoric Molecules: The Effect of Symmetry, *J. Chem. Phys*., 103, (12), **1995**

77) Skoog, D. A.; West, D. M.; Holler, F. J.; Crouch, S. R.; Fundamentals of Analytical Chemistry, 8th. Ed, *Brooks/Cole*, Belmont, California, **2004**

78) Skoog, D. A.; Holler, F. J.; Crouch, S. R., Principles of Instrumental Analysis, 6th Ed., *Thomson Brooks/Cole*, Belmont, California, **2007**

79) Karas, M.; Krüger, R. Ion Formation in MALDI: The Cluster Ionization Method, *Chem. Rev.*, **2003**, 103, 427-440

80) Ladaviére, C.; Lacroix-Desmazes, P.; Delolme, F. First Systematic MALDI/ESI Mass Spectrometry Comparison to Characterize Polystyrene Synthesized by Different Controlled Radical Polymerizations, *Macromolecules*, **2009**, 42, 70-84

81) Mansouri, A.; Cappello, C. D.; Houamer, S.; Charpentier, I.; Lahmam-Bennani, A.; Double Ionization of H_2 by Electron Impact: A Second Born Treatment, *J. Phys. B: At. Mol. Opt. Phys.*, 37, **2004**, 1203-1214

82) Baer, T.; Vacuum UV Photophysics and Photoionization Spectroscopy, *Ann. Rev. Phys. Chem.*, **1989**, 40, 637-669

83) Hoffman, E.; Stoobant, E., Mass Spectrometry: Principles and Applications, 3rd. Ed., *John Wiley & Sons, Ltd.*, West Essex, England, **2007**

84) Lias, S. G.; Bartmess, J. E.; National Institute of Standard and Technology Chemistry Webbook: Gas Phase Ion Thermochemistry **2016**, No. 69

85) Levy, D. H.; Laser Spectroscopy of Cold Gas-Phase Molecules, *Ann. Rev. Phys. Chem.*, **1980**, 31, 197-225

86) Murphy, H. R., Miller, D. R.; Effect of Nozzle Geometry on Kinetics in Free-Jet Expansions, *J. Phys. Chem.*, **1984**, 88, 4474-4478

87) Bernath, F. P.; Spectra of Atoms and Molecules, *Oxford University Press Inc.*, New York, New York, **1995**

88) Jenkins, J.; Savage, S.; A Theory for the Rapid Flow of Identical, Smooth, Nearly Elastic, Spherical Particle, *J. Fluid. Mech.*, **1983**, 130, 187-202

89) Louge, M.; Mastorakos, E.; Jenkins, J.; The role of particle collisions in pneumatic transport, *J. Fluid. Mech.*, 231 (**1991**), 345–359

90) Oh, J. J.; Park, I.; Wilson, R. J.; Peebles, S. A.; Kuczkowski, R. L. et. al.; Structure of the Chlorobenze-Argon Dimer: Microwave Spectrum and ab initio Analysis, *J. Chem. Phys.*, 113 9051, **2000**

91) Dao, P. D.; Morgan, S.; Castleman Jr, A. W.; Two-color Resonance Enhanced Multiphoton Ionization of van der Waals Molecules: Studies of Spectroscopy Shifts and Ionization Thresholds of Paraxylene Clustered with Argon, *Chem. Phys. Lett.*, 113, **1985**, 219-224

92) Kinsey, J. L.; Laser Induced Fluorescence, *Ann. Rev. Phys. Chem.*, **1977**, 28, 349-372

93) Zare, R. N.; Dagdigian, P. J.; Tunable Laser Fluorescence Method for Product State Analysis, *Science*, 185, **1974**, 739-747

94) Morse, M. D.; Experimental Methods in the Physical Sciences **1996**, Vol. 29B; *Academic Press Inc.*

95) Hollas, J. M.; Phillips, D.; Jet Spectroscopy and Molecular Dynamics, *Chapman & Hall*, Bishopbriggs, Glasgow G64 2NZ, **1995**

96) Foresman, J. B.; Frisch A.; Exploring Chemistry with Electronic Structure Methods, *Eleen Ed.*, Gaussian Inc: Pittsburg, **1993**

97) Ramachandran, K. I.; Deepa, G.; Namboori, K. Computational Chemistry and Molecular Modeling: Principles and Applications, *Springer,* Berlin, **2008**

98) Cramer, C. J., Ed. Essentials of Computational Chemistry: Theories and Models *John Wiley and Sons, Ltd*: West Sussex, **2004**

99) A.) Hanwell, M. D.; Curtis, D. E.; Lonie, D. C.; Vandermeersch, T.; Zurek, E.; Hutchison, G. R.; Avogadro: An Advanced Semantic Chemical Editor, Visualization, and Analysis Platform, *Journal of Cheminformatics*, 4, 17, **2012**. B.) Avogadro: an open-source molecular builder and visualization tool. Version 1.0.1

100) Rappé, A. K.; Casewit, C. J.; Colwell, C. S.; Goddard III, W. A.; Skiff, W. M.; UFF, A Full Periodic Table Force Field for Molecular Mechanics and Molecular Dynamics Simulations, *J. Am. Chem. Soc.*, **1992**, 114, 10024-10035

101) Halgren, T. A.; Merck Molecular Force Field. I. Basis, Form, Scope, Parameterization, and Performance of MMFF94, *J. Comput. Chem.*, 17, 490-510, **1996**

102) Raghavachari, K.; Trucks, G. W.; Pople, J. A.; Head-Gordon, M., A Fifth-Order Perturbation Comparison of Electron Correlation Theories, *Chem. Phys. Lett.* **1989**, 157, 479

103) Mardirossian, N.; Parkhill, J. A.; Head-Gordon, M.; Benchmark Results for Empirical post-GGA Functionals: Difficult Exchange Problems and Independent Tests, *Phys. Chem. Chem. Phys.*, **2011**, 13, 19325-19337

104) Zhao, Y.; Truhlar, D. G., The M06 Suite of Density Functionals for Main Group Thermochemistry, Thermochemical Kinetics, Noncovalent Interactions, Excited States, and Transition Elements: Two New Functionals and Systematic Testing of Four M06-Class Functionals and 12 Other Functionals, *Theoretical Chemistry Accounts,* **2008**, 120, 215-241

105) T. H. Dunning Jr.; Gaussian basis sets for use in correlated molecular calculations. I. The atoms boron through neon and hydrogen, *J. Chem. Phys.*, **1989**, 90, 1007-23

106) Förster, T; Kasper, K.; Ein Kozentrationsumschlag der Fluoreszenz, *Z. Phys. Chem.*, **1954**, 1, 275

107) Yip, W. T.; Levy, D. H.; Excimer/Exciplex Formation in van der Waals Dimers of Aromatic Molecules, *J. Phys. Chem.*, **1996**, 100, 11539-11545

108) Scholes, G. D.; Ghiggino, K. P.; Excitonic Interactions and Interchromophore Excitation Transfer, *J. Phys. Chem.*, **1994**, 98, 4580-4590

109) Auty, A. R.; Jones, A. C.; Phillips, D.; Spectroscopy and Decay Dynamics of Jet-Cooled Carbazole and N-ethylcarbazole and their Homocyclic Analogues, *Chem. Phys.*, Vol. 103, (**1986**), 163-182

110) Nebgen, B.; Emmert III, F. L.; Slipchenko, L. V.; Vibronic Coupling in Asymmetric Bichromophores: Theory and Application to Diphenylmethane, *J. Chem. Phys.*, 137, 084112, **2012**

111) Tubergen, M. J.; Levy, D. H.; Spectroscopy of Indole van der Waals Complexes: Evidence for a Conformation-Dependent Excited State, *J. Phys. Chem.*, 95, **1991**, 2175-2181

112) Das, A.; Mahato, K. K.; Chakraborty, T.; Excimer Formation in the Mixed Dimers of Naphthalene and 1-methoxynaphthalene in a Supersonic Jet, *Phys. Chem. Chem. Phys.*, **2001**, 3, 1813-1818

113) Ramanathan, V.; Pandey, P.; Chakraborty, T.; Laser Induced Fluorescence Spectroscopy of Jet-Cooled trans 1-methoxynapthalene: A Comparative Study with trans 1-hydroxynapthalene, *Chem. Phys. Lett.*, 456, (**2008**), 19-26

114) Fujiwara, T.; Lim, E. C.; Binding Energies of the Neutral and Ionic Clusters of Naphthalene in their Ground Electronic States, *J. Phys. Chem. A*, **2003**, 107, 4381-4386

115) Tretiak, S.; Zhang, W. M.; Chernyak, V.; Mukamel, S.; Excitonic Couplings and Electronic Coherence in Bridged Naphthalene Dimers, *PNAS*, **1999**, 96, 13003-13008

116) Kaziska, A. J.; Wittmeyer, S. A.; Topp, M. R.; Picosecond Time Resolution of Vibrational Relaxation in Molecular van der Waals Complexes: Perylene with Naphthalene and Benzene, *J. Phys. Chem.*, **1991**, 95, 3663-3670

117) Groswasser, D.; Speiser, S.; Laser-Induced Fluorescence Excitation Spectroscopy and Photophysics of Naphthalene Bichromophoric Molecules in Supersonic Jets, *Journal of Fluorescence*, 10, **2000**, 113-126

118) Wessel, J. E.; Syage, J. A.; Excitonic Interactions in Naphthalene Clusters, *J. Phys. Chem.*, **1990**, 94, 737

119) Ottiger, P.; Leutwyler, S.; Köppel, H.; S1 / S2 Excitonic Splittings and Vibronic Coupling in the Excited State of the Jet-Cooled 2-aminopyridine Dimer, *J. Chem. Phys.*, 131, 204208, **2009**

120) Saigusa, H.; Lim, E. C.; Excited State Dynamics of Fluorene/Substituted Benzene van der Waals Complexes in Supersonic Jets: Dependence of Exciplex Formation on the Relative Energies of the Lowest Excited Singlet States of Component Molecules, *J. Phys. Chem.*, **1990**, 94, 2631-2637

121) Saigusa, H.; Lim, E. C.; Localized and Delocalized Excited States of Fluorene Dimers, *J. Phys. Chem.*, **1991**, 95, 1194-120

122) Saigusa, H.; Lim, E. C. Lim; Excited State Dynamics of Aromatic Clusters: Correlation between Excitonic Interactions and Excimer Formation Dynamics, *J. Phys. Chem.*, **1995**, 99, 15738-15747

123) Pinkham, C. A.; Wait Jr., S. C.; The Electronic Spectra of Fluorene, Dibenzofuan, and Carbazole, *J. Mol. Spec.*, Vol. 27, (**1968**), 326-342

124) Kauffman, J. F.; Côté, M. J.; Smith, P. G.; McDonald, J. D.; Picosecond Fluorescence Depletion Spectroscopy. II. Intramolecular Vibrational Relaxation in the Excited Electronic State of Fluorene, *J. Chem. Phys*., 90, 2874, **1989**

125) Boo, B. H.; Kang, H. K.; Lee, S, Y.; Lee, J. K.; Lim, E. C.; Fluorescence Excitation and Resonant Two-Photon Ionization Spectroscopy of Fluorene Cooled in Pulsed Molecular Beams: Vibronic Assignment Based on a RCIS Calculation, *J. Kor. Phys. Soc*., Vol. 51, **2007**, 340-344

126) Coropceanu, V.; Nakano, T.; Gruhn, N. E.; Kwon, O.; Yade, T.; Katsukawa, K.; Brédas, J.; Probing Charge Transport in Pi-Stacked Fluorene-Based Systems, *J. Phys. Chem. B*, **2006**, 110, 9482-9487

127) Wang, L.; Puodziukynaite, E.; Vary, R. P.; Grumstrup, E. M.; Walczak, R. M.; Zolotarskaya, O. Y.; Schanze, K. S.; Reynolds, J. R.; Papanikolas, J. M.; Competition between Ultrafast Energy Flow and Electron Transfer in a Ru(II)-Loaded Polyfluorene Light-Harvesting Polymer, *J. Phys. Chem. Lett*., **2012**, 3, 2453-2457

128) Saigusa, H.; Lim, E. C.; Excimer Formation in van der Waals Dimers and Clusters of Aromatic Molecules, *Acc. Chem. Res*., Vol. 29, No. 4, **1996**

129) Cuff, L.; Kertesz, M.; Theoretical Prediction of the Vibrational Spectrum of Fluorene and Planarized Poly(p-phenylene), *J. Phys. Chem*., **1994**, 98, 12223-12231

130) Lee, S. Y.; Boo, B. H.; Density Functional Theory Study of Vibrational Spectra of Fluorene, *J. Phys. Chem*., 96, 100, 8782-8785

131) Gerbich, T.; Herterich, J.; Köhler, J.; Fischer, I.; Time-Domain Study of the S_3 State of 9-Fluorenone, *J. Chem. Phys. A*, **2014**, 118, 1397-1402

132) Nakano, T.; Synthesis, Structure and Function of Pi-Stacked Polymers, *Polymer Journal*, **(2010)**, 42, 103-123

133) IUPAC. Compendium of Chemical Terminology, 2nd ed. (the "Gold Book"). Compiled by A. D. McNaught and A. Wilkinson. *Blackwell Scientific Publications*, Oxford (1997). XML on-line corrected version: http://goldbook.iupac.org (2006-) created by M. Nic, J. Jirat, B. Kosata; updates compiled by A. Jenkins. ISBN 0-9678550-9-8

134) Guzei, I. A.; Abdelwahed, S. H.; Rathore, R.; Synthesis, Structure, and Evaluation of the Effect of Multiple Stacking on the Electron-Donor Properties of Pi-Stacked Polyfluorenes, *J. Am. Chem. Soc*., **2003**, 125, 8712-8713

135) Wessel, J.; Beck, S.; Highstrete, C.; Excitonic Interaction in the Fluorene Dimer, *J. Chem. Phys*., 101 (12), **1994**

136) Saigusa, H.; Itoh, M.; Dimer-Excimer Transformation of Fluorene in a Supersonic Expansion, *J. Phys. Chem*., **1985**, 89, 5436

137)Mautner, M.; Dimer Cations of Polycyclic Aromatics. Experimental Bonding Energies and Resonance Stabilization, *J. Phys. Chem.*, **1980,** 84, 2724-2728

138)Clark, A. E.; Qin, C.; Li, A. D. Q.; Beyond Exciton Theory: A Time-Dependent DFT and Franck-Condon Study of Perylene Diimide and its Chromophoric Dimer, *J. Am. Chem. Soc.*, **2007**, 129, 7586-7595

139)Dierksen, M.; Grimme, S.; Density Functional Calculations of the Vibronic Structure of Electronic Absorption Spectra, *J. Chem. Phys.*, 120, 3544, **2004**

140)Ottiger, P.; Leutwyler, S.; Köppel, H.; Vibrational Quenching of Excitonic Splittings in H-Bonded Molecular Dimers: The Electronic Davydov Splittings Cannot Match Experiment, *J. Chem. Phys.*, 136 174308, **2012**

141)Kopec, S.; Ottiger, P.; Leutwyler, S.; Köppel, H; Vibrational Quenching of Excitonic Splittings in H-Bonded Molecular Dimers: Adiabatic Description and Effective Mode Approximation, *J. Chem. Phys.*, 137 184312, **2012**

142)Miyazaki, M.; Fujii, M.; Real Time Observation of the Excimer Formation Dynamics of a Gas Phase Benzene Dimer by Picosecond Pump-Probe Spectroscopy, *Phys. Chem. Chem. Phys.*, **2015**, 17, 25989

143)Balmer, F. A.; Trachsel, M. A.; Avoird, A.; Leutwyler, S; The Elusive S2 State, the S1/S2 Splitting, and the Excimer States of the Benzene Dimer, *J. Chem. Phys.*, 142 234306, **2015**

144)Lu, K.; Eiden, G. C.; Weisshaar, J. C.; Toluene Cation: Nearly Free Rotation of the Methyl Group, *J. Phys. Chem.*, **1992**, 96, 9742-9748

145)Kim, W. S.; Kim, J.; Parl. J. K.; Mukamel, S.; Rhee, S. K.; Choi, Y. K.; Lee, J. Y.; Stacking Effect of Polyfluorene on the Chemical Shift and Electron Transport, *J. Chem. Phys. B*, **2005**, 109, 2686-2692

146)Talipov, M. R.; Ivanov, M. V.; Reid, S. A.; Rathore, R.; Two's Company, Three's a Crowd: Exciton Localization in Cofacially Arrayed Polyfluorenes, *J. Phys. Chem. Lett.*, **2016**, 7, 2915-2920

147)Nakano, T.; Pi-Stacked Polymers and Molecules **2014**, 1-49

148)Talipov, M.; Boddeda, A.; Timerghazin, Q.; Rathore, R.; Key Role of End-Capping Groups in Optoelecttonic Properties of Poly-p-phenylene Cation Radicals, *J. Phys. Chem. C*, **2014**, 118, 21400-21408

149)Yip, W. T.; Levy, D. H.; and Kobetic, R.; Piotrowiak, P.; Energy Transfer in Bichromophoric Molecules: The Effect of Symmetry and Donor/Acceptor Energy Gap, *J. Phys. Chem. A*, **1999**, 103, 10-20

150)Lang, M.; Holzmeier, F.; Fischer, I.; Hemberger, P.; Threshold Photoionization of Fluorenyl, Benzhydryl, Diphenylmethylene, and their Dimers, *J. Phys. Chem. A*, **2013**, 117, 5260-5268

151) Talipov, M.; Abdelwahed, S. H.; Thakur, K.; Reid, S. A.; Rathore, R. From Wired to Cables: Attempted Synthesis of 1,3,5-trifluorenylcyclohexane as a Platform for Molecular Cables, *J. Org. Chem.*, **2016**, 81, 1627-1634

152) Born, M.; Oppenheimer, J. R.; On the Quantum Theory of Molecules, *Annalen der Physik*, **1927**, 84, 457-484. (Translated by Blinder, S. M.)

153) Gaussian 09, Revision **E.01**, M. J. Frisch, G. W. Trucks, H. B. Schlegel, G. E. Scuseria, M. A. Robb, J. R. Cheeseman, G. Scalmani, V. Barone, B. Mennucci, G. A. Petersson, H. Nakatsuji, M. Caricato, X. Li, H. P. Hratchian, A. F. Izmaylov, J. Bloino, G. Zheng, J. L. Sonnenberg, M. Hada, M. Ehara, K. Toyota, R. Fukuda, J. Hasegawa, M. Ishida, T. Nakajima, Y. Honda, O. Kitao, H. Nakai, T. Vreven, J. A. Montgomery, Jr., J. E. Peralta, F. Ogliaro, M. Bearpark, J. J. Heyd, E. Brothers, K. N. Kudin, V. N. Staroverov, R. Kobayashi, J. Normand, K. Raghavachari, A. Rendell, J. C. Burant, S. S. Iyengar, J. Tomasi, M. Cossi, N. Rega, J. M. Millam, M. Klene, J. E. Knox, J. B. Cross, V. Bakken, C. Adamo, J. Jaramillo, R. Gomperts, R. E. Stratmann, O. Yazyev, A. J. Austin, R. Cammi, C. Pomelli, J. W. Ochterski, R. L. Martin, K. Morokuma, V. G. Zakrzewski, G. A. Voth, P. Salvador, J. J. Dannenberg, S. Dapprich, A. D. Daniels, Ö. Farkas, J. B. Foresman, J. V. Ortiz, J. Cioslowski, and D. J. Fox, Gaussian, Inc., Wallingford CT, 2009

154) Leist, R.; Frey, J. A.; Leutwyler, S.; Fluorobenzene−Nucleobase Interactions: Hydrogen Bonding or Pi-Stacking?, *J. Phys. Chem. A*, **2006**, 110, 4180-4187

155) Scholes, G. D.; Ghiggino, K. P.; Oliver, A. M.; Paddon-Row, M. N.; Through-Space and Through-Bond Effects on Exciton Interactions in Rigidly Linked Dinaphthyl Molecules, *J. Am. Chem. Soc.*, **1993**, 115, 4345-4349

156) Yoshida, Y.; Isomura, K.; Kumagai, Y.; Maesato, M.; Kishida, H.; Mizuno, M.; Saito, G.; Coronene-Based Charge-Transfer Complexes, *J. Phys.: Condens. Matter*, 28, **2016**, 304001

157) Reilly, N.; Ivanov, M.; Uhler, B.; Talipov, M.; Rathore, R.; Reid, S. A.; First experimental Evidence for the Diverse Requirements of Excimer vs Hole Stabilization in π-stacked Assemblies, *J. Phys. Chem. Lett.*, **2016**, 7, 3042-3045

158) Hoeben, F. J. M.; Jonkheijm, P.; Meijer, E. W.; Schenning, A. P. H. J.; About Supramolecular Assemblies of π-conjugated Systems, *Chem. Rev.*, **2005**, 105, 1491-1546

159) Birks, J. B.; Excimers, *Rep. Prog. Phys.*, **1975**, 38, 903-974